9 本科生以第一作者发表的论文

序号	文章名称	作者	杂志	影响因子	年份	网络连接
1	Preparation of Fucoidan-Based Electrospun Nanofibers and Their Interaction With Endothelial Cells.	Yiwen Chen,Huilin Zhu,Yuanping Hao,Zhanyi Sun,Peili Shen,Qihui Zhou	Frontiers in Bioengineering and Biotechnology	5.89	2021	https://www.x-mol.com/paper/search/q?selectSearchType=0&option=Preparation of+Fucoidan-Based+Electrospun+NanofibersandTheirInteractionWithEndothelialCells
2	Aptamer-based biosensors for the diagnosis of sepsis	Lubin Liu, Zeyu Han, Fei An, Xuening Gong, Chenguang Zhao, Weiping Zheng, Li Mei, Qihui Zhou	Journal of Nanobiotechnology	10.435	2021	https://www.x-mol.com/paper/1417203731817058304?adv
3	Diagnostic Value of CircRNAs as Potential Biomarkers in Oral Squamous Cell Carcinoma: A Meta-analysis	Mingfei Wang, Linfeng Zhang, Ling Gao, Wenhao Ren, Shaoming Li, Jingjing Zheng	Frontiers in Oncology	6.244	2021	https://www.x-mol.com/paper/1407436441050886144?adv

frontiers in Bioengineering and Biotechnology

ORIGINAL RESEARCH
published: 06 September 2021
doi: 10.3389/fbioe.2021.739209

Preparation of Fucoidan-Based Electrospun Nanofibers and Their Interaction With Endothelial Cells

Yiwen Chen[1,2†], Huilin Zhu[1,2†], Yuanping Hao[1], Zhanyi Sun[3], Peili Shen[3] and Qihui Zhou[1,2]*

[1]Department of Stomatology, Institute for Translational Medicine, The Affiliated Hospital of Qingdao University, Qingdao University, Qingdao, China, [2]School of Stomatology, Qingdao University, Qingdao, China, [3]State Key Laboratory of Bioactive Seaweed Substances, Qingdao Bright Moon Seaweed Group Co., Ltd., Qingdao, China

Sulfated polysaccharide fucoidan (FD) is widely applied in biomedical applications owing to its outstanding bioactivities. In addition to the biochemical features, the architecture of biomaterials plays a critical role in tissue repair and regeneration. Particularly, nanofibers have elicited great interest due to their extracellular matrix-like structure, high specific surface area, and favorable biological properties. Herein, chitosan-modified FD/ultra-high molecular weight polyethylene oxide (UHMWPEO) nanofibers are developed *via* green electrospinning and electrostatic interaction for studying their interaction with endothelial cells. The appropriate solvent is screened to dissolve FD. The electrospinnability of FD/UHMWPEO aqueous solutions is greatly dependent on the weight ratios of FD/UHMWPEO. The incorporation of UHMWPEO significantly improves the electrospinnability of solution and thermo-stability of nanofibers. Also, it is found that there is good miscibility or no phase separation in FD/UHMWPEO solutions. *In vitro* biological experiments show that the chitosan-modified FD/UHMWPEO nanofibers greatly facilitate the adhesion of endothelial cells and inhibit the attachment of monocytes. Thus, the designed FD-based nanofibers are promising bio-scaffolds in building tissue-engineered blood vessels.

Keywords: fucoidan, electrospun nanofibers, extracellular matrix, endothelial cells, biointerface, cell-material interface

OPEN ACCESS

Edited by:
Yilong Cheng,
Xi'an Jiaotong University, China

Reviewed by:
Shixian Lv,
University of Washington, United States
Jue Ling,
Nantong University, China

Correspondence:
Qihui Zhou
qihuizhou@qdu.edu.cn

†These authors have contributed equally to this work

Specialty section:
This article was submitted to Biomaterials, a section of the journal Frontiers in Bioengineering and Biotechnology

Received: *10 July 2021*
Accepted: *23 August 2021*
Published: *06 September 2021*

Citation:
Chen Y, Zhu H, Hao Y, Sun Z, Shen P and Zhou Q (2021) Preparation of Fucoidan-Based Electrospun Nanofibers and Their Interaction With Endothelial Cells. Front. Bioeng. Biotechnol. 9:739209. doi: 10.3389/fbioe.2021.739209

INTRODUCTION

In the past few decades, marine polysaccharides have gained increasing attention in the area of diversified biomedical applications owing to their inherent (bio)physicochemical features, such as biocompatibility, biodegradability, favorable bioactive, biomechanical properties, and structural functionalities (Bidarra et al., 2014; Fernando et al., 2019; Hao et al., 2020; Jana et al., 2020; Yin et al., 2021; Zheng et al., 2021). Particularly, sulfated polysaccharide fucoidan, extracted from marine brown seaweed, has been well-known to possess various biological activities, e.g., antibacterial, antiviral, antioxidant, anticoagulant, anti-inflammatory, antitumor, antithrombotic, antifibrotic, and immunomodulatory activities, facilitating the generation of angiogenesis and fibrillar collagen matrix (Li et al., 2008; Senthilkumar et al., 2017; Oka et al., 2020; Yao et al., 2020). These unique characteristics make them remarkable candidates for blood vessel tissue engineering, which has not been examined closely.

Besides the biochemical properties, their biophysical structure can significantly mediate cell attachment, shape, viability, the differentiation or pluripotency of stem cells, and even tissue repair

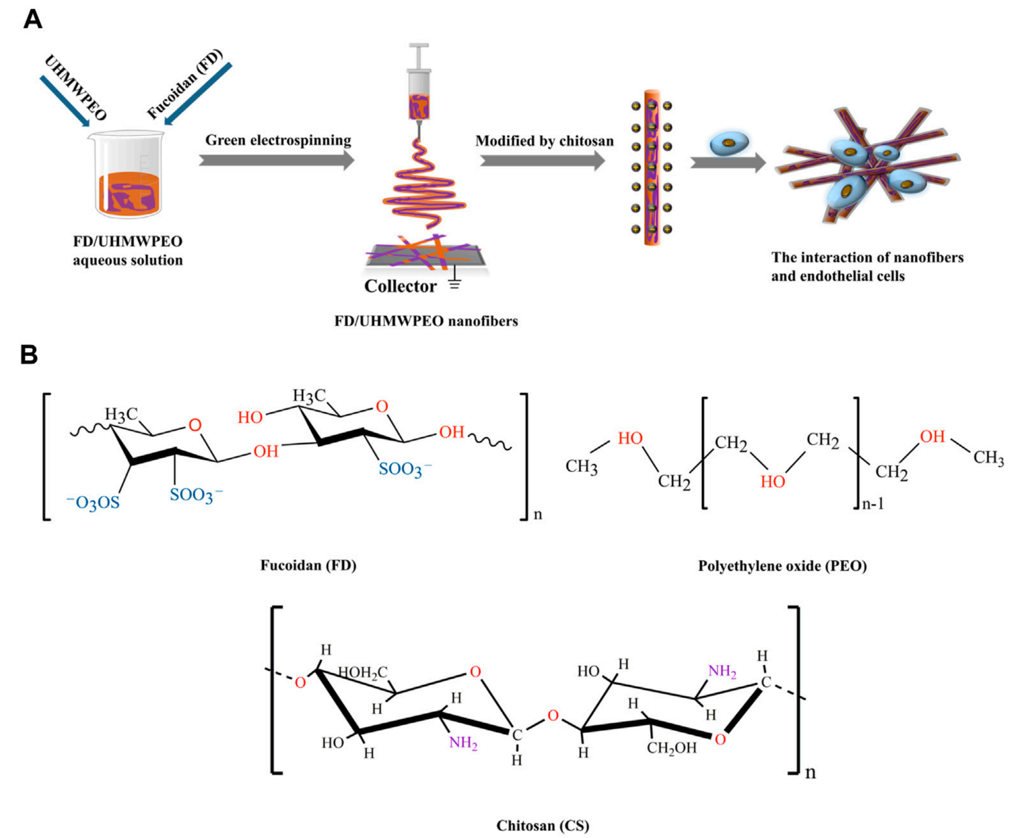

FIGURE 1 | (A) Schematic diagram of the preparation of CS-modified FD/UHMWPEO nanofibers and their interaction with HUVECs. **(B)** Chemical structures of FD, CS, and PEO.

and regeneration (Li et al., 2018; Cui et al., 2020; Yu et al., 2020; Yu et al., 2021; Zhou et al., 2020; Liu et al., 2021; Yang et al., 2021a; Yang et al., 2021b). Recently, the development of nanofibrous materials has received increasing attention in tissue engineering and regenerative medicine due to their outstanding properties, such as their favorable biological properties, sufficient mechanical strength, highly porous mesh with interconnectivity, extremely high specific surface area, and aspect ratio (Zhou et al., 2015; Zhou et al., 2017; Kenry and Lim, 2017; Xue et al., 2019; Ahmadi et al., 2021). In addition, nanofibers can mimic the natural extracellular matrix (ECM) structure in the blood vessel and have been widely used as a blood vessel tissue-engineering scaffold (Xu et al., 2004; Devolder et al., 2011). In the recent 2 decades, the electrospinning technique has been widely used to prepare polymeric fibers with diameters typically ranging from tens of nanometers to several micrometers (Zhang et al., 2005; Xue et al., 2019; Daraeinejad and Shabani, 2021; Fetz et al., 2021; Peng et al., 2021). However, the electrospinning of fucoidan (FD) remains a challenge due to its low viscoelasticity and solubility issues. It was reported that other nature polymers [e.g., chitosan (CS), cellulose, sodium alginate, protein] with a small amount of ultra-high molecular weight polymer (UHMWP) [e.g., polyethylene oxide (PEO), polyvinyl alcohol (PVA), polyvinyl pyrrolidone (PVP)] can allow their preparation in nanofibers *via* electrospinning (Zhang et al., 2008; Li et al., 2015). In this sense, the combination of FD and UHMWP could also be considered to address the issue of spinnability.

Vascular endothelial cells (VECs) are the predominant cell type and generate a continuous inner monolayer of blood vessels, which are responsible for regulating inflammation and vascular homeostasis in healthy blood vessels (Coultas et al., 2005). Also, the attachment of monocytes to VECs is vital for the occurrence of atherosclerosis and inflammation (Rajendran et al., 2013; Yang et al., 2019; Li et al., 2021a; Li et al., 2021b; Zong et al., 2021). Herein we hypothesize that FD-based nanofibers would be able to exhibit favorable physicochemical properties to mediate VEC responses in engineering vascular tissues. To test the hypothesis, FD/UHMWPEO nanofibrous films were fabricated using green electrospinning. **Figure 1A** displays the overall strategy to develop CS-modified FD/UHMWPEO nanofibers and their interaction with VECs. H_2O and a small amount of UHMWPEO were selected as the solvent and co-spinning polymer for electrospinning of FD. Then, positively charged CS was selected to interact with negatively charged FD *via* the electrostatic interaction. The chemical structures of FD, UHMWPEO and CS used are shown in **Figure 1B**. The physicochemical features of FD-based nanofibers, i.e., morphology, crystallization, and thermal properties, were systematically tested by different characterization techniques. Further, FD-based nanofibers were seeded with human umbilical VECs (HUVECs) to investigate the effects of material physicochemical properties on cellular attachment and the adhesion of monocytes to HUVECs.

MATERIALS AND METHODS

Materials

Fucoidan (FD, Mw = 276 kDa, sulfate: 29.65%) was provided by Qingdao Bright Moon Seaweed Group Co., Ltd. (Qingdao, China). UHMWPEO (Mv = ~6,000,000 g/mol^{-1}), chitosan (CS, Mv = 300 kDa and deacetylation degree ≥90%), and acetic acid (HAc, purity ≥99.8%) were supplied by Shanghai Macklin Biochemical Co., Ltd. (Shanghai, China). Both the human umbilical vein endothelial cells (HUVECs) and human acute monocytic leukemia cells (THP-1) were bought from the Shanghai Institutes for Biological Sciences (Shanghai, China). Dulbecco's Modified Eagle Medium/Nutrient Mixture F-12, RPMI 1640 media, and fetal bovine serum were supplied by Biological Industries (Israel). FITC phalloidin and DAPI were provided by Solarbio (Beijing, China). Cell Counting Kit-8 was purchased from Absin Bioscience Inc. (China). Carboxyfluorescein diacetate succinimidyl ester was provided by MedChemExpress (Shanghai, China). Other chemical reagents were of analytical grade and used without further purification. Ultrapure water used in all experiments was obtained with a Milli-Q apparatus (Millipore, Bedford, MA, USA).

Preparation of Electrospun FD-Based Nanofibers

The FD aqueous solutions were doped with a small amount of UHMWPEO (i.e., FD/UHMWPEO = 100/0, 98/2, 97/3, 96/4, 95/5, 94/6, 93/7, 92/8, 91/9, and 90/10). The mixed solutions were stirred for ~6 h at room temperature prior to processing to ensure thorough mixing. The solution was loaded into a 20 ml plastic syringe attached with a 25-gauge blunt-ended needle as the spinneret which was charged at a high electric potential of 10–15 kV by a high voltage power supply (Tianjin Dongwen High Voltage Power Supply Plant, China). The solution feeding rate (0.3–1 ml/h) was precisely controlled by a syringe pump (Baoding Longer Precision Pump Co., Ltd., China). The FD-based nanofibers were collected onto an aluminum foil-covered collector placed 15 cm away from the needle tip. Electrospinning processes were performed on a horizontal electrospinning setup at 20–25°C with an ambient humidity of 30–35%.

Modification of FD-Based Nanofibers by CS

FD-based nanofibers prepared from FD/PEO (90/10) were particularly selected for modification with CS. First, 1% CS was dissolved in an aqueous mixed solvent system consisting of 30, 60, and 90 wt% HAc, respectively. The FD-based nanofibers were immersed in the CS/HAc solution for ~60 s. All modified samples were dried for 2–3 days in a vacuum oven (DZF-6050AB, Beijing, China) at 35°C to remove any potential residual solvent.

Characterization

The morphological structure of the prepared nanofibers was observed using a scanning electron microscope (SEM) (VEGA3, TESCAN, Czech) operated at an acceleration voltage of 8–10 kV. Prior to observation, samples were sputter-coated with gold for 120 s to increase the electronic conductivity. The mean diameter of nanofibers was identified by randomly detecting at least 50 fibers from various SEM images for each type of sample using Image J software.

The rheometer (MCR301, Anton Paar, China) equipped with a parallel plate (20 mm) was used to measure the viscous property of FD/PEO aqueous solutions.

A Nicolet iN10 FTIR spectrometer (Thermo Fisher Scientific, Waltham, MA, USA) was used to characterize Fourier transform-infrared (FTIR) spectra of the samples over the range of 500–4,000 cm^{-1} at a scanning resolution of 2 cm^{-1} during 32 scans.

X-ray diffraction (XRD) spectroscopy was performed by DX2700 (Dandong, China) to measure the crystal structures of nanofiber samples. The samples were tested between 10 and 80° (2θ) at a scanning rate of 0.05° (2θ) per min operating with voltage 40 kV and current 30 mA equipped with Cu Kα radiation (λ = 1.5418 Å).

Thermogravimetric analysis on the nanofiber samples was conducted in a thermogravimetric analyzer (NETZSCH, Germany) at a scan range from 0 to 800°C with continuous nitrogen flow.

Differential scanning calorimetry (DSC, TA, USA) was used to measure the thermal properties of the electrospun FD-based nanofibers. A nitrogen atmosphere (flow rate = 50 ml/min) was used throughout. All samples were first quenched to -80°C with liquid nitrogen and then heated at a rate of 10°C/min to 180°C.

Cellular Assays

HUVECs (passage: 3–5) were cultured in Dulbecco's Modified Eagle Medium/Nutrient Mixture F-12 (Biological Industries, Israel) supplemented with 10% fetal bovine serum (Biological Industries, Israel) and 1% Penicillin-Streptomycin Liquid (Biological Industries, Israel) in a humidified incubator of 5% CO_2 at 37°C. THP-1 cells were cultured in RPMI 1640 media (Biological Industries, Israel) supplemented with 10% FBS in a humidified 37°C and 5% CO_2 incubator. THP-1 cells were used in the following experiments.

All substrates (Ø14 mm) were immersed into 75% ethanol for 2 min and then irradiated with UV for 1 h, placed in 24-wells, and washed by PBS. After that, HUVECs were incubated on the substrates in 24-well plates at a density of 3×10^4 cells/well for cell adhesion. All plates were stored in an incubator at 37°C and 5% CO_2 for 24 h. Then, HUVECs were fixated by 4% paraformaldehyde (Solarbio, Beijing, China) for 20 min. Subsequently, the cell membrane was permeabilized with 0.5% Triton X-100 (Sigma) solution for 3 min. Finally, the cells were stained by FITC phalloidin and DAPI for 30 and 10 min, respectively (Solarbio, Beijing, China). The images were captured by Fluorescence Microscopy (Nikon A1 MP, Japan).

TABLE 1 | The solubility of FD in different solvents.

H_2O	DCM	EA	DMSO	TCM	DMF	Diox	CCl_4	CAN	Hex	THF
+	–	–	–	–	–	–	–	–	–	–

DCM, Dichloromethane; EA, Ethyl acetate; DMSO, Dimethyl Sulphoxide; TCM, Trichloromethane; DMF, Dimethyl Formamidine; Diox, Dioxane; CCl_4, Carbon Tetrachloride; CAN, Acetonitrile; Hex, Hexyl hydride; THF, Tetrahydrofuran. "–" means insolubilization; "+" means solubilization.

HUVECs were seeded onto the sterilized substrate (Ø14 mm) in 24-well plates at a density of 5×10^4 cells/well for forming cell monolayers. After 1 day, THP-1 cells (1.5×10^5 cells/well) stained by Carboxyfluorescein diacetate succinimidyl ester (CFSE, MCE, China) were seeded onto HUVEC monolayer, and co-cultured for 4 h. Afterward, each well was washed with PBS three times and counted the number of THP-1 adhered by HUVECs using the Fluorescence Microscopy (Nikon A1 MP, Japan).

Statistical Analysis

All data were expressed as mean ± SD. Statistical analysis was performed using Origin 9.0. All the data were analyzed using one-way analysis of variance (ANOVA) with Tukey's test to determine differences between groups. A value of $p < 0.05$ was considered to be statistically significant.

RESULTS AND DISCUSSION

Solubility of FD in Various Solvents

It was demonstrated that the selection of solvent is critical to determine material solubility, viscoelasticity, electrical conductivity and electrospinnability of the solution, as well as the productivity and morphology of nanofibers (Zhou et al., 2013; Casasola et al., 2014). However, no studies have been performed to find out which solvents FD could dissolve in. In our study, FD was first dispersed into 11 solvents as shown in **Table 1** under magnetic stirring at room temperature. After 12 h, it was found that FD was only dissolved in the water (**Table 1**), which formed a hazel homogeneous solution (data not shown). The maximum solubility of FD in the water at room temperature is 10%. When water was heated to 40°C, FD dissolved faster and the amount of dissolved FD significantly increased. Therefore, in the following experiment water was used as a solvent to prepare FD nanofibers *via* electrospinning. Also, water-based electrospinning, also named "green electrospinning," has several advantages of being environmentally friendly, non-toxic, and non-flammable. It was reported that organic solvents remaining in the fibers had a negative effect on cellular adhesion and proliferation both *in vitro* and *in vivo* (Mooney et al., 1996; Lv et al., 2018). The water-based electrospinning strategy here for preparing FD nanofibers is a safe and versatile route to numerous applications in biology, medicine, and pharmacy.

Preparation of FD-Based Electrospun Nanofibers

To obtain the adequate viscosity of FD solution, the maximum FD concentration (10% w/v) at room temperature was used in the following experiment. However, when 10% w/v FD aqueous solution was used for electrospinning, only droplets were formed as shown in **Figure 2A**, probably because the used FD solution still did not have enough viscosity.

As reported, the electrospinnability of naturally derived polymer solutions can be greatly improved by introducing a small amount of UHMWPEO (Zhang et al., 2008; Li et al., 2015). As shown in **Figure 2B**, with the decrement of the weight ratios of FD/PEO from 100:0 to 98:2, FD/PEO microbeads were fabricated. When the mass ratio of FD/PEO was further decreased from 97:3 to 91:9, the nanofibers with bead-string morphology were generated, the microspheres were elongated, and the average diameter of nanofibers decreased (**Figures 2C–E**). The defect-free nanofibers with an average diameter (560 ± 88 nm) were prepared in the electrospinning of the FD/PEO (90:10) solution (**Figure 2F**). **Figure 2G** showed the variation in viscosity with the weight ratios of FD/PEO solutions. By adding PEO with different ratios relative to FD (FD/PEO = 98/2, 95/5, and 90/10), it was found that the viscosity of solutions was increased from 0.0114 to 0.0879 Pa·s. It was reported that the chain entanglements caused by the increased polymer concentration can play a vital role in fiber formation during electrospinning (Shenoy et al., 2005; Zhou et al., 2013).

Quantification shows that the fiber diameter first decreased and then increased with increasing the amount of PEO (**Figure 2H**). The size of microbeads initially increased with increasing the amount of PEO and then was relatively independent of the amount of PEO. The increased chain entanglements can serve to stabilize the electrospinning jet by inhibiting jet breakup, which elongated beads (Shenoy et al., 2005). These results indicate that the morphology and diameter of electrospun FD/PEO nanofibers greatly depended on the weight ratios of FD/PEO. Also, UHMWPEO as the co-spinning polymer significantly improved the spinnability of FD.

It was well-demonstrated that the diameter of nanofibers can affect the drug release, modulate cell adhesion, migration, proliferation, differentiation, siRNA uptake, and gene silencing, as well as even tissue repair and regeneration (Jaiswal and Brown, 2012; Higgins et al., 2015; Pelipenko et al., 2015; Yau et al., 2015). As depicted in **Figures 3A,B**, the diameter of FD/PEO nanofibers slightly increased and then decreased with increasing the applied voltage and collecting distance. The nanofiber diameter remained unchanged with the increment of feed rate (**Figure 3C**).

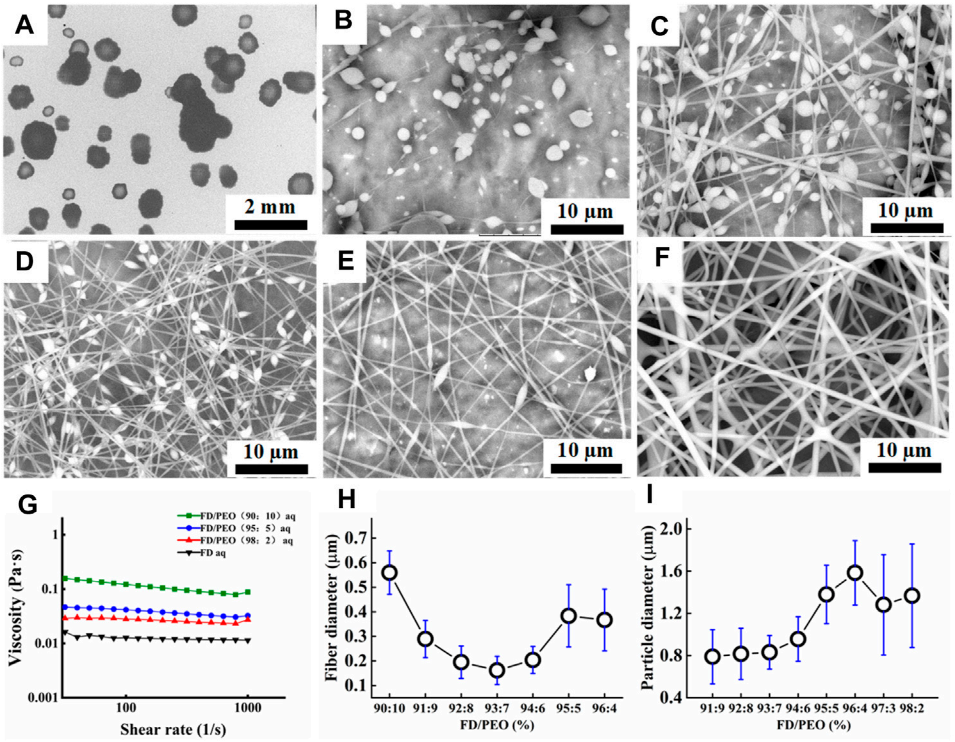

FIGURE 2 | (A–F) SEM images of FD/PEO electrospun nanofibers with different weight ratios of FD/PEO (i.e., 100/0, 98/2, 97/3, 93/7, 91/9, and 90/10). **(G)** The viscosity of FD/PEO solutions with different weight ratios. **(H, I)** Dependence of fiber diameter and microbead size on different weight ratios of FD/PEO, respectively.

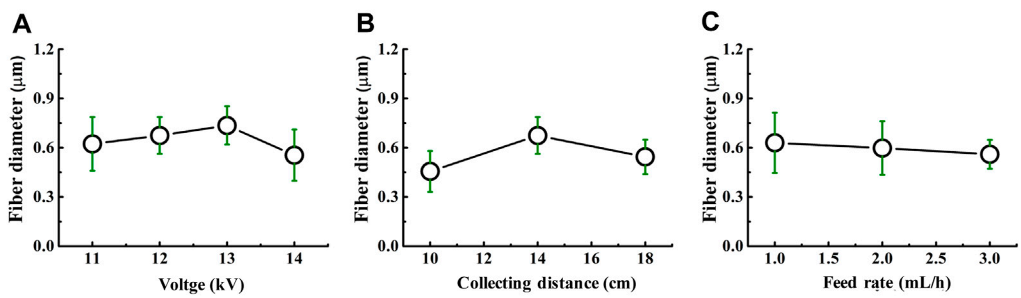

FIGURE 3 | Dependence of the fiber diameter on **(A)** voltage, **(B)** collecting distance, and **(C)** feed rate.

Characterization of the FD-Based Nanofibers

FT-IR spectra were performed to ascertain the molecular interactions in FD/PEO nanofibers (**Figure 4A**). PEO revealed a relatively sharp peak at 2,938 cm^{-1}, which is attributed to—CH_2 stretching (Shariful et al., 2017). And its typical peaks at 1,148 and 1,110 cm^{-1} correspond to C-O-C vibration. In addition, FD showed absorption bands at 3,434 cm^{-1} (O-H stretching), 1,642 cm^{-1} (C=O stretching), 1,232 cm^{-1} (S=O bending), and 833 cm^{-1} (C-O-S bending). The absorption band associated with C-O-C disappeared in FD/PEO nanofibers, probably because C-O-C is a proton acceptor and may form hydrogen bonding with the OH group in FD molecules (Kondo et al., 1994).

Figure 4B displays the XRD patterns of raw materials and the beaded nanofibers (FD/PEO = 95:5), nanofibers (FD/PEO = 90: 10). The PEO powder showed two characteristic diffraction peaks at 19.2 and 23.3°, corresponding to (120) and (112) planes, respectively. Pure FD powder at 23° displayed low overall crystallinity, which suggests that it is a semicrystalline polymer, which is consistent with other reports (Saravana et al., 2016). The XRD patterns of FD-based nanomaterials were similar to that of FD. There were no significant differences between nanomaterials with different ratios. Also, the diffraction peaks of PEO were largely depressed in the nanomaterials probably due to a small amount of added PEO and/or good miscibility between FD and PEO.

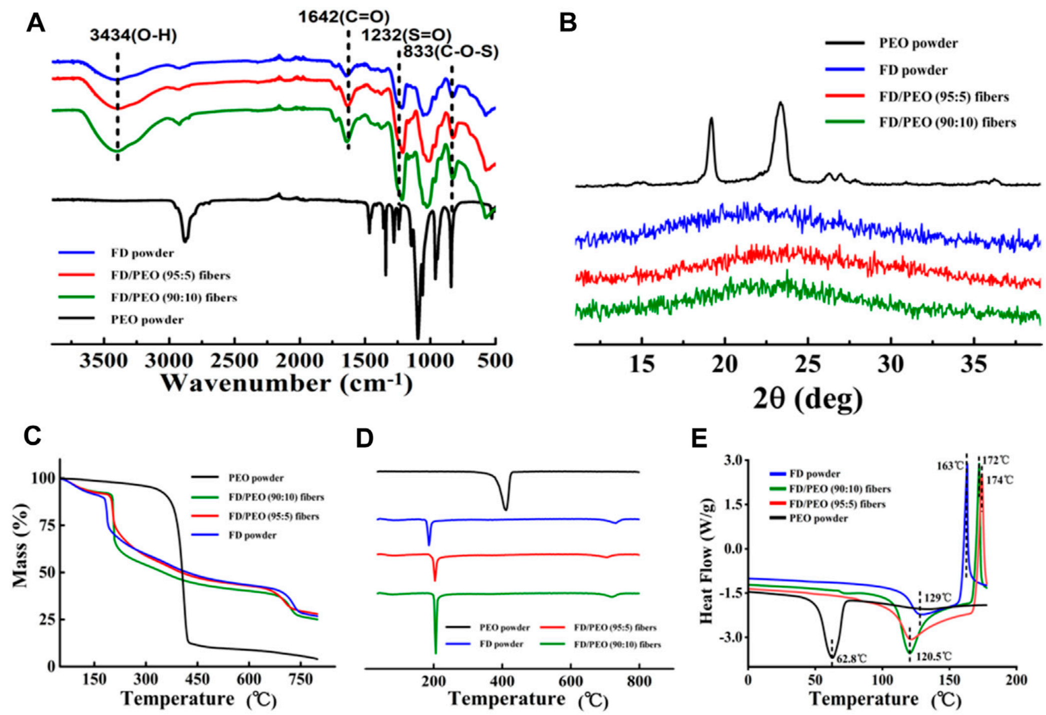

FIGURE 4 | (A) FT-IR spectra, **(B)** XRD diffraction patterns, **(C)** Raw TGA thermograms and **(D)** their first-order derivative curves, and **(E)** DSC curves of FD powder, PEO powder, FD/PEO (95/5) beaded nanofibers, and FD/PEO (90:10) nanofibers.

Raw TGA thermograms and their first-order derivative curves are shown in **Figures 4C,D**. It was found that the pure PEO is found to thermally decompose at 375°C and decomposed completely at 433°C. The FD powder showed a weight loss of approximately 28% between 35 and 200°C and a continuous weight loss until the temperature reaches 800°C. The thermal behavior of FD/PEO nanomaterials displayed a similar trend to that of FD powder. The first stage of weight loss (<100 °C) was due to moisture evaporation. The second stage exhibited a sharp decrease in weight owing to the decomposition of FD. With an increased amount of PEO, the maximum decomposition rate of FD/PEO nanomaterials slightly increased from 186 to 206°C. The reason may be due to a small amount of added PEO in composite nanofibers. Also, the introduction of PEO increased the thermal stability of FD/PEO nanomaterials.

Moreover, DSC analysis of the prepared FD/PEO nanomaterials displayed shifts in glass transition temperature with the incorporation of PEO to FD. No extra transition signals appeared as compared to the DSC curve of FD. Taken together, these results indicate that there was good miscibility or no obvious phase separation between FD and PEO.

FD/PEO Nanofibers Modified by CS

Because PEO and FD have a high solubility in water, the structure of prepared FD/PEO fibrous membranes in the aqueous environment can be destroyed. To maintain the structure of FD/PEO nanofibers in the cell culture medium, it is necessary to modify the nanofiber surface with an H_2O-insoluble polymer. Here, positively charged CS was selected which could interact with negatively charged FD *via* the electrostatic interaction. The FD/PEO nanofibers were soaked in 2 wt% CS solutions with various HAc/H_2O percentages (i.e., 30, 60, and 90%). Representative SEM images of FD/PEO nanofibers before and after modification are shown in **Figure 5**. After the treatment of CS solution in HAc/H_2O = 30 wt%, the integrity of the fiber structure was retained (**Figure 5A**). After the modification of CS solution in HAc/H_2O = 60 and 90 wt%, the fibers swelled largely and the fiber structure was disappeared (**Figures 5B,C**). Next, CS-modified FD/PEO nanofibers were soaked in water for 30 min and their fiber morphology remained. However, the nanofibers had obvious swelling and adhesion (**Figure 5D**). Although chemical crosslinking has been widely used to make natural polymers stable, the crosslinkers used are cytotoxic. Meanwhile, the chemical crosslinking of fucoidan has been not reported. Therefore, positively charged CS was selected which could interact with negatively charged FD *via* the electrostatic interaction.

HUVEC Attachment and Their Interactions With Monocytes

HUVECs were selected because they are the main cell type and play a critical role in the function of the blood vessel (Yang et al., 2017; Kang et al., 2019; Rocha et al., 2020). Cell attachment is regarded as the first and critical response of cells with their surrounding bio-scaffold, which precedes all

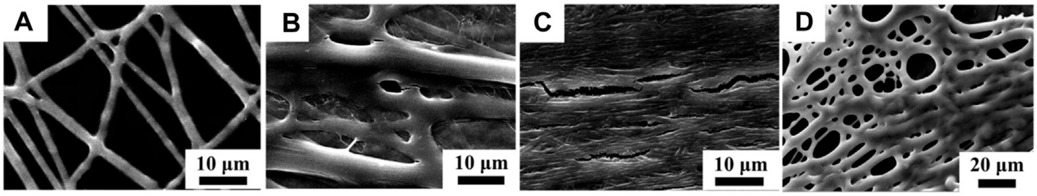

FIGURE 5 | SEM images of CS-modified FD nanofibers with different weight ratios of HAc/H_2O [i.e., **(A)** 30%, **(B)** 60%, and **(C)** 90%]. **(D)** The SEM image of CS-modified FD-based nanofibers in HAc/H_2O = 30% after infiltrating with H_2O.

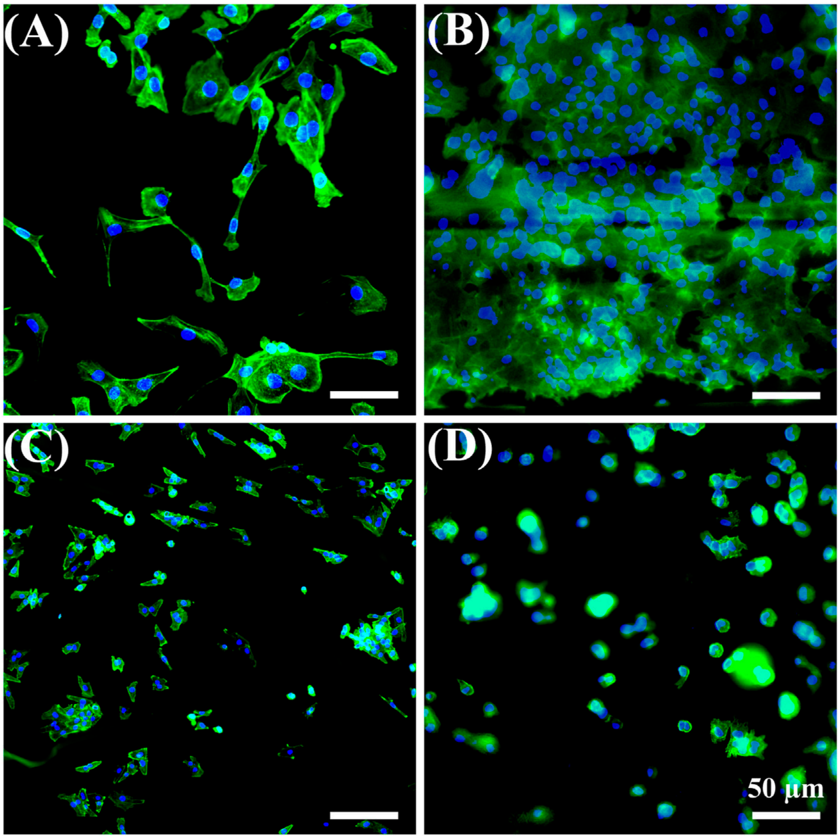

FIGURE 6 | Fluorescent images of HUVECs for 1 day on the **(A)** coverslip control, **(B)** CS-modified FD/UHMWPEO nanofibers, **(C)** CS/UHMWPEO nanofibers, and **(D)** FD/CS/UHMWPEO nonfibrous film. Scale bars = 50 μm.

other cellular events, e.g., survival, viability, function, and differentiation (Zhou et al., 2015; Zhou et al., 2020). As shown in **Figure 6,** HUVEC adhesion in all samples after 1 day of cell culture was studied with a double-label fluorescence staining of the nucleus (blue) and actin cytoskeleton (green). More adhered cells were found on the CS-modified FD/UHMWPEO nanofibers compared to the CS/UHMWPEO nanofibers and FD/CS/UHMWPEO nonfibrous films, indicating that FD and fiber structure could greatly promote cell adhesion. This result suggests that the CS-modified FD/UHMWPEO nanofibers possessed excellent cytocompatibility as a bio-scaffold for blood vessel tissue engineering.

The adhesion and migration of monocytes to endothelial cells is a process of the inflammatory response, which is mediated by specific molecules on endothelial cells and monocytes (Ross, 1999; Bian et al., 2017; Lin et al., 2018; Liu et al., 2020). THP-1 cells were seeded on HUVECs exposed to different materials. As shown in **Figure 7A**, the number of adhered monocytes on HUVECs cultured on the CS-modified FD/UHMWPEO nanofibers was less than those of other groups, indicating that the CS-modified FD/UHMWPEO nanofibers could inhibit the inflammatory response. Quantification shows that there were no significant differences among the samples.

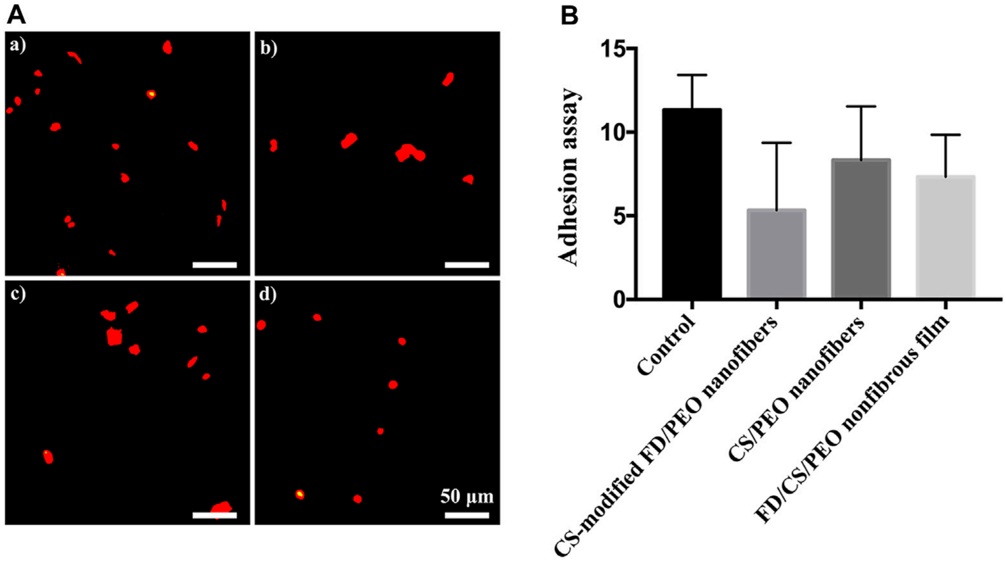

FIGURE 7 | (A) Fluorescent images of THP-1 cells on HUVECs cultured on the (a) the coverslip control, (b) CS-modified FD/UHMWPEO nanofibers, (c) CS/UHMWPEO nanofibers, and (d) FD/CS/UHMWPEO nonfibrous film. Scale bar = 50 μm. **(B)** The number of THP-1 cells on HUVECs cultured on different samples.

CONCLUSION

In summary, chitosan-modified FD/UHMWPEO nanofibers were fabricated using green electrospinning. Water was screened and used as a solvent to dissolve FD. The defect-free nanofibers with an average diameter (560 ± 88 nm) were prepared in the electrospinning of the FD/UHMWPEO (90:10) solution. The addition of UHMWPEO greatly improved the electrospinnability of the solution and thermo-stability of nanofibers. Cellular experiments demonstrated that the chitosan-modified FD/UHMWPEO nanofibers facilitate HUVEC adhesion and suppressed the attachment of monocytes. Thus, the developed FD-based nanofibers display great potential for vascular tissue engineering.

DATA AVAILABILITY STATEMENT

The original contributions presented in the study are included in the article/Supplementary Material, further inquiries can be directed to the corresponding author.

AUTHOR CONTRIBUTIONS

QZ contributed to the conception and design of the study. YC, HZ, YH, ZS, and PS performed the experiment. YC and HZ analyzed the data and performed the statistical analysis. YC and HZ wrote the first draft of the manuscript. QZ revised the manuscript. All authors contributed to manuscript revision, read, and approved the submitted version.

FUNDING

The authors are very grateful for the financial support of the National Natural Science Foundation of China (Grant No. 31900957), Shandong Provincial Natural Science Foundation (Grant No. ZR2019QC007), Innovation and technology program for the excellent youth scholars of higher education of Shandong province (Grant No. 2019KJE015), and China Postdoctoral Science Foundation (Grant No. 2019M652326).

REFERENCES

Ahmadi, A., Ahmadi, P., Sani, M. A., Ehsani, A., and Ghanbarzadeh, B. (2021). Functional Biocompatible Nanocomposite Films Consisting of Selenium and Zinc Oxide Nanoparticles Embedded in Gelatin/cellulose Nanofiber Matrices. *Int. J. Biol. Macromolecules* 175, 87–97. doi:10.1016/j.ijbiomac.2021.01.135

Bian, T., Li, H., Zhou, Q., Ni, C., Zhang, Y., and Yan, F. (2017). Human β-Defensin 3 Reduces TNF-α-Induced Inflammation and Monocyte Adhesion in Human Umbilical Vein Endothelial Cells. *Mediators Inflamm.* 2017, 8529542. doi:10.1155/2017/8529542

Bidarra, S. J., Barrias, C. C., and Granja, P. L. (2014). Injectable Alginate Hydrogels for Cell Delivery in Tissue Engineering. *Acta Biomater.* 10, 1646–1662. doi:10.1016/j.actbio.2013.12.006

Casasola, R., Thomas, N. L., Trybala, A., and Georgiadou, S. (2014). Electrospun Poly Lactic Acid (PLA) Fibres: Effect of Different Solvent Systems on Fibre Morphology and Diameter. *Polymer* 55, 4728–4737. doi:10.1016/j.polymer.2014.06.032

Coultas, L., Chawengsaksophak, K., and Rossant, J. (2005). Endothelial Cells and VEGF in Vascular Development. *Nature* 438, 937–945. doi:10.1038/nature04479

Cui, C., Chen, X., Ma, L., Zhong, Q., Li, Z., Mariappan, A., et al. (2020). Polythiourethane Covalent Adaptable Networks for Strong and Reworkable Adhesives and Fully Recyclable Carbon Fiber-Reinforced Composites. *ACS Appl. Mater. Inter.* 12, 47975–47983. doi:10.1021/acsami.0c14189

Daraeinejad, Z., and Shabani, I. (2021). Enhancing Cellular Infiltration on Fluffy Polyaniline-Based Electrospun Nanofibers. *Front. Bioeng. Biotechnol.* 9, 641371. doi:10.3389/fbioe.2021.641371

Devolder, R. J., Bae, H., Lee, J., and Kong, H. (2011). Directed Blood Vessel Growth Using an Angiogenic Microfiber/microparticle Composite Patch. *Adv. Mater.* 23, 3139–3143. doi:10.1002/adma.201100823

Fernando, I. P. S., Kim, D., Nah, J.-W., and Jeon, Y.-J. (2019). Advances in Functionalizing Fucoidans and Alginates (Bio)polymers by Structural Modifications: A Review. *Chem. Eng. J.* 355, 33–48. doi:10.1016/j.cej.2018.08.115

Fetz, A. E., Wallace, S. E., and Bowlin, G. L. (2021). Electrospun Polydioxanone Loaded with Chloroquine Modulates Template-Induced NET Release and Inflammatory Responses from Human Neutrophils. *Front. Bioeng. Biotechnol.* 9, 268. doi:10.3389/fbioe.2021.652055

Hao, Y., Zhao, W., Zhang, L., Zeng, X., Sun, Z., Zhang, D., et al. (2020). Bio-Multifunctional Alginate/Chitosan/Fucoidan Sponges with Enhanced Angiogenesis and Hair Follicle Regeneration for Promoting Full-Thickness Wound Healing. *Mater. Des.* 193, 108863. doi:10.1016/j.matdes.2020.108863

Higgins, A. M., Banik, B. L., and Brown, J. L. (2015). Geometry Sensing through POR1 Regulates Rac1 Activity Controlling Early Osteoblast Differentiation in Response to Nanofiber Diameter. *Integr. Biol.* 7, 229–236. doi:10.1039/c4ib00225c

Jaiswal, D., and Brown, J. L. (2012). Nanofiber Diameter-Dependent MAPK Activity in Osteoblasts. *J. Biomed. Mater. Res.* 100A, 2921–2928. doi:10.1002/jbm.a.34234

Jana, S., Gandhi, A., and Roy, C. (2020). "Marine Biomaterials-Based Systems," in *Marine Biomaterials-Based Systems*. Editor S-K Kim (John Wiley & Sons Ltd), 1141–1174 . doi:10.1002/9781119143802.ch47

Kang, P. L., Huang, H. H., Chen, T., Ju, K. C., and Kuo, S. M. (2019). Angiogenesis-promoting Effect of LIPUS on hADSCs and HUVECs Cultured on Collagen/hyaluronan Scaffolds. *Mater. Sci. Eng. C* 102, 22–33. doi:10.1016/j.msec.2019.04.045

Kenryand Lim, C. T. (2017). Nanofiber Technology: Current Status and Emerging Developments. *Prog. Polym. Sci.* 70, 1–17. doi:10.1016/j.progpolymsci.2017.03.002

Kondo, T., Sawatari, C., Manley, R. S. J., and Gray, D. G. (1994). Characterization of Hydrogen Bonding in Cellulose-Synthetic Polymer Blend Systems with Regioselectively Substituted Methylcellulose. *Macromolecules* 27, 210–215. doi:10.1021/ma00079a031

Li, B., Lu, F., Wei, X., and Zhao, R. (2008). Fucoidan: Structure and Bioactivity. *Molecules* 13, 1671–1695. doi:10.3390/molecules13081671

Li, Q., Wang, X., Lou, X., Yuan, H., Tu, H., Li, B., et al. (2015). Genipin-crosslinked Electrospun Chitosan Nanofibers: Determination of Crosslinking Conditions and Evaluation of Cytocompatibility. *Carbohydr. Polym.* 130, 166–174. doi:10.1016/j.carbpol.2015.05.039

Li, W., Yan, Z., Ren, J., and Qu, X. (2018). Manipulating Cell Fate: Dynamic Control of Cell Behaviors on Functional Platforms. *Chem. Soc. Rev.* 47, 8639–8684. doi:10.1039/c8cs00053k

Li, D., Yang, Y., Wang, S., He, X., Liu, M., Bai, B., et al. (2021a). Role of Acetylation in Doxorubicin-Induced Cardiotoxicity. *Redox Biol.* 46, 102089. doi:10.1016/j.redox.2021.102089

Li, X., Yang, Y., Wang, Z., Jiang, S., Meng, Y., Song, X., et al. (2021b). Targeting Non-Coding RNAs in Unstable Atherosclerotic Plaques: Mechanism, Regulation, Possibilities, and Limitations. *Int. J. Biol. Sci.* 17, 3413–3427. doi:10.7150/ijbs.62506

Lin, Z., Jin, J., Bai, W., Li, J., and Shan, X. (2018). Netrin-1 Prevents the Attachment of Monocytes to Endothelial Cells via an Anti-inflammatory Effect. *Mol. Immunol.* 103, 166–172. doi:10.1016/j.molimm.2018.08.021

Liu, Y., Deng, W., Yang, L., Fu, X., Wang, Z., van Rijn, P., et al. (2020). Biointerface Topography Mediates the Interplay between Endothelial Cells and Monocytes. *RSC Adv.* 10, 13848–13854. doi:10.1039/d0ra00704h

Liu, L., Han, Z., An, F., Gong, X., Zhao, C., Zheng, W., et al. (2021). Aptamer-Based Biosensors for the Diagnosis of Sepsis. *J. Nanobiotechnology* 19, 1–22. doi:10.1186/s12951-021-00959-5

Lv, D., Zhu, M., Jiang, Z., Jiang, S., Zhang, Q., Xiong, R., et al. (2018). Green Electrospun Nanofibers and Their Application in Air Filtration. *Macromol. Mater. Eng.* 303, 1–18. doi:10.1002/mame.201800336

Mooney, D. J., Baldwin, D. F., Suh, N. P., Vacanti, J. P., and Langer, R. (1996). Novel Approach to Fabricate Porous Sponges of Poly(d,l-Lactic-Co-Glycolic Acid) without the Use of Organic Solvents. *Biomaterials* 17, 1417–1422. doi:10.1016/0142-9612(96)87284-x

Oka, S., Okabe, M., Tsubura, S., Mikami, M., and Imai, A. (2020). Properties of Fucoidans Beneficial to Oral Healthcare. *Odontology* 108, 34–42. doi:10.1007/s10266-019-00437-3

Pelipenko, J., Kocbek, P., and Kristl, J. (2015). Nanofiber Diameter as a Critical Parameter Affecting Skin Cell Response. *Eur. J. Pharm. Sci.* 66, 29–35. doi:10.1016/j.ejps.2014.09.022

Peng, W., Ren, S., Zhang, Y., Fan, R., Zhou, Y., Li, L., et al. (2021). MgO Nanoparticles-Incorporated PCL/Gelatin-Derived Coaxial Electrospinning Nanocellulose Membranes for Periodontal Tissue Regeneration. *Front. Bioeng. Biotechnol.* 9, 216. doi:10.3389/fbioe.2021.668428

Rajendran, P., Rengarajan, T., Thangavel, J., Nishigaki, Y., Sakthisekaran, D., Sethi, G., et al. (2013). The Vascular Endothelium and Human Diseases. *Int. J. Biol. Sci.* 9, 1057–1069. doi:10.7150/ijbs.7502

Rocha, L. A., Gomes, E. D., Afonso, J. L., Granja, S., Baltazar, F., Silva, N. A., et al. (2020). *In Vitro* evaluation of ASCs and HUVECs Co-cultures in 3D Biodegradable Hydrogels on Neurite Outgrowth and Vascular Organization. *Front. Cel Dev. Biol.* 8, 489. doi:10.3389/fcell.2020.00489

Ross, R. (1999). Atherosclerosis - An Inflammatory Disease. *N. Engl. J. Med.* 340, 115–126. doi:10.1056/nejm199901143400207

Saravana, P. S., Cho, Y.-J., Park, Y.-B., Woo, H.-C., and Chun, B.-S. (2016). Structural, Antioxidant, and Emulsifying Activities of Fucoidan from Saccharina Japonica Using Pressurized Liquid Extraction. *Carbohydr. Polym.* 153, 518–525. doi:10.1016/j.carbpol.2016.08.014

Senthilkumar, K., Ramajayam, G., Venkatesan, J., Kim, S.-K., and Ahn, B.-C. (2017). "Biomedical Applications of Fucoidan, Seaweed Polysaccharides," in *Seaweed Polysaccharides*. Editors J Venkatesan, S Anil, and S.-K Kim (Elsevier), 269–281. doi:10.1016/b978-0-12-809816-5.00014-1

Shariful, M. I., Sharif, S. B., Lee, J. J. L., Habiba, U., Ang, B. C., and Amalina, M. A. (2017). Adsorption of Divalent Heavy Metal Ion by Mesoporous-High Surface Area Chitosan/poly (Ethylene Oxide) Nanofibrous Membrane. *Carbohydr. Polym.* 157, 57–64. doi:10.1016/j.carbpol.2016.09.063

Shenoy, S. L., Bates, W. D., Frisch, H. L., and Wnek, G. E. (2005). Role of Chain Entanglements on Fiber Formation during Electrospinning of Polymer Solutions: Good Solvent, Non-specific Polymer-Polymer Interaction Limit. *Polymer* 46, 3372–3384. doi:10.1016/j.polymer.2005.03.011

Xu, C., Inai, R., Kotaki, M., and Ramakrishna, S. (2004). Aligned Biodegradable Nanofibrous Structure: A Potential Scaffold for Blood Vessel Engineering. *Biomaterials* 25, 877–886. doi:10.1016/s0142-9612(03)00593-3

Xue, J., Wu, T., Dai, Y., and Xia, Y. (2019). Electrospinning and Electrospun Nanofibers: Methods, Materials, and Applications. *Chem. Rev.* 119, 5298–5415. doi:10.1021/acs.chemrev.8b00593

Yang, J., Hao, X., Li, Q., Akpanyung, M., Nejjari, A., Neve, A. L., et al. (2017). CAGW Peptide- and PEG-Modified Gene Carrier for Selective Gene Delivery and Promotion of Angiogenesis in HUVECs *In Vivo*. *ACS Appl. Mater. Inter.* 9, 4485–4497. doi:10.1021/acsami.6b14769

Yang, L., Han, D., Zhan, Q., Li, X., Shan, P., Hu, Y., et al. (2019). Blood TfR+ Exosomes Separated by a pH-Responsive Method Deliver Chemotherapeutics for Tumor Therapy. *Theranostics* 9, 7680–7696. doi:10.7150/thno.37220

Yang, L., Pijuan-Galito, S., Rho, H. S., Vasilevich, A. S., Eren, A. D., Ge, L., et al. (2021a). High-Throughput Methods in the Discovery and Study of Biomaterials and Materiobiology. *Chem. Rev.* 121, 4561–4677. doi:10.1021/acs.chemrev.0c00752

Yang, Y., Zhao, X., Yu, J., Chen, X., Wang, R., Zhang, M., et al. (2021b). Bioactive Skin-Mimicking Hydrogel Band-Aids for Diabetic Wound Healing and Infectious Skin Incision Treatment. *Bioactive Mater.* 6, 3962–3975. doi:10.1016/j.bioactmat.2021.04.007

Yao, Y., Zaw, A. M., Anderson, D. E. J., Hinds, M. T., and Yim, E. K. F. (2020). Fucoidan Functionalization on Poly(vinyl Alcohol) Hydrogels for Improved Endothelialization and Hemocompatibility. *Biomaterials* 249, 120011–120024. doi:10.1016/j.biomaterials.2020.120011

Yau, W. W. Y., Long, H., Gauthier, N. C., Chan, J. K. Y., and Chew, S. Y. (2015). The Effects of Nanofiber Diameter and Orientation on siRNA Uptake and Gene Silencing. *Biomaterials* 37, 94–106. doi:10.1016/j.biomaterials.2014.10.003

Yin, X., Hao, Y., Lu, Y., Zhang, D., Zhao, Y., Mei, L., et al. (2021). Bio-Multifunctional Hydrogel Patches for Repairing Full-Thickness Abdominal Wall Defect. *Adv. Funct. Mater.*, 2105614. doi:10.1002/adfm.202105614

Yu, Z., Li, Q., Wang, J., Yu, Y., Wang, Y., Zhou, Q., et al. (2020). Reactive Oxygen Species-Related Nanoparticle Toxicity in the Biomedical Field. *Nanoscale Res. Lett.* 15, 115. doi:10.1186/s11671-020-03344-7

Yu, J., Xu, K., Chen, X., Zhao, X., Yang, Y., Chu, D., et al. (2021). Highly Stretchable, Tough, Resilient, and Antifatigue Hydrogels Based on Multiple Hydrogen

Bonding Interactions Formed by Phenylalanine Derivatives. *Biomacromolecules* 22, 1297–1304. doi:10.1021/acs.biomac.0c01788

Zhang, Y., Lim, C. T., Ramakrishna, S., and Huang, Z.-M. (2005). Recent Development of Polymer Nanofibers for Biomedical and Biotechnological Applications. *J. Mater. Sci. Mater. Med.* 16, 933–946. doi:10.1007/s10856-005-4428-x

Zhang, Y., Venugopal, J. R., El-Turki, A., Ramakrishna, S., Su, B., and Lim, C. T. (2008). Electrospun Biomimetic Nanocomposite Nanofibers of Hydroxyapatite/chitosan for Bone Tissue Engineering. *Biomaterials* 29 (32), 4314–4322. doi:10.1016/j.biomaterials.2008.07.038

Zheng, W., Hao, Y., Wang, D., Huang, H., Guo, F., Sun, Z., et al. (2021). Preparation of Triamcinolone Acetonide-Loaded Chitosan/fucoidan Hydrogel and its Potential Application as an Oral Mucosa Patch. *Carbohydr. Polym.* 272, 118493. doi:10.1016/j.carbpol.2021.118493

Zhou, Q., Bao, M., Yuan, H., Zhao, S., Dong, W., and Zhang, Y. (2013). Implication of Stable Jet Length in Electrospinning for Collecting Well-Aligned Ultrafine PLLA Fibers. *Polymer* 54, 6867–6876. doi:10.1016/j.polymer.2013.10.042

Zhou, Q., Xie, J., Bao, M., Yuan, H., Ye, Z., Lou, X., et al. (2015). Engineering Aligned Electrospun PLLA Microfibers with Nano-Porous Surface Nanotopography for Modulating the Responses of Vascular Smooth Muscle Cells. *J. Mater. Chem. B* 3, 4439–4450. doi:10.1039/c5tb00051c

Zhou, Q., Zhang, H., Zhou, Y., Yu, Z., Yuan, H., Feng, B., et al. (2017). Alkali-Mediated Miscibility of Gelatin/Polycaprolactone for Electrospinning Homogeneous Composite Nanofibers for Tissue Scaffolding. *Macromol. Biosci.* 17, 1–10. doi:10.1002/mabi.201700268

Zhou, Q., Chen, J., Luan, Y., Vainikka, P. A., Thallmair, S., Marrink, S. J., et al. (2020). Unidirectional Rotating Molecular Motors Dynamically Interact with Adsorbed Proteins to Direct the Fate of Mesenchymal Stem Cells. *Sci. Adv.* 6, eaay2756. doi:10.1126/sciadv.aay2756

Zong, T., Yang, Y., Lin, X., Jiang, S., Zhao, H., Liu, M., et al. (2021). 5′-tiRNA-Cys-GCA Regulates VSMC Proliferation and Phenotypic Transition by Targeting STAT4 in Aortic Dissection. *Mol. Ther. Acids*. doi:10.1016/j.omtn.2021.07.013

Conflict of Interest: ZS and PS are employed by Qingdao Bright Moon Seaweed Group Co., Ltd.

The remaining authors declare that the research was conducted in the absence of any commercial or financial relationships that could be construed as a potential conflict of interest.

Liu et al. J Nanobiotechnol (2021) 19:216
https://doi.org/10.1186/s12951-021-00959-5

Journal of Nanobiotechnology

REVIEW

Open Access

Aptamer-based biosensors for the diagnosis of sepsis

Lubin Liu[1,2†], Zeyu Han[1,2†], Fei An[1,2], Xuening Gong[1,2], Chenguang Zhao[1,2], Weiping Zheng[1,2], Li Mei[2] and Qihui Zhou[1,2*]

Abstract

Sepsis, the syndrome of infection complicated by acute organ dysfunction, is a serious and growing global problem, which not only leads to enormous economic losses but also becomes one of the leading causes of mortality in the intensive care unit. The detection of sepsis-related pathogens and biomarkers in the early stage plays a critical role in selecting appropriate antibiotics or other drugs, thereby preventing the emergence of dangerous phases and saving human lives. There are numerous demerits in conventional detection strategies, such as high cost, low efficiency, as well as lacking of sensitivity and selectivity. Recently, the aptamer-based biosensor is an emerging strategy for reasonable sepsis diagnosis because of its accessibility, rapidity, and stability. In this review, we first introduce the screening of suitable aptamer. Further, recent advances of aptamer-based biosensors in the detection of bacteria and biomarkers for the diagnosis of sepsis are summarized. Finally, the review proposes a brief forecast of challenges and future directions with highly promising aptamer-based biosensors.

Keywords: Aptamer-based biosensors, Nanomaterials, Diagnosis, Sepsis

Introduction

Sepsis, the syndrome of multiple organ dysfunction caused by immune disorders, is one of the most critical global issues in medicine due to the unacceptably high mortality rate [1–3]. Sepsis is an inflammatory disease mediated by the activation of the innate immune system which was induced by bacterial invasion either directly or indirectly [4, 5]. In particular, the most popular gram-positive isolates are *Staphylococcus aureus* (*S. aureus*) and *Streptococcus pneumoniae*. Meanwhile, *Escherichia coli* (*E. coli*), *Klebsiella*, and *Pseudomonas aeruginosa* dominate among gram-negative isolates [6, 7]. An epidemic international study of infection and sepsis containing more than 14,000 patients in 1265 participating intensive care units (ICUs) from 75 countries showed that 62% of the positive isolates were gram-negative organisms, 47% were gram-positive, and 19% were fungi [8]. The massive invasion of bacteria makes immunocytes activate and release kinds of cytokines. Some pathogenic components, such as lipopolysaccharide (LPS), can interact with the toll-like receptors (TLRs) of monocytes to activate transcription factor NF-kB which can promote the release of pro-inflammatory cytokines, such as tumor necrosis factor α (TNF-α) and interleukin 6 (IL-6) [9]. C-reactive protein (CRP), an acute-phase protein released by macrophages, remains the most frequently used biomarker for both infection and inflammation diagnosis in clinical practice [10].

According to a primary extrapolation of data from high-income countries, there are 19.4 million cases of severe sepsis annually around the world among 31.5 million cases of sepsis, with potentially 5.3 million death each year [11]. Although overall mortality decreases due to preventive measures, a more rapidly increasingly

*Correspondence: qihuizhou@qdu.edu.cn
†Lubin Liu and Zeyu Han contributed equally to this work
[1] Institute for Translational Medicine, Department of Stomatology, The Affiliated Hospital of Qingdao University, Qingdao University, Qingdao 266003, China
Full list of author information is available at the end of the article

overall incidence rate of sepsis is revealed, demonstrating a continuing challenge [5]. However, the initial symptoms of sepsis are atypical and nonspecific, which is a clinical syndrome defined by a series of signs, symptoms, laboratory abnormalities, and characteristic pathophysiological derangements, resulting in a delayed diagnosis [5]. As research reported in *Critical Care Medicine*, over one-third of septic patients with atypical symptoms of infection are more likely to have a higher possibility to delay antibiotic administration and a higher risk of mortality [12]. The potential survival rate of sepsis falls dramatically up to 7.6% per hour without effective antibiotic treatment [13]. It is necessary to achieve the early diagnosis of sepsis to prevent the development of the disease. Sequential Sepsis-related Organ Failure Assessment (SOFA) score and bedside clinical score termed qSOFA (for quick SOFA) are recommended for early identification of sepsis [14]. Clinically, it is necessary to determine the species of pathogenic bacteria in time for the diagnosis of sepsis but conventional methods, such as blood cultures and molecular techniques, require multi-steps, resulting in time-consuming and demanding. They display low sensitivity which delays extremely the treatment of sepsis. The polymerase chain reaction (PCR), based on the detection of bacterial DNA, has the potential to reduce the diagnosis time to hours, but it still fails to detect the low-level blood infection [15–17]. Additionally, these methods are laboratory-based, and trained personnel for operation are needed a lot. In addition, blood biomarkers provide a valuable auxiliary role in the clinical status assessment of sepsis as the markers reflecting the severity of organism after infection and inflammation. Therefore, a rapid and sensitive method to diagnose sepsis in early stages is required urgently to ensure the rapid administration of appropriate antibiotics and prevent the occurrence of severe disease conditions, thereby saving human lives.

Recently, the occurrence of aptamer-based sensors has attracted considerable attention for the diagnosis of sepsis owing to the dramatic efficiency for targets and the accuracy for detection [18]. Nucleic acid aptamers, identified by an *in-vitro* selection procedure called Systematic Evolution of Ligands by EXponential enrichment (SELEX), are single-stranded oligonucleotides (DNA or RNA) molecules that can bind to targets with high specificity and affinity [19, 20]. The aptamer is becoming increasingly popular nowadays because of the stability, easy accessibility, affordable prices, and minimal immune response compared with antibodies. Interestingly, a drug based on modified RNA aptamer, called Macugen (pegaptanib), has been approved by the Food and Drug Administration (FDA) for the treatment of age-related macular degeneration, showing the first successful commercial commodity [21]. Aptamers composed of nucleic acids can be modified easily by fluorescent dyes to achieve the detection visually [22]. In addition, aptamers are also used in homogenous assays which do not need to separate or wash because they bind to the target directly in a sequence-specific manner [23–25]. Recently, nucleic acid aptamers have been used widely as affinity receptors in combination with various signal transduction strategies based on nanomaterials in different kinds of biosensing platforms, including colorimetry, chemiluminometry, electrochemistry, fluorometry, and fluorescence anisotropy [26–31]. The aptamer-based biosensors have high detection sensitivity because aptamer can easily integrate with the signal amplification strategies, such as rolling circle amplification, CRISPR technology, PCR technology, LAMP technology, and magnetic separation technology. Xu et al. reported a dramatic increase in the sensitivity of bacteria detection through the combination of dual-functional aptamer and CRISPR-Cas12a assisted RCA [32]. Furthermore, the specificity of biosensing platforms comes from aptamer which can interact with the target by the unique structure transformation property of nucleic acid. The stability of aptamers has been improved significantly through the post-selection modification of aptamers and the direct selection of aptamers from libraries bearing modified backbones or nucleobases to ensure the stable functions of aptamer-based sensors [21, 33]. In addition, their inherent physicochemical characteristics of nanomaterials, including ultra-small size, high reactivity, and tunable surface modification, have enabled them to overcome some of the limitations and achieve the expected diagnostic and therapeutic effect [34–42]. The biosensors consist of (nano)biointerface and aptamer have been explored widely to detect bacteria and biomarkers, such as gold nanoparticles (NPs), graphene oxide, and carbon nanotubes, which play an indispensable role in improving the sensitivity and shortening the time in the detection for the target [22, 29, 30, 43]. The VOSviewer bibliometric visualization software was used to analyze co-occurrences on aptamer and (nano)biointerface (Fig. 1).

In this review, the selection method of the nucleic acid aptamer is introduced briefly in the first. Also, recent advances of aptamer-based biosensors (Fig. 2) in the detection of bacteria and biomarkers (Table 1) for the diagnosis of sepsis are summarized. Finally, we summarize the mechanism and notable advantages or disadvantages of aptamer-based sensors in sepsis diagnosis (Table 2).

The SELEX of aptamer

Nowadays, the selection of aptamers is on the basis of systematic evolution of ligands by SELEX which is a gold-standard strategy that can select specific and sensitive

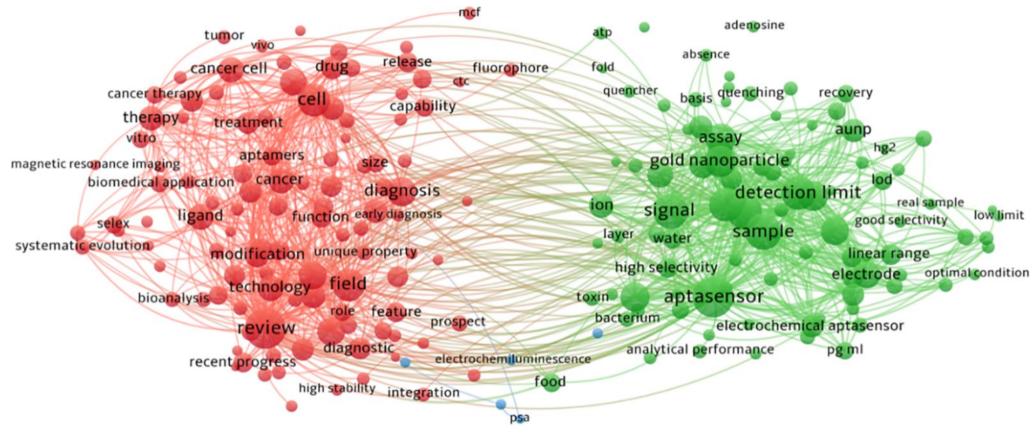

Fig. 1 The analysis of keyword co-occurrences on aptamer and (nano)biointerface

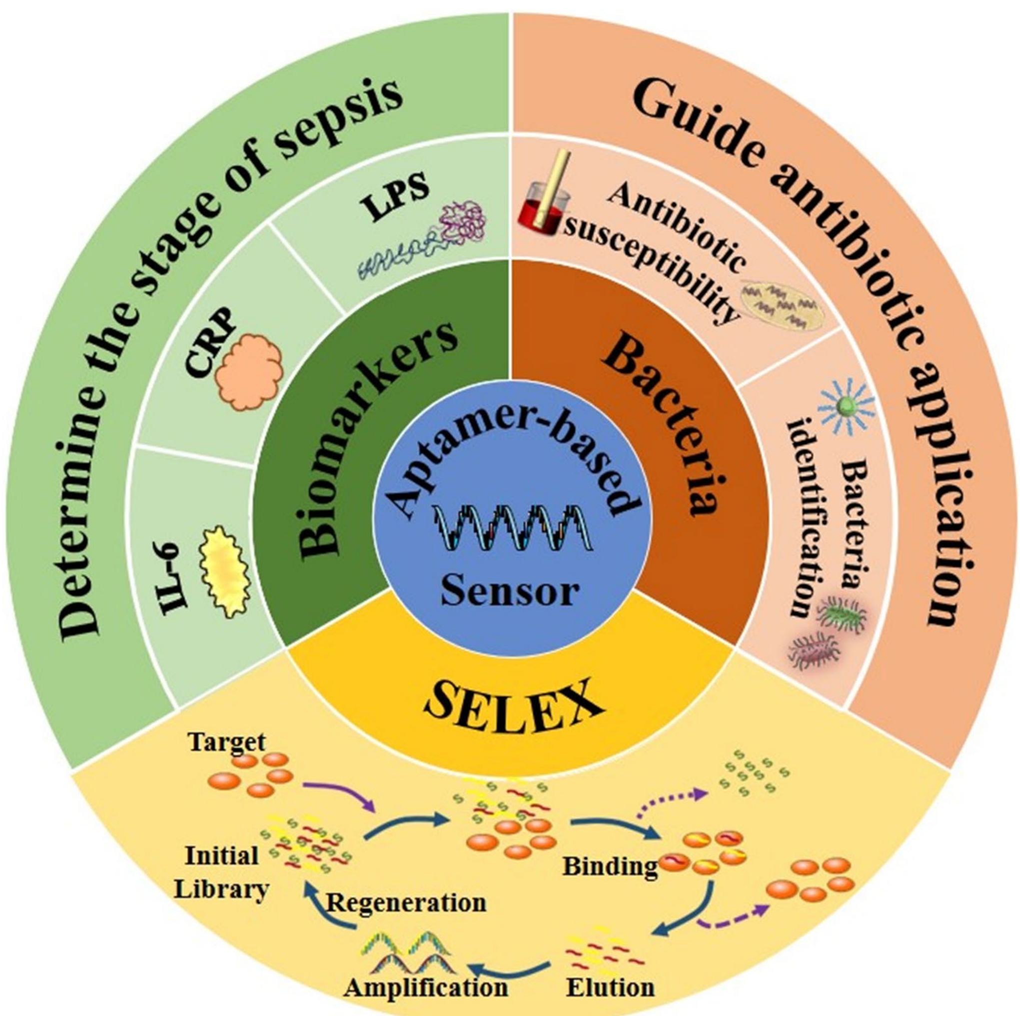

Fig. 2 Aptamer-based biosensors in the detection of bacteria and biomarkers for the diagnosis of sepsis

Table 1 Summary of aptamer-based detection of sepsis-related pathogens and biomarkers

Targets	Aptamer sequences	Nanomaterials	Sensor type/method	Type of aptamer	Length (nt)[a)]	Limit of detection (LOD)	References
S. aureus	I: 5′-TCC CTA CGG CGC TAA CCC CCC CAG TCC GTC CTC CCA GCC TCA CAC CGC CAC CGT GCT ACA AC-3′ II: 5′-TCC CTA CGG CGC TAA CCT CCC AAC CGC TCC ACC CTG CCT CCG CCT CGC CAC CGT GCT ACA AC-3′	AuNPs	Aptamer-conjugated GNPs and a resonance light-scattering detection system	DNA	40	–	[44]
	I: 5′-TCC CTA CGG CGC TAA CCC CCC CAG TCC GTC CTC CCA GCC TCA CAC CGC CAC CGT GCT ACA ACT TTT TTT TT-3′ II: 5′-TCC CTA CGG CGC TAA CCC CCC CAG TCC GTC CTC CCA GCC TCA CAC CGC CAC CGT GCT ACA ACT TTT TTT T-3′	Fe_3O_4@mTiO_2	Capture platform based on Fe_3O_4@mTiO_2 modified with target aptamer	DNA	71	10–2000 CFU/mL	[45]
	apt: 5′-GCA ATG GTA CGG TAC TTC CTC GGC ACG TTC TCA GTA GCG CTC GCT GGT CAT CCC ACA GCT ACG TCA AAA GTG CAC GCT ACT TTG CTA A-3′	–	Vertical capacitance apta-sensors	DNA	88	10^0 CFU/mL Biofilm: 20% of the area	[46]
	apt: 5′-GCA ATG GTA CGG TAC TTC CTC GGC ACG TTC TCA GTA GCG CTC GCT GGT CAT CCC ACA GCT ACG TCA AAA GTG CAC GCT ACT TTG CTA A-3′	–	Electrical antimicrobial suscepti-bility test (e-AST) system	DNA	88	–	[47]
MASA	–	Streptavidin Mag-netic Beads	CRISPR-Cas12a assisted RCA	–	–	10^2–10^6 CFU/mL	[32]
E. coli	apt: 5′-ATC CGT CAC ACC TGC TCT ACT GGC CGG CTC AGC ATG ACT AAG AAG GAA GTT ATG TGG TGT TGG CTC CCG TAT TTT TTT TTT-3′	Fe_3O_4@mTiO_2	–	DNA	81		[45]
	apt: 5′-GCA ATG GTA CGG TAC TTC CCC ATG AGT GTT GTG AAA TGT TGG GAC ACT AGG TGG CAT AGA GCC GCA AAA GTG CAC GCT ACT TTG CTA A-3′	–	Vertical capacitance ap-tasensors	DNA	88	10^0 CFU/mL Biofilm: 20% of the area	[46]

Table 1 (continued)

Targets	Aptamer sequences	Nanomaterials	Sensor type/method	Type of aptamer	Length (nt)[a)]	Limit of detection (LOD)	References
	apt: 5′-GCA ATG GTA CGG TAC TTC CCC ATG AGT GTT GTG AAA TGT TGG GAC ACT AGG TGG CAT AGA GCC GCA AAA GTG CAC GCT ACT TTG CTA A-3′	–	Electrical antimicrobial susceptibility test (e-AST) system	DNA	88	–	[47]
Peptidoglycan	I: 5′-TCG CGC GAG TCG TCT GGG GAC AGG GAG TGC GCT GCT CCC CCC GCA TCG TCC TCC C-3′ II: 5′-TCG CGC GAG TCG TCT GGG GGA CTA GAG GAC TTG TGC GGC CCC GCA TCG TCC TCC C-3′	–	–	DNA	I/II: 55	–	[48]
OMVs	I: 5′-ATA CCA GCT TAT TCA ATT GGG TGA GGG GGG GTT CAC AAC GTT AAA GAT AGA CGG GGG AAG ATA GTA AGT GCA ATC T-3′ II: 5′-ATA CCA GCT TAT TCA ATT CCG AGT CCA GAC TCA CCG CCG CCT CCT CAA GAC GTG CTG GAG ATA GTA AGT GCA ATC T-3′	–	Enzyme-linked aptamer assay	DNA	I/II: 76	*E. coli* DH5α: 0.13 ± 0.01 μg/mL *E. coli* K12: 3.70 ± 0.98 μg/mL *S.marcescens*: 0.23 ± 0.16 μg/m	[49]
P.aeruginosa	apt: 5′-CCC CCG TTG CTT TCG CTT TTC CTT TCG CTT TTG TTC GTT TCG TCC CTG CTT CCT TTC TTG-3′	–	Vertical capacitance aptasensors	DNA	60	10^0 CFU/mL Biofilm: 20% of the area	[46]
	apt: 5′-CCC CCG TTG CTT TCG CTT TTC CTT TCG CTT TTG TTC GTT TCG TCC CTG CTT CCT TTC TTG-3′	–	Electrical antimicrobial susceptibility test (e-AST) system	DNA	60	–	[47]
K.pneumoniae	apt: 5′-GCA ATG GTA CGG TAC TTC C(N45)-CAA AAG TGC ACG CTA CTT TGC TAA-3′	–	Electrical antimicrobial susceptibility test (e-AST) system	DNA	44	–	[47]
E. faecalis	apt: 5′-ATC CAG AGT GAC GCA GCA CGA CAC GTT AGG TTG GTT AGG TTG GTT AGT TTC TTG TGG ACA CGG TGG CTT A-3′	–	Electrical antimicrobial susceptibility test (e-AST) system	DNA	70	–	[47]
LPS	apt: 5′-CTT CTG CCC GCC TCC TTC C-(45 N)-GGA GAC GAG ATA GGC GGA CAC T-3′	Gold disk electrodes	Electrochemical	DNA	86	0.01–1 ng/mL	[50]
		Gra AuNPs	Electrochemical			8.7 fg/mL 10–50 fg/mL	[51]

Table 1 (continued)

Targets	Aptamer sequences	Nanomaterials	Sensor type/method	Type of aptamer	Length (nt)[a)]	Limit of detection (LOD)	References
		Gold atomic cluster	Electrochemical			7.94×10^{-21} M and 0.01aM–1 pM	[52]
		RGO/AuNPs	Electrochemical			1 fg/mL	[53]
		RGO/AuNPs	Electrochemical			0.2 fg/mLand 0.001–0.01 pg/mL	[54]
		MoS_2 AuNPs RGO	Voltammetric biosensor			3.01×10^{-5} ng/mL and 5.0×10^{-5} ng/mL to 2.0×10^{-2} ng/mL	[55]
		–	Optical sensor			5.5 pg/mL– 100 ng/mL	[56]
		SLG	Acoustic wave biosensor			3.53 ng/mL 0–100 ng/mL	[57]
		GO	Fluorescence quenching efficiency			15.7 ng/mL and 25–1600 ng/mL	[58]
		RGO	Fluorescence quenching efficiency Continuous Injection-Electrostacking			8.3 fM	[59]
IL-6	Model number: ATW0082 ATW0077	AuNPs	Optical approach	–	–	1.95 μg/mL	[60]
	apt: 5′-GTC TCT GTG TGC GCC AGA GAC ACT GGG GCA GAT ATG GGC CAG CAC AGA ATG AGG CCC-3′	AuNPs	Electrochemical	–	–	1.6 pg/ml	[61]
	Model number: ATW0077	Carbon nanotube	Microfluidic-based approach	–	–	1 pg/mL–10 ng/mL	[62]
	apt: 5′- GGT GGC AGG AGG ACT ATT TAT TTG CTT TTC T -3′	GR	Field-Effect Transistor-Based Approach	–	–	139 fM	[63]
	–	GR	Field-Effect Transistor-Based Approach	–	–	618 fM	[64]
CRP	apt: 5′-GGC AGG AAG ACA AAC ACG ATG GGG GGG TAT GAT TTG ATG TGG TTG TTG CAT GAT CGT GGT CTG TGG TGC TGT-3′	–	Optical fiber sensor	DNA	72	2–20 mg/mL	[65]
	apt: 5′-GCC UGU AAG GUG GUC GGU GUG GCG AGU GUG UUA GGA GAG AUU GC-3′	–	Luminex xMAP technology	RNA	44	0.4 mg/L	[66]
	apt: 5′-CGA AGG GGA TTC GAG GGG TGA TTG CGT GCT CCA TTT GGT G- 3′	AuNPs	Optical nanosensor	DNA	40	1.77 pM	[67]

Table 2 The mechanism and notable advantages or disadvantages of aptamer-based biosensors

Sensor Type/Method	Mechanism of Action	Comments	References
Aptamer-conjugated GNPs and a resonance light-scattering detection system	Aptamers are combined onto GNPs followed by bead-based amplification, one bacterial cell was capable of generating more than 10^4 GNPs after amplification, and amplified GNPs could be detected by the light-scattering–sensing system	Very short detection time. The detection of a single cell can be reached within 1.5 h without complicated equipment such as thermal cyclers or centrifuges	[44]
CRISPR-Cas12a assisted RCA	The specificity based on the dual functionalized aptamers can initiate bioconjugation to specifically recognize the protein targets and can also convert the protein recognition to nucleic acid signals	Accurate identification and high-sensitive detection of MRSA. Dual amplification of the nucleic acid signal	[32]
Capture platform based on Fe_3O_4@ $mTiO_2$ modified with target aptamer	First, the complex was incubated with blood samples and the aptamer would connect with the target bacteria. After that, the bacteria captured by Apt-Fe_3O_4@$mTiO_2$ NPs were concentrated with the help of the magnetic field	High bacterial-captured efficiency of about 80%, short detection time within 2 h, and little cross-react with the nontarget components in blood	[45]
Fe_3O_4-Ce6-Apt nanosystem	Simultaneous blood bacterial species identification and enrichment can be achieved in a single step, and then, enriched bacteria can be detected with fluorescence microscopic determination	Identify and enrich the bacteria in the sepsis blood sample for 1 h. Blood disinfection	[68]
Enzyme-linked aptamer assay	Construct ELAA	High sensitivity to bacterial OMVs as low as 25 ng/mL. A new possibility for the development of cell-free bacterial sensors using bacterial OMVs instead of living bacterial cells	[49]
Vertical capacitance aptasensors	Some bacteria, culture in blood culture media comprising blood (0.2 mL) and culture media (0.8 mL), the biofilm formation and bacterial growth could be detected by measuring capacitance changes at f = 0.5 and 10 kHz, respectively. After treated with antibiotics, the sensitivity of bacteria to antibiotics can be judged by this change	Short AST time within 12 h	[46]
e-AST system	The e-AST system is composed of 60 aptamer-functionalized capacitance sensors, of which 2 sensors were used for the negative control, 3 sensors for positive control, and other 55 sensors for the determination of antibiotic sensitivity to 11 antibiotics at 5 different concentrations	Short AST time within 6 h	[47]
Voltammetric biosensor	After using aptamers immobilized by RGO, and MoS_2 is also applied as the matrix of the biosensor with the application of RGO and AuNPs	Simplified operation sequence with fast response and high recovery rate. PEI-rGO-MoS_2 nanocomposite with a larger specific surface area, thermal stability and electrical conductivity increases the sensitivity of the sensor	[55]
Acoustic wave biosensor	The SLG film first connects with CS, and then the amino groups in the CS react with the aldehyde in GA to form C = N bonds. After that, the aldehydes groups in GA react with the amine-functionalized aptamer, which is ready for the specific detection of endotoxin	Rapid, simple operations and low costs. Excellent stability from the air phase to the liquid phase	[57]
Microfluidic-based approach	Real-time response of the sensor conductance is monitored with increasing concentration of IL-6, exposure to the sensing surface in buffer solution, and clinically relevant spiked blood samples	Sensitive detection of IL-6 at low concentrations	[62]
Luminex xMAP technology	xMAP assays typically employ a sandwich-type format using antibodies for the capture. For this assay, an RNA aptamer that binds CRP is conjugated to beads to act as the capture agent	The number and type of analytes by using aptamers alone or in conjunction with antibodies expand and the use of sample volumes is low	[66]
Optical sensor	The signal output mode is an optical image, small changes can be converted into optical signals for output	Compatibility to a wide range of surface modifications. The detection limit of the sensor slightly changed with increased use. Some cross-reactivity towards the unspiked human serum	[56, 60, 65, 67]

Table 2 (continued)

Sensor Type/Method	Mechanism of Action	Comments	References
Fluorescence quenching efficiency	The concentration of LPS can be quantitatively analyzed by observing fluorescence changes	Little consumption of sample. Low recovery of serum sample	[58, 59]
Field-Effect Transistor-Based Approach	The graphene surface immobilized aptamer is unfolded without IL-6 and it would fold after binding with the target. These aptamer structural changes bring the negative charges in IL-6 to the proximity of the graphene-liquid interface	Low-voltage operation (< 1 V), inherent gain amplification, biocompatibility and miniaturization	[63, 64]
Electrochemical	Electrochemical sensors are constructed using various nanomaterials	Gold disk electrodes: Short detection time and little cross-interaction reactivity to plasmid DNA, RNA, proteins, saccharides, and/or lipids which are most likely to coexist with LPS assay Gra AuNPs: Overcome the disadvantage of limited nicking endonuclease recognition and integrate molecular biological technology and nano-biotechnology with electrochemical detection to cascade signal amplification, which can detect target LPS down to the femtogram level Gold atomic cluster: Simple sensor fabrication compared with other electrochemical sensors for LPS RGO/AuNPs: Short LPS detection time within 35 min. Enhanced electrode performance and low LOD down to femtomolar level AuNPs: Label-free detection, simple experimental protocol, high selectivity and low limit of detection	[50–54, 61]

aptamers from random single-stranded nucleic acid sequence library [69]. In 1990, Ellington and Szostak successfully screened out oligonucleotides and named the "aptamer", which is the first time to get aptamer from RNA library through this method [19, 20]. Briefly, there are three steps included in the selection cycle for DNA [70]. First of all, targets are incubated with the library containing randomized sequences, obtaining a complex of target and sequences. Secondly, nonspecific aptamers and the targets are separated respectively, and bound sequences are preserved. Finally, the proper sequences will be amplified through PCR. The selection cycle is then repeated until the sequence of the desired affinity is enriched. In every selection round, more affiliative aptamers are selected (Fig. 3). There are tiny differences of the SELEX for RNA aptamers that RNA should reverse transcription into DNA first and homologous DNA is transcribed into RNA after the selection.

However, there are some demerits in the traditional methods, such as time-consuming and huge costs [71]. Nowadays, some new methods based on traditional SELEX have been developed to overcome shortcomings, like cell SELEX, magnetic bead-based SELEX, in vivo SELEX, in Silico SELEX and so on, which aims to save time, use expediently and raise efficiency [69, 70, 72].

Aptamer-based detection of pathogenic bacteria

Sepsis, a serious infection syndrome that can cause tissue damage and multisystem organ failure, is usually due to the presence of pathogenic bacteria in the bloodstream, resulting in high mortality in the world [73]. Importantly, sepsis has a high mortality rate due to the inability to quickly identify pathogens in the early stages of infection. Conventionally, blood culture, called the "gold standard", is mostly used for bacteria detection in clinical, hence time-consuming, costly, and trained personnel for the operation needed in great demand.

Therefore, the rapid, accurate, and easy detection of bacteria is required urgently for the early diagnosis and therapy of sepsis. Aptamer-based sensors have a great potential to solve this problem because of sensitivity, specificity, and rapidity. Here, we discuss some articles about the detection of sepsis-related bacteria through aptamer-based sensors.

Aptamer-based detection of a single type of pathogenic bacteria

This section pays attention to sensors designed for detecting pathogenic whole cells that can be targeted by aptamers. The first example of aptamer-based sensors that will be introduced was created to detect *S. aureus*, a common pathogen of sepsis [44, 74]. First of all, SA17 and SA61, two DNA aptamers that showing high specificity and nanomolar affinity with *S. aureus*, were modified on magnetic beads and gold nanoparticles (GNPs) separately. After that, quantitative PCR (qPCR) was used to quantify the number of aptamers or aptamer-conjugated GNPs linked with single *S. aureus* cells. To improve the sensitivity of detection to *S. aureus*, aptamers were attached with NPs followed by amplification based on magnetic beads (Fig. 4). Using this ingenious way, a single *S. aureus* cell could be detected within 1.5 h without expensive equipment.

In another study, Xu et al. realized the detection for *Methicillin-Resistant Staphylococcus aureus* (MRSA) using dual-functional aptamer and CRISPR-Cas12a assisted RCA[32]. Different from the recognition of the whole cell, the aptamer recognizes MRSA depending on the penicillin-binding proteins2a (PBP2a), which shows a low affinity for β-lactam antibiotics. The biosensing

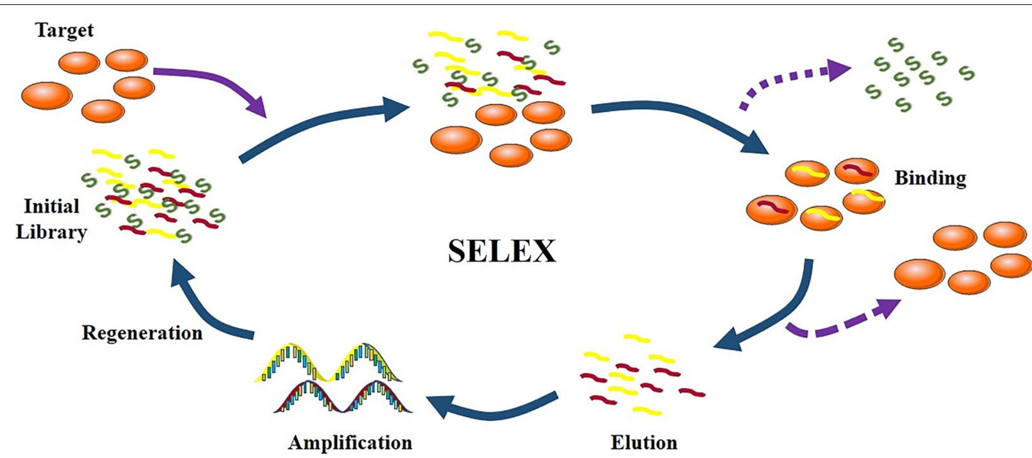

Fig. 3 The process of SELEX

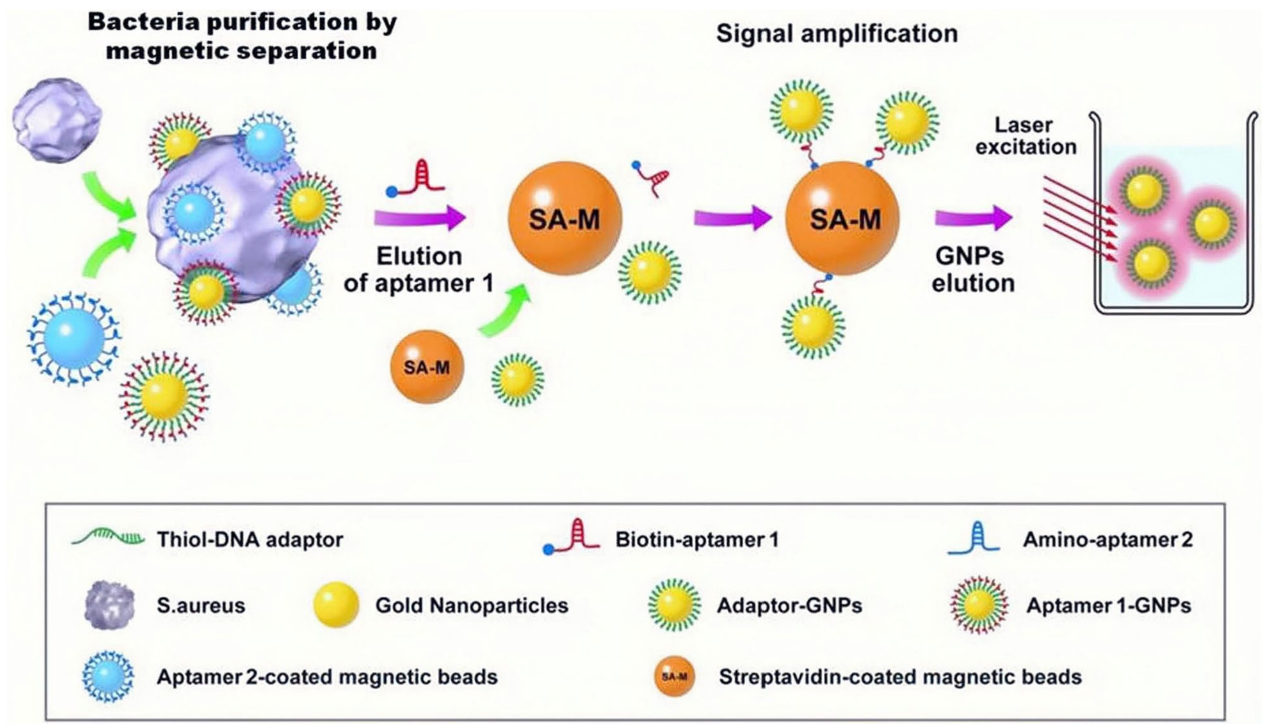

Fig. 4 Bead-based amplification in the detection of unbound *S. aureus* using aptamer-conjugated GNPs [44]

process could be divided into two steps: bacteria isolation based on the protein A aptamer (Apt A) and signal amplification. Protein A is a membrane protein shared by both MRSA and *S. aureus*. In the first step, Streptavidin Magnetic Beads (SMBs) were mixed with Apt A to get the capture complex (SMBs-Apt A), and the protein A positive bacteria could be enriched by the SMBs-Apt A complex via the aptamer-protein interaction for the next step. The second aptamer (Apt B) was made of PBP2a specific aptamer and a Blocker. The Blocker was released from Apt B to touch off the following RCA when the Apt B connected with PBP2a on the surface of MRSA. Via the integration of attached RCA and CRISPR-Cas12a assisted trans-cleavage, dual amplification of the nucleic acid signal was obtained. Furthermore, the output above was consistent with the traditional colony count in the four groups of serum samples, which proved the feasibility of this method for clinical sample detection.

There are some studies that specific target aptamers and magnetic NPs were used together to identify and collect pathogenic bacteria in blood samples with low bacterial concentrations and achieved the rapid qualitative or quantitative detection of bacteria. Shen et al. created a capture platform that consisted of a mesoporous TiO_2 coated magnetic NP and modified with target aptamer (Apt-Fe_3O_4@mTiO_2) to reduce the time of detection [45]. First, the complex was incubated with blood samples and the aptamer would connect with target bacteria by folding into the sequence-defined unique structure when it was exposed to bacteria. After that, the bacteria captured by Apt-Fe_3O_4@mTiO_2 NPs were concentrated with the help of the magnetic field to recognize pathogenic bacteria (Fig. 5A). Compared with the control group, the number of *S. aureus* decreased markedly in the supernatant after captured by a bar magnet within 2 min (Fig. 5B). Meanwhile, the Apt-Fe_3O_4@mTiO_2 nanosensor had a higher efficiency (2 h) than conventional blood culture (8 h) to capture bacteria when 10^4 CFU/mL bacteria were spiked into blood (Fig. 5C). To verify the reliability of the capture platform at low bacterial concentrations, two representative bacteria, *S. aureus* and *E. coli*, were used as model bacteria and the results showed that bacterial capture was up to 80% (10–2000 CFU/mL) (Fig. 5D). In addition to bacterial capture for diagnosis, Wang et al. accomplished efficient extracorporeal blood disinfection taking advantage of magnetic NPs functionalized with chlorin e6 molecules and bacterial species-identifiable aptamers (Fe_3O_4-Ce6-Apt) (Fig. 5E) [68]. Fe_3O_4-Ce6-Apt nanosystem could identify and enrich the bacteria through incubated with sepsis blood sample for 1 h and the enriched bacteria were imaged by fluorescence microscopy to quantitatively evaluate the number (Fig. 5F). After near-infrared (NIR) laser irradiation for 5 min (660 nm, 0.8 W/cm^2), the agar plate showed a few bacteria (Fig. 5G). Through the conditions of the mice, the treatment for sepsis therapy based on blood disinfection by Fe_3O_4-Ce6-Apt was evaluated preliminarily (Fig. 5H). Although this aptamer-based sensor has shown advantages in the detection and therapy of sepsis, there is still much unknown about long-term safety in the human body.

Aptamer-based detection of several types of pathogenic bacteria

In clinical practice, sepsis is commonly caused by the infection of a variety of bacteria, therefore, some scholars have constructed aptamers aiming at common components of bacteria, such as peptidoglycan and membrane vesicles [48, 49]. Compared with detecting one type of bacteria, these kinds of aptamers can simultaneously detect the existence of multiple types of sepsis-related bacteria, enabling patients to be diagnosed in an early and timely manner, guiding the use of antibiotics and reducing the mortality rate of patients.

Peptidoglycan is a kind of cell wall polymer shared by both gram-positive and gram-negative bacteria, which plays a critical role in the survival of bacteria and is closely related to the pathogenicity of bacteria [75, 76]. Ana et al. developed adapters that could recognize bacterial peptidoglycans, called Antibac1 (AT1) and Antibac2 (AT2), and found that both AT1 and AT2 have a high affinity for *E. coli* and *S. aureus* [77]. In subsequent work, they went on to explore the ability of AT1 and AT2 to bind to causative agents of bacterial-borne sepsis [48]. The results showed that these aptamers bound with high efficiency to the main agents of bacterial sepsis, including four gram-positive and seven gram-negative bacterial, and the affinity of AT1 and AT2 to bacteria was assessed by real-time quantitative PCR. This work demonstrated that ssDNA aptamers targeting bacterial peptidoglycan can recognize multiple types of septic pathogens and can be used to develop universal biosensor probes, which is of great significance for the rapid and sensitive detection of sepsis in clinical practice.

Gram-negative bacteria are the main pathogenic bacteria leading to clinical sepsis. Their outer membrane produces and secretes outer membrane vesicles (OMVs) that can carry several virulence biomolecules and endotoxins [78]. OMVs are known to be important pathogenic agents that improve bacterial survival and trigger immune responses in host cells [79]. Therefore, Shin et al. developed a kind of broadly cross-reactive aptamers for the OMVs from gram-negative bacteria and built an Enzyme-linked aptamer assay (ELAA) (Fig. 6) [49]. The results showed that ELAA successfully detected OMVs from a variety of gram-negative bacteria, which provides a new possibility for the development of cell-free bacterial sensors using bacterial OMVs instead of living bacterial cells. Detection of live bacteria in the blood is difficult due to the immunomodulatory nature of host cells and the bactericidal activity of serum, suggesting that detecting bacterial OMVs in clinical blood samples may be more effective than detecting bacterial cells.

Real-time monitoring of bacterial growth and AST

It is well-known that the survival rate of sepsis falls by an average of 7.6% for every hour of delay ineffective antibiotic treatment [13]. Patients' survival could be highly improved if they received timely and effective antibiotic treatment, but antimicrobial susceptibility test (AST) results usually require more than three days with conventional methods [80–82]. In addition to the quantitative and qualitative detection of bacteria, the aptamer sensor can monitor the real-time growth of bacteria and biofilm, which continuously and timely evaluate the internal infections and the effectiveness of antibiotics [46, 47]. For instance, Song et al. developed a vertical capacitance aptamer-functionalized sensor (Fig. 7) that significantly shorten the AST time to within 12 h [46]. They found that when bacteria, including *E. coli, S. aureus,* and *Pseudomonas aeruginosa*, were cultured in blood culture media comprising blood (0.2 mL) and culture media (0.8 mL), the biofilm formation and bacterial growth could be detected by measuring capacitance changes at f = 0.5 and 10 kHz, respectively. After treated with antibiotics, the sensitivity of bacteria to antibiotics could be judged by this change. This study demonstrated that an aptamer-functionalized sensor could be used as an alternative tool for detecting bacteria and rapid AST in positive blood culture without the need for sub-culturing.

(See figure on next page.)

Fig. 5 The Apt-Fe_3O_4@mTiO_2 nanosensor (**A**–**D**). **A** Conceptual strategies to enrich and identify pathogenic bacteria in human blood. Top: conventional blood culture. Down: the aptamer-based capture platform. **B** Photographs and agar plates showing the bacteria capture with and without a bar magnet. **C** Schematic representation of detection time for enriching and identifying pathogen in human blood samples based on that aptamer-based capture platform (left) and conventional blood culture (right). **D** Bacteria counted numbers enriched by Apt-Fe_3O_4@mTiO_2 nanosensor at a low concentration range (10–2000 CFU/mL) [45]. The Fe_3O_4-Ce6-Apt nanosystem (**E–H**). **E** Schematic illustration of strategies for early sepsis diagnosis and extracorporeal blood disinfection based on Fe_3O_4-Ce6-Apt nanosystem. **F** Illustration of the process of Fe_3O_4-Ce6-Apt nanosystem-based strategy for the bacterial enrichment and identification within 1.5 h. **G** Agar plate photographs for live bacterial units. The blood samples containing *S. aureus* (10^6 CFU) were incubated with Fe_3O_4-Ce6-Apt nanosystem before and after NIR laser irradiation for 5 min. **H** Photographs of the mice transfused with the blood samples containing *S. aureus* (10^6 CFU) with and without disinfection treatment at different times [68]

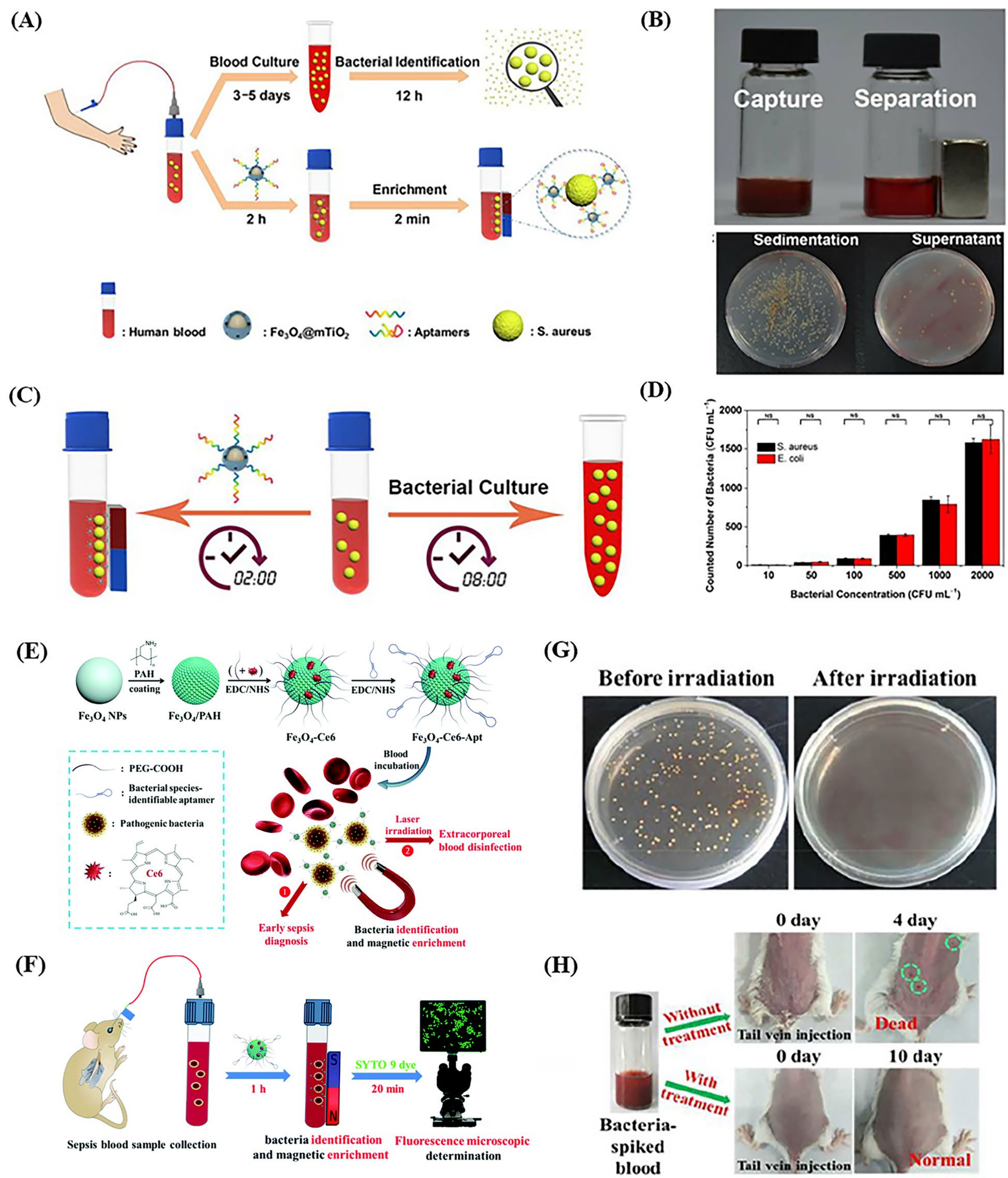

Fig. 5 (See legend on previous page.)

Furthermore, Lee et al. developed an electrical AST (e-AST) system, which shortens the AST time to only 6 h [47]. The e-AST system was composed of 60 aptamer-functionalized capacitance sensors, of which 2 sensors were used for the negative control, 3 sensors for positive control, and other 55 sensors for the determination of antibiotic sensitivity to 11 antibiotics at 5 different concentrations. To evaluate the performance of the e-AST

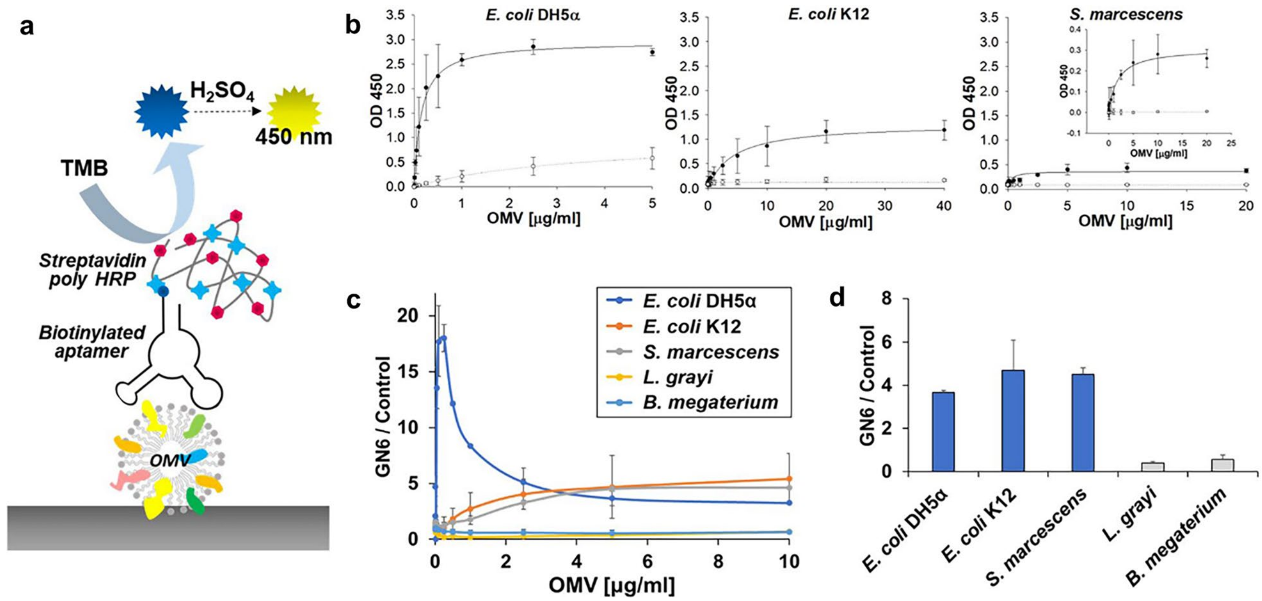

Fig. 6 The scheme of GN6 ELAA and the specificity of GN6 to some OMVs [49]

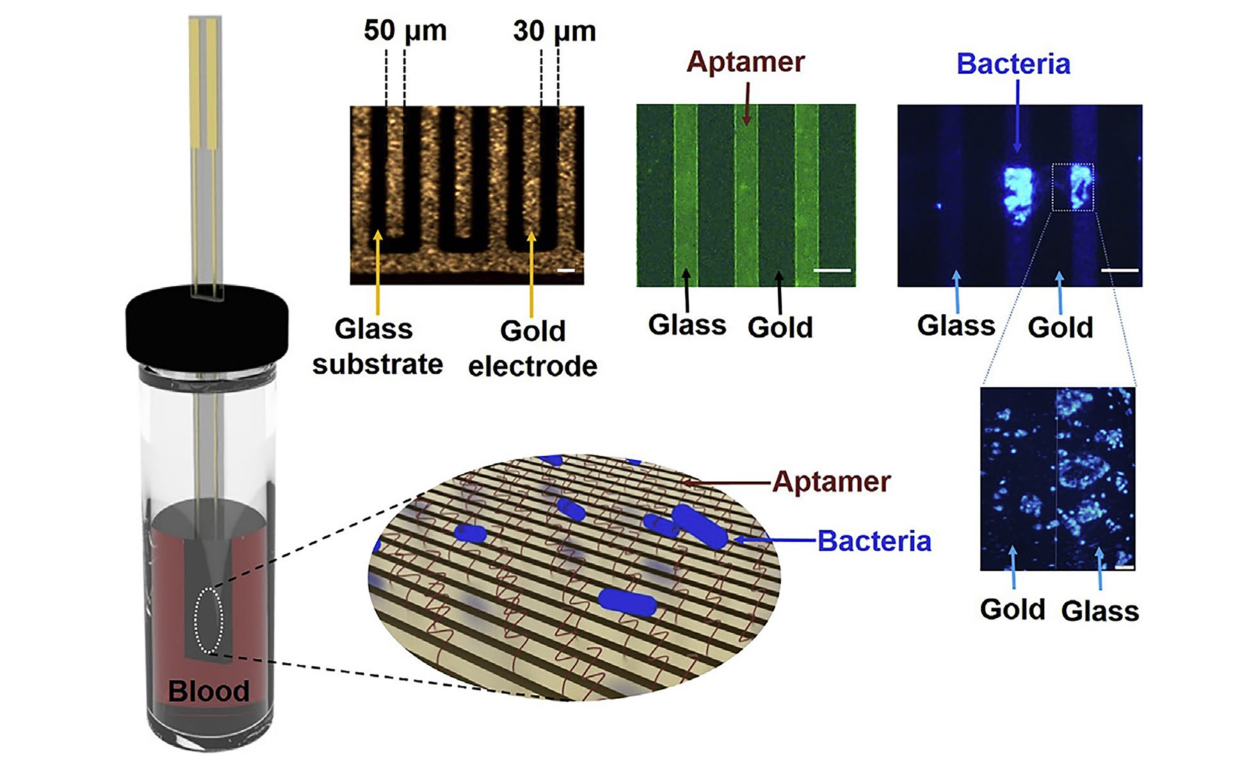

Fig. 7 Scheme of vertical capacitance aptamer-functionalized sensor [46]

system, 4,554 tests were conducted on 30 clinical strains isolated from septic patients. The results showed an estimated 97% classification agreement between the e-AST system and the gold standard broth microdilution (BMD) test, indicating its great potential for clinical application. Although the diagnosis of sepsis with e-AST may be more expensive, it is significant to save patients suffering from sepsis.

Aptamer-based detection of sepsis-related biomarkers

In addition to the successful detection of pathogenic bacteria in the early period of sepsis, it is necessary to monitor the biomarkers timely which are helpful to judge the occurrence and stage of sepsis and observe systematic conditions [83]. Biomarkers, especially from the blood, make significant changes of content when inflammatory responses occur in the early time with the happening of two molecular patterns [84]. Changes in their levels indicate a state of inflammatory response in the body that cannot be provided by the methods of diagnosing pathogens. However, it is still a challenge to find an accurate and quantitative way to detect biomarkers in the human blood. Compared with frequently-used methods of detecting biomarkers like mass spectrometry (MS) and antibody-based technologies, aptamer-based sensors have shown a huge potential in recent years because of their superiorities like low costs, wide detection ranges, low immunogenicity, and sufficient sensitivity [85–87]. Several biomarkers are associated with the occurrence and development of sepsis, such as LPS, IL-6, and CRP [88]. In the following sub-section, some aptamer-based sensors for detecting sepsis-related serum biomarkers are discussed.

LPS

LPS, called endotoxins, are the major glycolipid molecule in the cell walls of gram-negative bacteria which is the main difference between gram-negative and gram-positive bacteria [89]. Many investigations have highlighted the impact of LPS in the development of sepsis and LPS interacts with the special cellular receptors such as Toll-like receptor-4/MD2 and CD14 to produce inflammatory cytokines [90]. The release of LPS can cause a series of cascading inflammatory pathological reactions, which lead to the occurrence of sepsis. Therefore, LPS is considered an important biomarker for the diagnosis of sepsis.

Over the last few decades, the detection methods of LPS have been continuously developed. Previous methods, such as the rabbit pyrogen test (RPT) [91], the Limulus amoebocyte lysate (LAL) [92], the monocyte activation test (MAT) [93], the recombinant factor C (rFC) [94], and the EndoLISA [95], cannot be routinely used to analyze clinical sepsis samples because of their disadvantages of temperature dependence, high cost, inconsistent, and long testing time. However, studies have shown that the LPS test methods based on aptamers were used for the early diagnosis of sepsis in the past few years, which have the advantages of sensitivity, specificity, high affinity, low cost, and time-saving.

To capture LPS, electrodes have been modified by graphene oxide (GO) and GNPs to detect LPS. Kim et al. used a method based on the nonequilibrium capillary electrophoresis of equilibrium mixtures to identify LPS [50]. It did not include the systematic evolution of ligands by exponential enrichment (NECEEM-based non-SELEX) method. This method constructed an electrochemical aptamer sensor on a gold electrode with a high-affinity LPS binder B2. The linear detection range of the electrochemical aptamer sensor for LPS was from 0.01 to 1 ng/mL. Compared with the traditional strategy of diagnosing sepsis, the time of this method was significantly shorter, however, the extensive application of this aptamer sensor was limited by its low sensitivity. To improve their sensitivity, signal amplification strategies should be considered. Bai et al. designed a new type of aptamer-based electrochemical platform through the combination of two typical signal amplification strategies to achieve the ultra-sensitive detection of LPS [51]. Firstly, the three-way DNA junction-aided enzymatic recycling could increase the electrical signal by increasing the number of capture probes. Besides, the GO nanocomposite material further enhanced the electrochemical signal. The sensitivity of this method was down to femtogram level (8.7 fg/mL), with a linear range of 6 orders of magnitude (from 10 fg/mL to 50 ng/mL). This method obtained better sensitivity compared with the previous study, but the complex manufacturing process of the aptamer sensor would limit its clinical application. Interestingly, Posha and co-workers reported an ultrasensitive electrochemical biosensor that does not require additional signal amplification strategies [52]. Gold clusters were used as electrodes because of their excellent merits, such as fast electron transfer and good water solubility, and then the strong affinity of 5' end amino groups of the aptamer was fixed on the surface of the gold electrode. An electrochemical biosensor could be produced to monitor the concentration of LPS by using the allowed or blocked electron transfer in the surface-assembled molecule. Aptamers immobilized by gold atomic cluster were mediated in this biosensor. The lower detection limit of this sensor was 7.94×10^{-21} M, which was at the attomolar level. And the linear range was from 0.01 aM to 1 pM, which was with a linear response of 9 orders of magnitude (Fig. 8). Therefore, this aptamer biosensor had higher sensitivity, simple structure and preparation process, and had a broad application prospect in the detection of LPS in sepsis.

Besides, in the last few years, RGO and AuNPs have been used to immobilize aptamers. Compared with GO, RGO has higher electrical conductivity, better ductility,

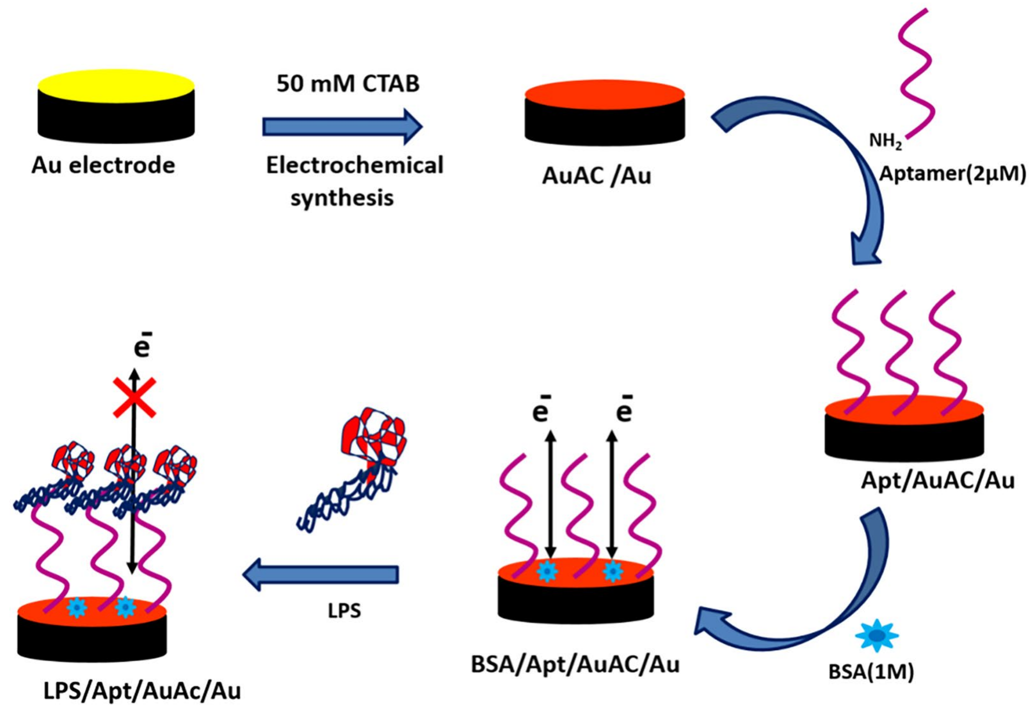

Fig. 8 Schematic diagram of the preparation and working principle of Apt/AuAC/Au sensor [52]

thermal stability, and has received more attention in the biological analysis [96]. For example, Pourmadadi et al. modified aptamers on the surface of a glassy carbon electrode (GCE) via RGO and AuNPs, which were successfully used in the analysis of serum of patients and normal people [53]. In another case, the research by Yazdian et al. used RGO-Au NPs to modify electrodes to immobilize thiolated aptamer that specifically binds to endotoxin [54]. After using aptamers immobilized by RGO, the nanomaterial with better performance enabled the aptamer sensor to possess higher sensitivity in LPS detection. The detection lower limit and dynamic range of the sensor were 0.2 fg/mL and 0.001–0.01 pg/mL, respectively. Further, molybdenum disulfide (MoS2) was also applied as the matrix of the biosensor with the application of RGO and AuNPs (Fig. 9) [55]. The high electrical conductivity and large specific surface area of the new nanocarrier can greatly amplify the electrochemical signal and enhance the sensitivity of the aptamer sensor. It was linear in the range of 5.0×10^{-5} to 2.0×10^{-2} ng/mL, and the lower LOD was 3.01×10^{-5} ng/mL. In addition, the method had a good recovery rate for serum samples and a broad application prospect in the field of trace analysis of LPS in sepsis diagnosis. The label-free aptamer sensor in this study could simplify the operation sequence and had a fast response speed. Some studies by An et al. and Ji et al. also used label-free aptamer sensors to detect LPS [56, 57].

Also, there were some studies using aptamers labeled with 6-carboxyfluorescein (6-FAM) to detect LPS. For instance, Zhang et al. designed a 6-FAM labeled aptamer as a fluorescent probe to detect LPS, by combining the advantages of the aptamer's specific binding ability and the fluorescence quenching effect of GO [58]. However, the linear range of this probe for LPS was 25–1600 ng/mL and the lower LOD was 15.7 ng/mL. Therefore, the detection sensitivity was low, and the study did not mention whether this method could be effectively applied in clinical practice. There was a significant improvement in Niu et al. [59]. Based on the fluorescence quenching effect in the study, they designed a microfluidic chip based on the continuous injection-electrostacking to couple RGO and FAM-aptamer so that the aptamer could be combined with LPS to achieve the purpose of detection. The detection limit of this method was 8.3 fM (8.3×10^{-4} Eu/mL) and the sensitivity is higher. This aptamer-based biosensor can detect LPS in injections and serum of human and sepsis model mice, and can quickly distinguish between gram-negative bacteria from gram-positive bacteria and fungus (Fig. 10). Taken together, this method is simple, sensitive and specific, and has a good correlation with the gold-standard LAL assay. As a practical application, it can be used for the detection of sepsis in the clinic.

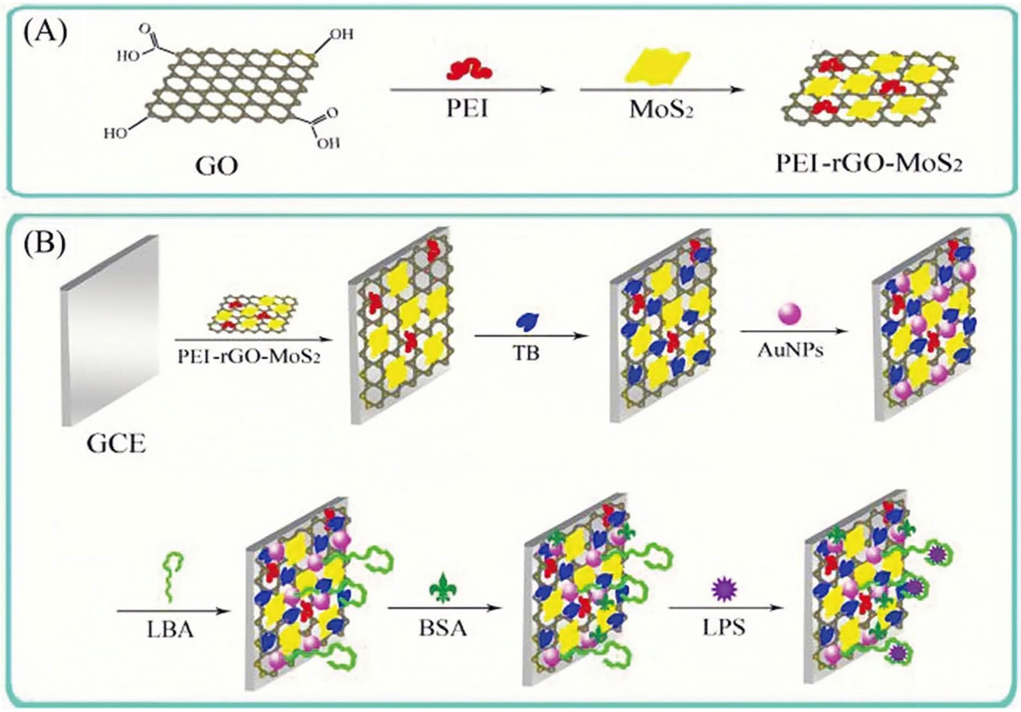

Fig. 9 **A** Schematic diagram of the fabrication of PEI-rGO-MoS2. **B** Schematic representation of the coating of the aptamer sensor [55]

IL-6

IL-6 is a cytokine that takes part in many immune and inflammatory responses [97]. It plays an important role in the process of the hepatic protein during acute inflammation[98]. In addition, the high level of the IL-6 is a symbol of the high risk of death especially in intra-abdominal sepsis [99]. Compared with a low concentration of IL-6 in the normal condition (lower than 10 pg/mL), the level of IL-6 rises rapidly (even more than 1 pg/ml) when sepsis occurs in adults [100]. Therefore, detecting the change of IL-6 concentration is of great significance for the early diagnosis of sepsis.

To detect IL-6 rapidly, aptamers are usually combined with NPs, such as AuNPs, graphene, nanotubes, to construct sensor systems.

For instance, to develop an optical sensor, Giorgi-Coll et al. combined many aptamers with gold nanoclusters, which was called "sandwich-style" (Fig. 11) [60]. When aptamers recognized and attached IL-6, the gold nanoclusters were aggregated and made the color of the solution change from red to pink in few minutes, which could be measured by a spectrophotometer or a plate reader. It provided a fast method for detecting the concentration of IL-6 in human serum albumin by an optical sensor, which contributes to diagnosing sepsis quickly in clinical.

Tertis et al. developed an electrochemical sensor that was made up of glassy carbon electrodes coated with GNPs and aptamers fixed via gold-sulfur bonds [61]. The designed sensors could test the concentration of IL-6 from 5 pg/mL to 100 ng/mL with a detection limit of 1.6 pg/mL. The sensor could be re-used and be applied to detect other biomarkers in the clinic, which was helpful to diagnose sepsis.

For another sensor like microfluidic sensor, Khosravi et al. modified aptamers conjugated 1-Pyrenebutanoic Acid Succinimidyl Ester (PASE) on the nanotube biosensors [62]. The conductance was reduced with the increase of IL-6 concentration, which caused the change of the electrical signal. This was the first time to use the PASE conjugated aptamers to detect IL-6 and the strategy not only achieved label-free techniques but also completed 10 pg/mL sensitivity in serum.

Hao et al. combined the aptamer with a graphene-based field-effect transistor (GFET) to build the aptameric graphene-based based field-effect transistor(A-GFET) [63]. By relying on online signal processing circuits, the detection of IL-6 was carried out in ten minutes with the limit of 140 fM. In addition, the transistor could detect IL-6 which was stored for a long time. After that, they improved the A-GFET by using PASE as a linker, which caused the range of detection was extended to 618 fM and the sensing performance of A-GFET was improved [64].

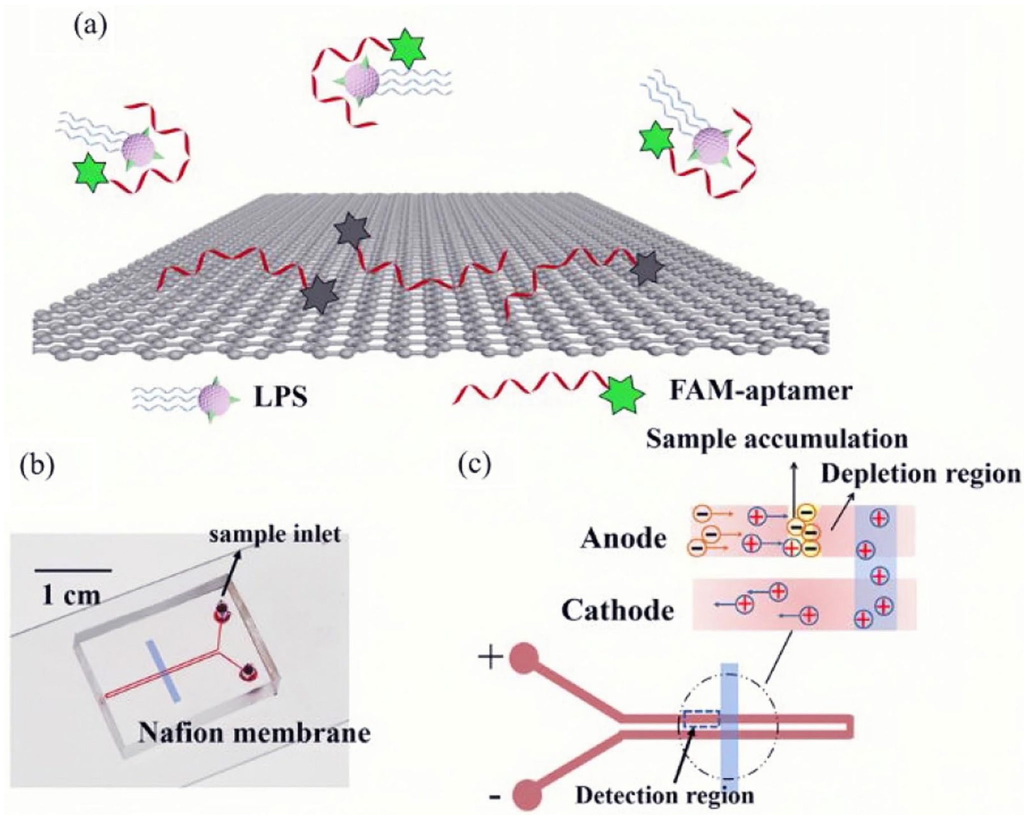

Fig. 10 The interaction principle of determination of LPS by coupling FAM-aptamer and rGO on a microfluidic biochip. **a** Schematic diagram of the fluorescence formation of LPS; **b** Schematic representation of the PDMS microfluidic CI-ES-chip; **c** Voltage scheme applied for the LPS preconcentration and the CI-ES mechanism [59]

CRP

CRP is an acute-phase protein produced by the liver, which is a common biomarker for the diagnosis of infection and inflammation in clinical treatment. The levels of CRP are elevated after infection and inflammation [101]. The level of CRP mostly depends on the amount of tissue damage currently occurring, and it can rise 1000-fold after infection or tissue damage within 24 to 48 h [102]. Elevated serum CRP concentration indicates a potential risk of organ failure and sepsis [103]. Besides, CRP has been widely used as biomarker of neonatal sepsis [104]. Therefore, detecting CRP is of great significance for the early diagnosis of sepsis.

Previous detection techniques, such as antibody-based tests [105] and enzyme-linked immunosorbent assay (ELISA) [106], have been proven to successfully detect CRP, however, some limitations are present. For example, antibody activity is not stable, and different animals have various immune responses, which leads to different specificity and sensitivity to CRP. ELISA can also cause inaccurate results by the color and composition of the medium used in assays [107].

Recently, aptamers have been applied in the detection of CRP. With the rapid development of optical fiber technology, the research of optical fiber sensors (OFS) received increasing attention. Generally, OFS works by detecting changes in light propagation caused by external stimuli. Compared with traditional sensor technologies, OFS is resistant to electromagnetic interference and high temperatures [108]. In addition, OFS has already been used to monitor pH, respiration rate, heart rate, and body temperature in the biomedical fields [109, 110]. Zamarreño and co-workers prepared a biosensor for rapid response and real-time monitoring of sepsis [65]. In this assay, researchers used a layer-by-layer (LbL) technique to combine CRP aptamer film with a fiber optic refractometer based on lossy mode resonances (LMRs). As aptamers bound to CRP, the refractive index of the sensitive coating changed (Fig. 12). The developed sensor could measure CRP in the range of 2–20 mg/L in less than 15 min. This experiment provided a new direction of diagnosis for early sepsis.

Besides, Luminex xMAP technology for clinical diagnosis is a hot topic in the field of bioscience. It allows

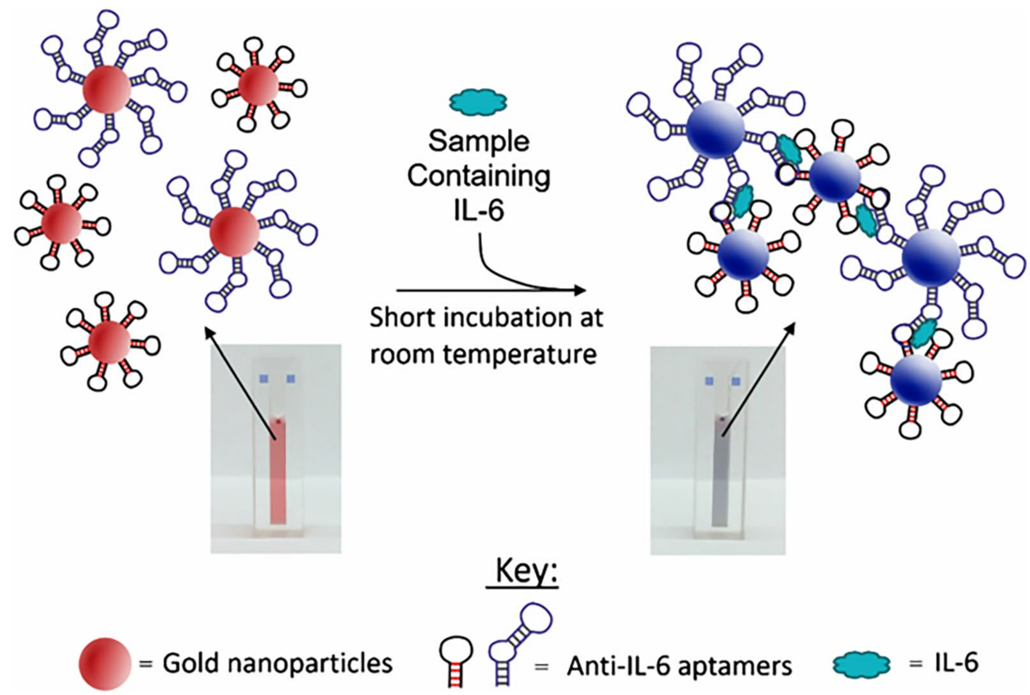

Fig. 11 The process of the sandwich-style and color changes [60]

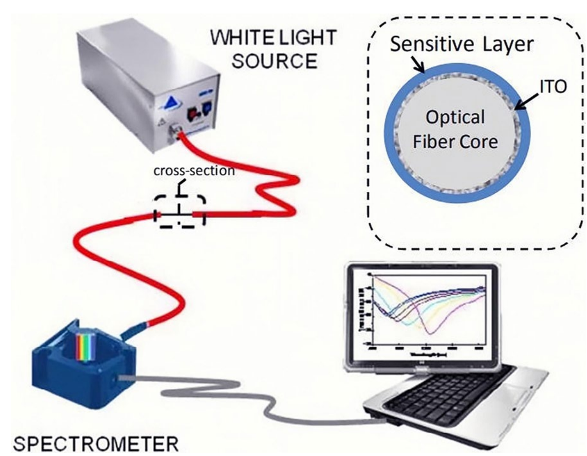

Fig. 12 The experimental setup of a fiber optic biosensor [65]

simultaneous detection of multiple analytes, using a lower sample size and shorter culture time. Furthermore, multiple types of aptamers can be incorporated into this technology [111]. Porschewski et al. reported the use of aptamers in the xMAP technology [112]. To expand the application of aptamers, Bernard et al. coupled an RNA aptamer that binds CRP to beads to act as the trapping agent [66]. Biotinylated anti-CRP antibody coupled to fluorescently labeled streptavidin was used to quantify CRP. An assay for the detection of CRP was successfully established with the detection limit of 0.4 mg/L in diluted serum.

In the last few years, NPs have been used to detect CRP in sepsis. Ghosh et al. reported an optical nanosensor using DNA aptamer as the main sensing element [67]. This biosensor combined a deoxyribonucleic acid aptamer with a quantum dot on the 5' terminus and a GNPs on the 3' terminus. When the aptamer bound to CRP, the photoluminescence intensity decreased based on the principle of fluorescence resonance energy transfer (FRET) (Fig. 13). The nanosensor was highly specific for CRP and the minimum detection limit was 1.77 pM. This detection system was synthesized by the wet chemical method and was simple in design. By using specific DNA aptamers, it could also be applied to detect other molecules.

CRP is also a generic biomarker for inflammation, cancer, cardiovascular, and neurological diseases. Currently, several aptamer-based detection strategies have been constructed, e.g., surface plasmon resonance [113], electrochemical [114], Photoelectrochemical (PEC) [115], etc.

Conclusions and perspectives

Diagnosing sepsis at the early stage is of great significance, which could guide doctors to use effective symptomatic and antibiotic treatment. Aptamer-based

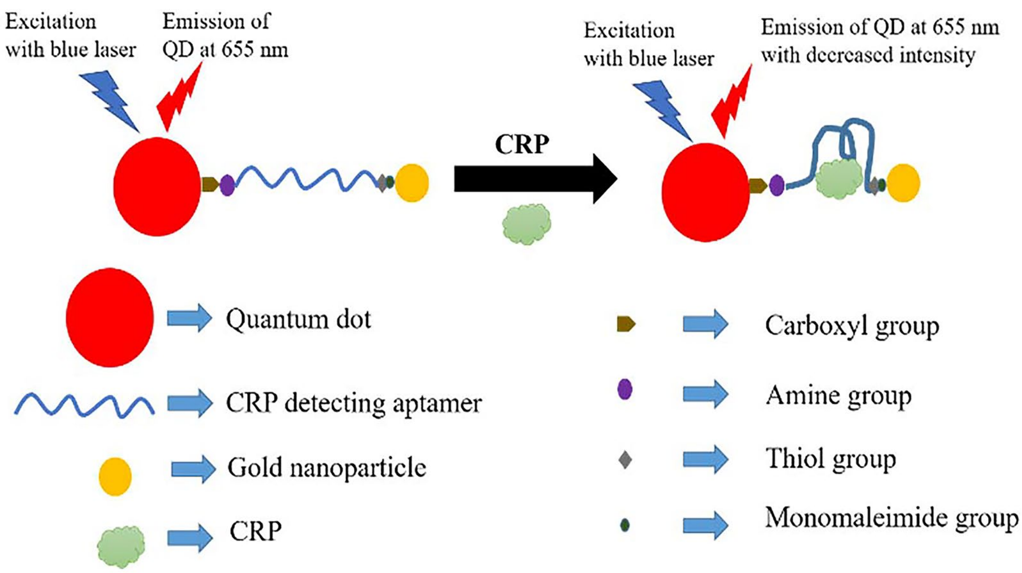

Fig. 13 A decrease in the photoluminescence of the nanosensor when CRP binds to the DNA aptamer [67]

biosensors may be a powerful complement to the traditional diagnostic method "blood culture" because of their accessibility, rapidity, and stability. The review summarized the recent progress of aptamer-based biosensors in the detection of bacteria and biomarkers for the diagnosis of sepsis. It is highly expected that innovative aptamer-based applications will emerge through rational design and development to achieve an excellent clinical performance.

Although some preliminary success has been achieved in the area of sepsis diagnosis by taking advantage of aptamer-based nano-biosensing systems, some challenges still remain for advancing this technology.

First, many aptamers have been selected against the sepsis-related targets, but only a tiny minority of aptamers' properties have been investigated. The safety of most aptamers has not been demonstrated, which limits their biological/clinical applications. In addition, the aptamer secondary and tertiary structures can be easily affected by temperature. To maintain its spatial configuration, the aptamers used for sepsis diagnosis should be selected according to the temperature at the time of clinical testing. Cold storage may also change their optimal folded conformation, which leads to lower detection accuracy. Thus, it is very important to develop a technique to avoid such potential thermally-induced conformational issues. Besides, the binding performance of aptamers may be affected in complex matrices. Therefore, it is necessary to keep aptamers' normal function in working matrices, such as using chemical modifications to enhance their stability, and testing the performance of aptamer-based biosensor in its specific working environment is also needed.

Second, although numerous work has been reported for proof-of-concept, there is still no available kits that can be applied at clinical or industrial level. Developing more efficient platforms, which may remedy the cost and inconvenience of aptamer-based nano-biosensing systems, will accelerate the translation from the bench to the clinic. Therefore, aptamer-integrated high-throughput analysis platforms could offer an ideal strategy to detect multiple pathogens and biomarkers from human biofluids that are commonly involved in the occurrence and development of clinical sepsis.

Third, it is critical to have the ability to design an aptamer-based nano-biosensor to offer ultra-high sensitivity and reproducibility with a large dynamic range simultaneously, because the signals of the sensor could be interfered from the biological molecules and aptamer are susceptible to degradation in biological media. A promising strategy may be the appropriate chemical modification in aptamer-based nanosensors, e.g., using polyethylene glycol to enhance resistance to exonucleases.

Fourth, it was reported that some specific aptamers have potential applications in the treatment of sepsis. Integration of the diagnosis and treatment in sepsis could be a promising strategy in the future research direction.

Overall, the aptamer-based sensor systems have a great potential for the early diagnosis of sepsis due to their excellent merits, such as high sensitivity, fast detection speed, wide detection range, easy mass production, etc. The specificity of this type of detecting technique makes it possible to detect different targets only by changing the type of aptamers. In addition to detect pathogens and biomarkers, it can monitor the real-time growth of bacteria and biofilms and also conduct drug sensitivity tests. With the continuous development of interdisciplinary research, it is predictable that the aptamer sensor system will become a crucial diagnostic tool for sepsis.

Acknowledgements
The authors acknowledge Yanjing Ji for the discussion.

Authors' contributions
LL and ZH collected literatures and wrote the original draft. FA, XG, and CZ wrote the original draft and prepared the table. WZ and LM prepared the figures. QZ conceived the idea and revised the manuscript. All authors read and approved the final manuscript.

Funding
The authors are very grateful for the financial support of by the National Natural Science Foundation of China (Grant No. 31900957), Shandong Provincial Natural Science Foundation (Grant No. ZR2019QC007), Innovation and technology program for the excellent youth scholars of higher education of Shandong province (Grant No. 2019KJE015), China Postdoctoral Science Foundation (Grant No. 2019M652326), and National College Students Innovation and Entrepreneurship Training Program of China (S202011065031).

Availability of data and materials
Without restrictions.

Declarations

Ethics approval and consent to participate
Not applicable.

Consent for publication
All authors gave their consent for publication.

Competing interests
The authors declare that they have no competing interests.

Author details
[1] Institute for Translational Medicine, Department of Stomatology, The Affiliated Hospital of Qingdao University, Qingdao University, Qingdao 266003, China. [2] School of Stomatology, Qingdao University, Qingdao 266003, China.

Received: 30 April 2021 Accepted: 9 July 2021
Published online: 19 July 2021

References

1. Hotchkiss RS, Karl IE. The pathophysiology and treatment of sepsis. N Engl J Med. 2003;348:138–50.
2. Cohen J. The immunopathogenesis of sepsis. Nature. 2002;420:885–91.
3. Bone RC. The pathogenesis of sepsis. Ann Intern Med. 1991;115:457–69.
4. Kanashiro A, Sônego F, Ferreira RG, Castanheira FVS, Leite CA, Borges VF, et al. Therapeutic potential and limitations of cholinergic anti-inflammatory pathway in sepsis. Pharmacol Res . 2017;117:1–8.
5. Hotchkiss RS, Moldawer LL, Opal SM, Reinhart K, Turnbull IR, Vincent JL. Sepsis and septic shock. Nat Rev Dis Prim. 2016. https://doi.org/10.1038/nrdp.2016.45.
6. Thompson BT. Drotrecogin alfa (activated) did not reduce mortality at 28 or 90 days in patients with septic shock. Ann Intern Med. 2012;157:24774.
7. Opal SM, Garber GE, LaRosa SP, Maki DG, Freebairn RC, Kinasewitz GT, et al. Systemic host responses in severe sepsis analyzed by causative microorganism and treatment effects of drotrecogin alfa (activated). Clin Infect Dis. 2003;37:50–8.
8. Vincent JL, Rello J, Marshall J, Silva E, Anzueto A, Martin CD, Moreno R, Lipman J, Gomersall C. International study of the prevalence and outcomes of infection in intensive care units. JAMA. 2009;302:2323–9.
9. Zhang G, Ghosh S. Molecular mechanisms of NF-κB activation induced by bacterial lipopolysaccharide through Toll-like receptors. J Endotoxin Res. 2000;6:453–7.
10. Lin KH, Wang FL, Wu MS, Jiang BY, Kao WL, Chao HY, et al. Serum procalcitonin and C-reactive protein levels as markers of bacterial infection in patients with liver cirrhosis: A systematic review and meta-analysis. Diagn Microbiol Infect Dis. 2014;80:72–8.
11. Fleischmann C, Scherag A, Adhikari NKJ, Hartog CS, Tsaganos T, Schlattmann P, et al. Assessment of global incidence and mortality of hospital-treated sepsis current estimates and limitations. Am J Respir Crit Care Med. 2016;193:259–72.
12. Filbin MR, Lynch J, Gillingham TD, Thorsen JE, Pasakarnis CL, Nepal S, et al. Presenting symptoms independently predict mortality in septic shock: Importance of a previously unmeasured confounder. Crit Care Med. 2018;46:1592–9.
13. Kumar A, Ellis P, Arabi Y, Roberts D, Light B, Parrillo JE, et al. Initiation of inappropriate antimicrobial therapy results in a fivefold reduction of survival in human septic shock. Chest. 2009;136:1237–48.
14. Singer M, Deutschman CS, Seymour C, Shankar-Hari M, Annane D, Bauer M, et al. The third international consensus definitions for sepsis and septic shock (sepsis-3). JAMA. 2016;315:801–10.
15. Ottesen EA, Hong JW, Quake SR, Leadbetter JR. Microfluidic digital PCR enables multigene analysis of individual environmental bacteria. Science. 2006;314:1464−67.
16. Burtscher C, Wuertz S. Evaluation of the use of PCR and reverse transcriptase PCR for detection of pathogenic bacteria in biosolids from anaerobic digestors and aerobic composters. Appl Environ Microbiol. 2003;69:4618–27.
17. Pechorsky A, Nitzan Y, Lazarovitch T. Identification of pathogenic bacteria in blood cultures: comparison between conventional and PCR methods. J Microbiol Methods. 2009;78:325–30.
18. Park KS. Nucleic acid aptamer-based methods for diagnosis of infections. Biosens Bioelectron. 2018;102:179–88.
19. Tuerk C, Gold L. Systematic evolution of ligands by exponential enrichment: RNA ligands to bacteriophage T4 DNA polymerase. Science. 1990;249:505–10.
20. Ad E, Jw S. In vitro selection of RNA molecules that bind specific ligands. Nature. 1990;346:818–22.
21. Meek KN, Rangel AE, Heemstra JM. Enhancing aptamer function and stability via in vitro selection using modified nucleic acids. Methods. 2016;106:29–36.
22. Zhou S, Lu C, Li Y, Xue L, Zhao C, Tian G, et al. Gold nanobones enhanced ultrasensitive surface-enhanced raman scattering aptasensor for detecting *Escherichia coli* O157:H7. ACS Sens. 2020;5:588–96.
23. Deng B, Lin Y, Wang C, Li F, Wang Z, Zhang H, et al. Aptamer binding assays for proteins: the thrombin example-A review. Anal Chim Acta. 2014;837:1–15.
24. Sung TC, Chen WY, Shah P, Chen CS. A replaceable liposomal aptamer for the ultrasensitive and rapid detection of biotin. Sci Rep . 2016;6:1–8.
25. He JL, Wu ZS, Zhou H, Wang HQ, Jiang JH, Shen GL, et al. Fluorescence aptameric sensor for strand displacement amplification detection of cocaine. Anal Chem. 2010;82:1358–64.
26. Fan Y, Zhang W, Liu Y, Zeng Z, Quan X, Zhao H. Three-dimensional branched crystal carbon nitride with enhanced intrinsic peroxidase-like activity: a hypersensitive platform for colorimetric detection. ACS Appl Mater Interfaces. 2019;11:17467–74.
27. Li N, Ho CM. Aptamer-based optical probes with separated molecular recognition and signal transduction modules. J Am Chem Soc. 2008;130:2380–1.
28. Lautner G, Balogh Z, Bardóczy V, Mészáros T, Gyurcsányi RE. Aptamer-based biochips for label-free detection of plant virus coat proteins by SPR imaging. Analyst. 2010;135:918–26.
29. Simeonov Y, Weber U, Penchev P, Ringbæk TP, Schuy C, Brons S, et al. 3D range-modulator for scanned particle therapy: development, Monte Carlo simulations and experimental evaluation. Phys Med Biol. 2017;62:7075–96.

30. Beiranvand ZS, Abbasi AR, Dehdashtian S, Karimi Z, Azadbakht A. Aptamer-based electrochemical biosensor by using Au-Pt nanoparticles, carbon nanotubes and acriflavine platform. Anal Biochem Elsevier Ltd. 2017;518:35–45.
31. Mok W, Li Y. Recent progress in nucleic acid aptamer-based biosensors and bioassays. Sensors. 2008;8:7050–84.
32. Xu L, Dai Q, Shi Z, Liu X, Gao L, Wang Z, et al. Accurate MRSA identification through dual-functional aptamer and CRISPR-Cas12a assisted rolling circle amplification. J Microbiol Methods. 2020;173:105917.
33. Zhou J, Bobbin ML, Burnett JC, Rossi JJ. Current progress of RNA aptamer-based therapeutics. Front Genet. 2012;3:1–14.
34. Yang L, Pijuan-Galito S, Rho HS, Vasilevich AS, Eren AD, Ge L, et al. High-throughput methods in the discovery and study of biomaterials and materiobiology. Chem Rev. 2021. https://doi.org/10.1021/acs.chemrev.0c00752.
35. Zhou Q, Chen J, Luan Y, Vainikka PA, Thallmair S, Marrink SJ, et al. Unidirectional rotating molecular motors dynamically interact with adsorbed proteins to direct the fate of mesenchymal stem cells. Sci Adv. 2020. https://doi.org/10.1126/sciadv.aay2756.
36. Zhou Q, Zhao Z, Zhou Z, Zhang G, Chiechi RC, van Rijn P. Directing mesenchymal stem cells with gold nanowire arrays. Adv Mater Interfaces. 2018;5:1–8.
37. Ji Y, Han Z, Ding H, Xu X, Wang D, Zhu Y, et al. Enhanced eradication of bacterial/fungi biofilms by glucose oxidase-modified magnetic nanoparticles as a potential treatment for persistent endodontic infections. ACS Appl Mater Interfaces. 2021. https://doi.org/10.1021/acsami.1c01748.
38. Fan Y, Liu Y, Zhou Q, Du H, Zhao X, Ye F, et al. Catalytic hairpin assembly indirectly covalent on Fe_3O_4@C nanoparticles with signal amplification for intracellular detection of miRNA. Talanta. 2021;223:121675.
39. Yu Z, Li Q, Wang J, Yu Y, Wang Y, Zhou Q, et al. Reactive oxygen species-related nanoparticle toxicity in the biomedical field. Nanoscale Res Lett. 2020;15:1–14.
40. Yao J, Yang M, Duan Y. Chemistry, biology, and medicine of fluorescent nanomaterials and related systems: New insights into biosensing, bioimaging, genomics, diagnostics, and therapy. Chem Rev. 2014;114:6130–78.
41. Biju V. Chemical modifications and bioconjugate reactions of nanomaterials for sensing, imaging, drug delivery and therapy. Chem Soc Rev. 2014;43:744–64.
42. Smith BR, Gambhir SS. Nanomaterials for in vivo imaging. Chem Rev . 2017;117:901–86.
43. Zu G, Cao Y, Dong J, Zhou Q, van Rijn P, Liu M, et al. Development of an Aptamer-Conjugated Polyrotaxane-Based Biodegradable Magnetic Resonance Contrast Agent for Tumor-Targeted Imaging. ACS Appl Bio Mater. 2019;2:406–16.
44. Chang YC, Yang CY, Sun RL, Cheng YF, Kao WC, Yang PC. Rapid single cell detection of Staphylococcus aureus by aptamer-conjugated gold nanoparticles. Sci Rep. 2013;3:1–7.
45. Shen H, Wang J, Liu H, Li Z, Jiang F, Wang FB, et al. Rapid and Selective Detection of Pathogenic Bacteria in Bloodstream Infections with Aptamer-Based Recognition. ACS Appl Mater Interfaces. 2016;8:19371–8.
46. Song JH, Lee SM, Park IH, Yong D, Lee KS, Shin JS, et al. Vertical capacitance aptasensors for real-time monitoring of bacterial growth and antibiotic susceptibility in blood. Biosens Bioelectron. 2019;143:111623.
47. Lee KS, Lee SM, Oh J, Park IH, Song JH, Han M, et al. Electrical antimicrobial susceptibility testing based on aptamer-functionalized capacitance sensor array for clinical isolates. Sci Rep . 2020;10:1–9.
48. Graziani AC, Stets MI, Lopes ALK, Schluga PHC, Marton S, Ferreira IM, et al. High efficiency binding aptamers for a wide range of bacterial sepsis agents. J Microbiol Biotechnol. 2017;27:838–43.
49. Shin HS, Gedi V, Kim JK, Lee DK. Detection of Gram-negative bacterial outer membrane vesicles using DNA aptamers. Sci Rep. 2019;9:1–8.
50. Kim SE, Su W, Cho M, Lee Y, Choe WS. Harnessing aptamers for electrochemical detection of endotoxin. Anal Biochem. 2012;424:12–20.
51. Bai L, Chai Y, Pu X, Yuan R. A signal-on electrochemical aptasensor for ultrasensitive detection of endotoxin using three-way DNA junction-aided enzymatic recycling and graphene nanohybrid for amplification. Nanoscale. 2014;6:2902–8.
52. Posha B, Nambiar SR, Sandhyarani N. Gold atomic cluster mediated electrochemical aptasensor for the detection of lipopolysaccharide. Biosens Bioelectron. 2018;101:199–205.
53. Pourmadadi M, Shayeh JS, Omidi M, Yazdian F, Alebouyeh M, Tayebi L. A glassy carbon electrode modified with reduced graphene oxide and gold nanoparticles for electrochemical aptasensing of lipopolysaccharides from *Escherichia coli* bacteria. Microchim Acta Microchimica Acta. 2019;186:2–9.
54. Yazdian F, Rashedi H. Applying reduced graphene oxide-gold nanoparticles for the electrochemical detection of endotoxin. In: Proceedings of the 7th international conference on innovation in science and technology. 2020. p. 280–94.
55. Yuan Y, Li L, Zhao M, Zhou J, Bai L. An aptamer based voltammetric biosensor for endotoxins using a functionalized graphene and molybdenum disulfide composite as a new nanocarrier. Anal R Soc Chem. 2018;144:1253–9.
56. An Z, Jang CH. Simple and label-free liquid crystal-based optical sensor for highly sensitive and selective endotoxin detection by aptamer binding and separation. ChemistrySelect. 2019;4:1416–22.
57. Ji J, Pang Y, Li D, Huang Z, Zhang Z, Xue N, et al. An aptamer-based shear horizontal surface acoustic wave biosensor with a CVD-grown single-layered graphene film for high-sensitivity detection of a label-free endotoxin. Microsyst Nanoeng. 2020. https://doi.org/10.1038/s41378-019-0118-6.
58. Zhang Z, Yang J, Pang W, Yan G. An aptamer-based fluorescence probe for facile detection of lipopolysaccharide in drinks. RSC Adv R Soc Chem. 2017;7:54920–6.
59. Niu J, Hu X, Ouyang W, Chen Y, Liu S, Han J, et al. Femtomolar detection of lipopolysaccharide in injectables and serum samples using aptamer-coupled reduced graphene oxide in a continuous injection-electrostacking biochip. Anal Chem. 2019;91:2360–7.
60. Giorgi-Coll S, Marín MJ, Sule O, Hutchinson PJ, Carpenter KLH. Aptamer-modified gold nanoparticles for rapid aggregation-based detection of inflammation: an optical assay for interleukin-6. Microchim Acta Microchimica Acta. 2020;187:1–11.
61. Tertis M, Leva PI, Bogdan D, Suciu M, Graur F, Cristea C. Impedimetric aptasensor for the label-free and selective detection of Interleukin-6 for colorectal cancer screening. Biosens Bioelectron. 2019;137:123–32.
62. Khosravi F, Loeian SM, Panchapakesan B. Ultrasensitive label-free sensing of IL-6 based on PASE functionalized carbon nanotube micro-arrays with RNA-aptamers as molecular recognition elements. Biosensors. 2017;7:1–13.
63. Hao Z, Pan Y, Huang C, Wang Z, Zhao X. Sensitive detection of lung cancer biomarkers using an aptameric graphene-based nanosensor with enhanced stability. Biomed Microdevices . 2019;21:1–9.
64. Hao Z, Pan Y, Huang C, Wang Z, Lin Q, Zhao X, et al. Modulating the linker immobilization density on aptameric graphene field effect transistors using an electric field. ACS Sensors. 2020;5:2503–13.
65. Zamarreño CR, Ardaiz I, Ruete L, Muñoz FJ, Matias IR, Arregui FJ. C-reactive protein aptasensor for early sepsis diagnosis by means of an optical fiber device. Proc IEEE Sensors 2013. 2013; p. 4–7.
66. Bernard ED, Nguyen KC, DeRosa MC, Tayabali AF, Aranda-Rodriguez R. Development of a bead-based aptamer/antibody detection system for C-reactive protein. Anal Biochem. 2015;472:67–74.
67. Ghosh S, Metlushko A, Chaudhry S, Dutta M, Stroscio MA. Detection of c-reactive protein using network-deployable DNA aptamer based optical nanosensor. In: 2019 IEEE EMBS International Conference on Biomedical & Health Informatics (BHI). 2019. p. 1–4.
68. Wang J, Wu H, Yang Y, Yan R, Zhao Y, Wang Y, et al. Bacterial species-identifiable magnetic nanosystems for early sepsis diagnosis and extracorporeal photodynamic blood disinfection. Nanoscale. 2018;10:132–41.
69. Saito S. SELEX-based DNA aptamer selection: a perspective from the advancement of separation techniques. Anal Sci. 2021;37:17–26.
70. Zhuo Z, Yu Y, Wang M, Li J, Zhang Z, Liu J, et al. Recent advances in SELEX technology and aptamer applications in biomedicine. Int J Mol Sci. 2017;18:1–19.
71. Darmostuk M, Rimpelova S, Gbelcova H, Ruml T. Current approaches in SELEX: an update to aptamer selection technology. Biotechnol Adv. 2014;33:1141–61.
72. Kaur H. Recent developments in cell-SELEX technology for aptamer selection. Biochim Biophys Acta Gen Subj. 2018;1862(10):2323–9.
73. Khilnani P. Severe sepsis and septic shock. In: Chawla R, Todi S, editors. ICU Protoc A stepwise approach. India: Springer; 2012. p. 703–7.

74. Cross AS, Zierdt CH, Roup B, Almazan R, Swan JC. A hospital-wide outbreak of septicemia due to a few strains of *Staphylococcus aureus*. Am J Clin Pathol. 1983;79:598–603.
75. Vollmer W, Blanot D, De Pedro MA. Peptidoglycan structure and architecture. FEMS Microbiol Rev. 2008;32:149–67.
76. Schumann P. Peptidoglycan structure. Methods Microbiol. Elsevier Ltd. 2011;38:101–29.
77. Ferreira IM, de Souza Lacerda CM, de Faria LS, Corrêa CR, de Andrade ASR. Selection of peptidoglycan-specific aptamers for bacterial cells identification. Appl Biochem Biotechnol. 2014;174:2548–56.
78. Beveridge TJ. Structures of gram-negative cell walls and their derived membrane vesicles. J Bacteriol. 1999;181:4725–33.
79. Jan AT. Outer Membrane Vesicles (OMVs) of gram-negative bacteria: a perspective update. Front Microbiol. 2017;8:1–11.
80. Khan ZA, Siddiqui MF, Park S. Current and emerging methods of antibiotic susceptibility testing. Diagnostics. 2019. https://doi.org/10.3390/diagnostics9020049.
81. Syal K, Mo M, Yu H, Iriya R, Jing W, Guodong S, et al. Current and emerging techniques for antibiotic susceptibility tests. Theranostics. 2017;7:1795–805.
82. Behera B, Anil Vishnu GK, Chatterjee S, Sitaramgupta VVSN, Sreekumar N, Nagabhushan A, et al. Emerging technologies for antibiotic susceptibility testing. Biosens Bioelectron. 2019;142:111552.
83. Kumar A, Roberts D, Wood KE, Light B, Parrillo JE, Sharma S, et al. Duration of hypotension before initiation of effective antimicrobial therapy is the critical determinant of survival in human septic shock*. Crit Care Med. 2006;34:1589–96.
84. Song J, Moon S, Park DW, Cho H, Kim JY, Park J, et al. Biomarker combination and SOFA score for the prediction of mortality in sepsis and septic shock. Medicine (Baltimore). 2020. https://doi.org/10.1097/MD.0000000000020495.
85. Bauer M, Strom M, Hammond DS. Anything You Can Do, I Can Do Better : can aptamers replace antibodies in clinical diagnostic applications? Molecules. 2019;24:1–13.
86. Alizadeh N, Yousef M, Reza S. Aptamer-assisted novel technologies for detecting bacterial pathogens. ScienceDirect. 2017;93:737–45.
87. Gold L, Ayers D, Bertino J, Bock C, Bock A, Brody EN, et al. Aptamer-based multiplexed proteomic technology for biomarker discovery. Nat Preced. 2010. https://doi.org/10.1371/journal.pone.0015004.
88. Liu Y, Hou J, Li Q, Chen K, Wang SN, Wang J. Biomarkers for diagnosis of sepsis in patients with systemic inflammatory response syndrome : a systematic review and meta—analysis. Springerplus. 2016. https://doi.org/10.1186/s40064-016-3591-5.
89. Preston A, Mandrell RE, Gibson BW, Apicella MA. The lipooligosaccharides of pathogenic gram-negative bacteria. Crit Rev Microbiol. 1996;22:139–80.
90. Rosadini CV, Kagan JC. Early innate immune responses to bacterial LPS. Curr Opin Immunol . 2017;44:14–9.
91. Welch H. Herbert 0. Calvery WTM and CWP, The Method of Preparation and Test for Bacterial Pyrogen. J Am Pharm Assoc. 1949;71:2955–7.
92. Iwanaga S, Miyata T, Tokunaga F, Muta T. Molecular mechanism of hemolymph clotting system in Limulus. Thromb Res. 1992;68(1):1–32.
93. Franco E, Garcia-Recio V, Jiménez P, Garrosa M, Girbés T, Cordoba-Diaz M, et al. Endotoxins from a pharmacopoeial point of view. Toxins (Basel). 2018;10:1–9.
94. Inoue KY, Ino K, Shiku H, Matsue T. Electrochemical detection of endotoxin using recombinant factor C zymogen. Electrochem commun. 2010;12:1066–9.
95. Demertzis N. Development of a multiplex sensing platform for the accurate and rapid diagnosis of Sepsis. (Doctoral dissertation, Cardiff University) 2020.
96. Lee BR, Kim JW, Kang D, Lee DW, Ko SJ, Lee HJ, et al. Highly efficient polymer light-emitting diodes using graphene oxide as a hole transport layer. ACS Nano. 2012;6:2984–91.
97. Meyer C, Eydeler K, Magbanua E, Zivkovic T, Piganeau N, Lorenzen I, et al. Interleukin-6 receptor specific RNA aptamers for cargo delivery into target cells. RNA Biol. 2012;9:67–80.
98. Pfäfflin A, Schleicher E. Inflammation markers in point-of-care testing (POCT). Anal Bioanal Chem. 2009;393:1473–80.
99. Clinical C, Unit T, Hospital QE. Interleukin 6 is a prognostic indicator of outcome in severe intra-abdominal sepsis. Br J Surg. 1994;81:1306–8.
100. Hunter CA, Jones SA. IL-6 as a keystone cytokine in health and disease. Nat Immunol . 2015;16:448–57.
101. Kumar S, Tripathy S, Jyoti A, Singh SG. Recent advances in biosensors for diagnosis and detection of sepsis: a comprehensive review. Biosens Bioelectron. 2019;124–125:205–15.
102. Hencst JM. The role of C-Reaction protein in the evaluation and management of infants with suspected sepsis. Adv Neonatal Care. 2003;3:3–13.
103. Pierrakos C, Vincent JL. Sepsis biomarkers: a review. Crit Care. 2010;14:1–18.
104. Yang AP, Liu J, Yue LH, Wang HQ, Yang WJ, Yang GH. Neutrophil CD64 combined with PCT, CRP and WBC improves the sensitivity for the early diagnosis of neonatal sepsis. Clin Chem Lab Med. 2016;54:345–51.
105. Meyer MHF, Hartmann M, Keusgen M. SPR-based immunosensor for the CRP detection—a new method to detect a well known protein. Biosens Bioelectron. 2006;21:1987–90.
106. Dominici R, Luraschi P, Franzini C. Measurement of C-reactive protein: two high sensitivity methods compared. J Clin Lab Anal. 2004;18:280–4.
107. Zubiate P, Zamarreño CR, Sánchez P, Matias IR, Arregui FJ. High sensitive and selective C-reactive protein detection by means of lossy mode resonance based optical fiber devices. Biosens Bioelectron . 2017;93:176–81.
108. Correia R, James S, Lee SW, Morgan SP, Korposh S. Biomedical application of optical fibre sensors. J Opt. 2018. https://doi.org/10.1088/2040-8986/aac68d.
109. Shao LY, Yin MJ, Tam HY, Albert J. Fiber optic pH sensor with self-assembled polymer multilayer nanocoatings. Sensors (Switzerland). 2013;13:1425–34.
110. Fajkus M, Nedoma J, Martinek R, Vasinek V, Nazeran H, Siska P. A non-invasive multichannel hybrid fiber-optic sensor system for vital sign monitoring. Sensors (Switzerland). 2017;17:1–17.
111. Wendt M, Cappuccilli G. Generating conformation and complex-specific synthetic antibodies. Methods Mol Biol. 2017;1575:303–22.
112. Porschewski P, Grättinger MAM, Klenzke K, Erpenbach A, Blind MR, Schäfer F. Using aptamers as capture reagents in bead-based assay systems for diagnostics and hit identification. J Biomol Screen. 2006;11:773–81.
113. Wu B, Jiang R, Wang Q, Huang J, Yang X, Wang K, et al. Detection of C-reactive protein using nanoparticle-enhanced surface plasmon resonance using an aptamer-antibody sandwich assay. Chem Commun. 2016;52:3568–71.
114. Jarczewska M, Rębiś J, Górski Ł, Malinowska E. Development of DNA aptamer-based sensor for electrochemical detection of C-reactive protein. Talanta. 2018;189:45–54.
115. Zhang X, Chi KN, Li DL, Deng Y, Ma YC, Xu QQ, et al. 2D-porphrinic covalent organic framework-based aptasensor with enhanced photoelectrochemical response for the detection of C-reactive protein. Biosens Bioelectron. 2019;129:64–71.

Publisher's Note

Springer Nature remains neutral with regard to jurisdictional claims in published maps and institutional affiliations.

frontiers in Oncology

SYSTEMATIC REVIEW
published: 08 July 2021
doi: 10.3389/fonc.2021.693284

Diagnostic Value of CircRNAs as Potential Biomarkers in Oral Squamous Cell Carcinoma: a Meta-Analysis

Mingfei Wang[1†], *Linfeng Zhang*[1†], *Wenhao Ren*[2], *Shaoming Li*[2], *Keqian Zhi*[2], *Jingjing Zheng*[3*] and *Ling Gao*[2*]

[1] School of Stomatology, Qingdao University, Qingdao, China, [2] Department of Oral and Maxillofacial Surgery, Key Laboratory of Oral Clinical Medicine, The Affiliated Hospital of Qingdao University, Qingdao, China, [3] Department of Endodontics, Key Laboratory of Oral Clinical Medicine, The Affiliated Hospital of Qingdao University, Qingdao, China

OPEN ACCESS

Edited by:
Die Wang,
Hudson Institute of Medical Research, Australia

Reviewed by:
Jaimanti Bakshi,
Post Graduate Institute of Medical Education and Research (PGIMER), India
Liang Ding,
Nanjing University, China

***Correspondence:**
Jingjing Zheng
zhengjingjing.1984@163.com
Ling Gao
coffee_smile@163.com

†These authors have contributed equally to this work and share first authorship

Specialty section:
This article was submitted to Head and Neck Cancer, a section of the journal Frontiers in Oncology

Received: 10 April 2021
Accepted: 22 June 2021
Published: 08 July 2021

Citation:
Wang M, Zhang L, Ren W, Li S, Zhi K, Zheng J and Gao L (2021) Diagnostic Value of CircRNAs as Potential Biomarkers in Oral Squamous Cell Carcinoma: a Meta-Analysis. Front. Oncol. 11:693284. doi: 10.3389/fonc.2021.693284

Introduction: Circular RNAs (CircRNAs), an emerging non-coding RNA, have been demonstrated to be involved in tumorigenesis, metastasis, and cancer progression, and could represent novel potential biomarkers for diagnosing oral squamous cell carcinoma (OSCC). However, no meta-analysis has investigated the diagnostic role of circRNAs in OSCC. Hence, to investigate whether circRNAs could serve as specific biomarkers for OSCC, the present systematic review and meta-analysis evaluated the diagnostic efficiency of circRNAs in patients with OSCC.

Materials and Methods: A thorough search of online databases (Pubmed, Web of Science, Embase, and the Cochrane Library) was conducted to collect relevant studies up to March 30th, 2021. All eligible studies were case-control studies. The quality of each study was evaluated by the Quality Assessment of Diagnostic Accuracy Studies-2 (QUADAS-2) tool. STATA (version 15.1) and Review Manager (version 5.4) were employed to conduct the meta-analysis, and the PRISMA statement was adopted in this study.

Results: A total of 16 studies were included in the meta-analysis, with five studies on upregulated circRNAs, and 11 on downregulated circRNAs. The enrolled studies that met our eligibility criteria all derived from China. The pooled sensitivity (SEN), specificity (SPE), diagnostic odds ratio (DOR), positive likelihood ratio (PLR), negative likelihood ratio (NLR), and the area under receiver operating characteristics curve (AUC) with the 95% confidence intervals (95% CIs) were 0.74 (0.69–0.79), 0.79 (0.73–0.84), 10.74 (7.81–14.77), 3.50 (2.78–4.45), 0.33 (0.27–0.39) and 0.83 (0.79–0.86), respectively. The subgroup analysis demonstrated that serum, plasma, and saliva specimens had a better diagnostic performance than tissue samples, with a high value of sensitivity, specificity, DOR, and AUC values. The results also showed that the subgroups of upregulated circRNAs and a sample size of ≥100 manifested higher specificity, DOR, and AUC for cancer detection than downregulated circRNAs and a sample size of < 100.

Conclusions: A strong association was demonstrated between the dysregulated expression of circRNAs and the diagnosis of OSCC. Hence, circRNAs have the potential to function as promising biomarkers and therapeutic targets for OSCC.

Systematic Review Registration: PROSPERO, number CRD42021256857.

Keywords: circular RNA, OSCC, oral oncology, meta-analysis, biomarker, diagnosis

INTRODUCTION

Head-and-neck squamous cell carcinoma (HNSCC) ranks the sixth most common neoplasm by incidence globally, accounting for 650,000 new cancer cases and 350,000 deaths worldwide annually (1). HNSCCs constitute a group of epithelial malignant tumors in the oral cavity, nose, sinuses, salivary gland, larynx, and pharynx. According to previous reports, males are more likely to be affected than females, with a ratio ranging from 2:1 to 4:1 (2). Among the subtypes of HNSCC, oral squamous cell carcinoma (OSCC) is the most common malignant neoplasm and has a poor prognosis with a 5-year survival rate of <50% (3, 4). The most widely applied therapies include surgery, chemotherapy, and radiotherapy, which significantly compromise the patients' quality of life. In etiology, the typical risk factors are mainly related to environmental carcinogens, such as tobacco and alcohol, and risky lifestyle habits, e.g., betel nut chewing (5). Recently, the human papillomavirus (HPV) has emerged as an etiologic factor contributing to the development of HNSCC (6). HPV-positive HNSCC cases, as a consequence of HPV infections, mainly occur in the oropharynx region within the lymphoid epithelium of the tongue or tonsils, primarily in patients with the HPV-16 subtype (7).

Currently, the gold standard for OSCC diagnosis is still conventional oral examination and the histological evaluation of biopsy tissue, constituting highly accurate and reliable diagnostic methods with high specificity and sensitivity. However, the clinical application is limited due to patient discomfort and sampling bias, leading to misdiagnosis (8). Some biomarkers (such as carcinoembryonic antigen [CEA] and CA199) have been developed and implemented clinically. However, they have low accuracy and have proven inefficient. Consequently, it is imperative for clinicians to search for novel biomarkers as non-invasive diagnostic tools to enhance the efficacy of OSCC diagnosis.

Circular RNAs (circRNAs), a novel class of endogenous non-coding RNAs, are derived from the back-splicing by the canonical spliceosome *via* exon or intron circularization (9). As the high-throughput sequencing technology has made great strides and been widely employed, several circRNAs have been captured and identified (10). Instead of the linear structure within a 5' cap and a 3' polyadenylated tail, this non-coding RNA is characterized by a covalently closed-loop structure (11). CircRNAs are exceedingly stable and play a pivotal role in various physiological and pathophysiological processes. Studies recently published implied that this newly found subclass of long non-coding RNA has significantly boosted research efforts in many diseases, such as heart failure, autism, diabetes mellitus, and cancer (12–15). Cumulative research has illustrated that circRNAs function as microRNA molecular sponges and regulate gene expression and other biological procedures, such as cell proliferation, invasion, and migration (16).

Considerable evidence has indicated that circRNAs could serve as a viable diagnostic option. Nonetheless, due to variations in the study design, specimen type, and sample size, no explicit clinical diagnostic significance of circRNA in OSCC has been elucidated in previous studies. Therefore, this systematic meta-analysis aimed to combine the results of previously published studies to estimate the diagnostic test accuracy of dysregulated circRNAs as biomarkers for OSCC.

MATERIALS AND METHODS

The process of study selection was conducted following the Preferred Reporting Items for Systematic Reviews and Meta-Analyses guideline for diagnostic test accuracy (PRISMA-DTA) (17).

Study Design

A systematic review and meta-analysis were applied to assess the clinical diagnostic capability of circRNAs in OSCC.

Bibliography Search Strategy

All the eligible studies in this meta-analysis were selected independently by two authors (MW and LZ). A thorough electronic search was carried out in PubMed, Web of Science, Embase, and Cochrane Library online databases up to March 30th, 2021. The full and reproducible keywords used in the search are provided in **Appendix 1**. In addition, the two authors independently and manually screened the titles, abstracts, and full texts to identify the relevant studies. Then the authors extracted the data from the relevant articles.

Inclusion and Exclusion Criteria

All the studies included in the meta-analysis met the following inclusion criteria.

The inclusion criteria were as follows:

a. case-control study or cohort study,
b. the diagnosis of oral squamous cell carcinoma was confirmed by histological examinations,
c. the studies analyzed the relationship between circRNAs and oral cancers,
d. circRNAs expression levels were assessed with quantitative real-time polymerase chain reaction(qRT-PCR) analysis, and

e. the sample size, sensitivity, specificity, and AUC were provided to calculate true positives (TP), false positives (FP), false negatives (FN), and true negatives (TN);

The exclusion criteria were as follows:

a. duplicate data from previous studies,
b. reviews, letters, case reports, and meeting abstracts, etc.,
c. non-English and animal studies, and
d. insufficient or unqualified data.

Data Extraction and Quality Assessment

The titles and abstracts of the articles were independently screened by two authors (MW and LZ) to determine their relevance to the topic, focusing on the diagnostic application of RNA in OSCC, defined by the International Classification of Diseases 10th Revision (ICD-10) codes C00-C06. Then LG and JZ evaluated the full text of the remaining articles, independently extracted the relevant data, and cross-checked to ensure data accuracy. The following data were extracted from each study: (a) basic information including the first author's name, publication year, country, circRNA type, circRNA expression, sample size, cancer type, specimen, and detection method; (b) clinicopathological features including gender, age, tumor size, lymph node metastasis, TNM, T-stage, differentiation, and extrathyroidal extension; and (c) diagnostic information including sample size, sensitivity, specificity, and area under the curve (AUC).

The quality of each study was assessed independently by two authors (WR and SL) using the Quality Assessment of Diagnostic Accuracy Studies-2 (QUADAS-2) tool, retaining all original domain questions in two dimensions ("Risk of Bias" and "Applicability Concerns") (18). Each risk of bias item was graded "yes", "no", or "unclear", while the applicability concerns were evaluated as "high", "low", or "unclear".

Summary Measures

The diagnostic sensitivity and specificity of the upregulated or downregulated circRNAs in the OSCC patients compared to the controls were considered the primary measures.

Statistical Analysis

The meta-analysis was conducted utilizing STATA 15.1 and Review Manager 5.4 statistical softwares to analyze the diagnostic performance of circRNAs in OSCC, constructing forest plots for sensitivity (SEN), specificity (SPE), negative likelihood ratio (NLR), positive likelihood ratio (PLR), and the diagnostic odds ratio (DOR). A summary receiver operator characteristics curve (SROC) was plotted to calculate the area under the SROC curve (AUC) and 95% confidence intervals (95% CIs) for the qualitative assessment of the diagnostic value. Deek's funnel plot and funnel chart were constructed to estimate the publication bias between the included studies (with $P > 0.05$ indicating no publication bias). Furthermore, the Harbord test plot was established to scrutinize the potential publication bias in the meta-analysis (with $P > 0.05$ indicating no publication bias). Fagan's nomogram was constructed to calculate post-test probabilities. An LR scatter matrix plot was utilized to assess the clinical significance of individual diagnostic studies, which was divided into four quadrants. Heterogeneity was estimated using I^2 statistics and the Cochrane Q-test (with $I^2 > 50\%$ and $P < 0.05$ suggesting significant heterogeneity). The analysis applied a random-effects model due to significant heterogeneity. Meta-regression and subgroup analyses were performed to identify the potential source of heterogeneity. Sensitivity analysis was conducted by omitting individual studies to test the reliability of our analyses.

Trial Sequential Analysis

Trial sequential analysis (TSA) was performed for the meta-analysis results using the TSA software V.0.9.5.5 beta (Copenhagen Trial Unit). This analysis was utilized to estimate the required information size (RIS) for the statistical significance of the present meta-analysis. When the actual sample size in the meta-analysis failed to reach the RIS, TSA was applied to combine the results and provide a cumulated sample size of the included studies with an adjusted threshold to test the statistical significance and considerably reduce type I errors (false-positive results). Theoretically, the cumulative z-curve crossing both the conventional and TSA monitoring boundaries indicated sufficient evidence for the diagnostic capability of dysregulated circRNAs for OSCC detection. The required information size, adopting an alpha risk of 5% and a beta risk of 20%, was estimated for this analysis.

RESULTS

Search Results

Figure 1 presents the detailed search process. A total of 2105 potentially eligible articles were identified from PubMed (903 records), Web of Science (603 records), Embase (598 records), and Cochrane Library (one record). A total of 671 records remained after eliminating 1434 duplicates. Furthermore, 615 articles were excluded for the following reasons: 56 were review articles, 553 were unrelated studies, and six were articles whose full texts were not available. After evaluating the full articles, 33 records were excluded without sufficient data, and 16 were removed because no relevant results were reported (**Appendix 2**). Finally, 872 cases and 900 controls from 16 studies were included in the meta-analysis (19–34).

Study Characteristics

In the meta-analysis, an evaluation was conducted on the association between circRNA expression levels and the type of OSCC to determine the accuracy of circRNA expression as an OSCC biomarker. **Table 1** presents the main characteristics of each study. All the studies were released between 2018 and 2021, which were all from China. Each included study adopted the conventional case-control design. Twelve studies used paired OSCC as cases and corresponding adjacent normal tissue as controls. Four studies used saliva, plasma, or serum samples

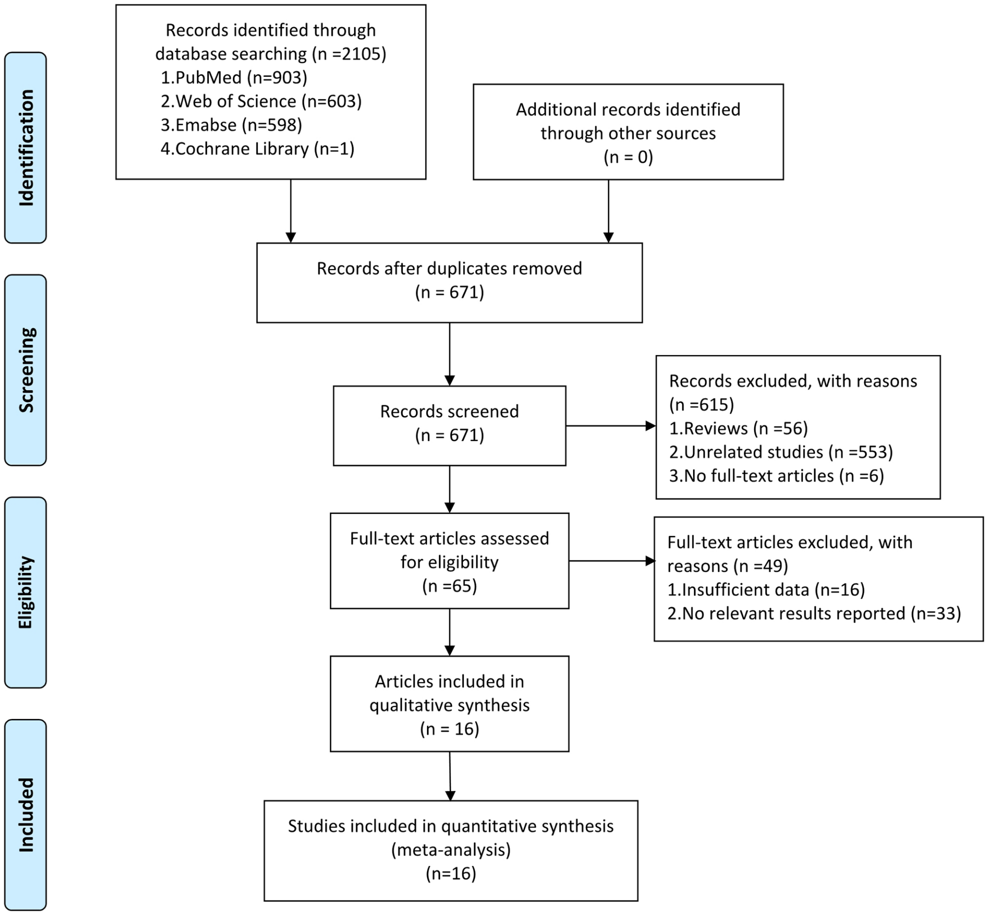

FIGURE 1 | The PRISMA flow diagram showing the process of eligible studies search and selection. This meta-analysis identified 16 eligible studies that used circRNAs as biomarkers for tumor diagnosis.

from OSCC patients as the cases and healthy volunteers as controls. The number of patients in the included studies ranged from 25 to 146. A total of 16 different circRNAs were assessed, among which five upregulated circRNAs were recognized as tumor promoters (22, 25, 29, 30, 32) and 11 were downregulated as tumor suppressors (19–21, 23, 24, 26–28, 31, 33, 34). All circRNA expression levels were detected using qRT-PCR in tissues (n = 12), plasma (n = 1), serum (n = 2), and saliva (n = 1). All the samples were collected before clinical treatment.

Risk of Bias and Applicability Concerns Within Studies

Not a single included study fulfilled all the domain criteria in the QUADAS-2 methodological quality tool. On average two out of four domains of risk of bias were fulfilled in each study. The case-control design and inappropriate exclusions(for the specific diagnosis) explained why no study was observed to have a low risk in patient selection and index test domain. Two of these studies were graded as high risk in patient selection because no exact time scope and continuity were mentioned. Items 4 and 7 were assessed as unclear because no information on blinding was reported. All the articles met the criteria of the three domains of applicability concerns (**Figure 2** and **Appendix 3**).

Meta-Analysis

The present meta-analysis of 16 cohorts in 872 patients and 900 controls included 16 circRNA types. A random-effects model was selected because of the significant heterogeneity ($I^2 > 50\%$) between the included studies. The meta-analysis was conducted, and the pooled sensitivity, specificity, PLR, NLR, DOR, and SROC were calculated for circRNA, as illustrated in **Figure 3**. The pooled statistical values for sensitivity (**Figure 3A**), specificity (**Figure 3B**), PLR (**Figure 3C**), NLR (**Figure 3D**), and DOR (**Figure 3E**) with the 95% confidence intervals for the enrolled studies in this study were 0.74 (95% CI: 0.69 – 0.79), 0.79 (95% CI: 0.73 – 0.84), 3.50 (95% CI: 2.76 – 4.45), 0.33 (95% CI: 0.27 – 0.39), and 10.74 (95% CI: 7.81 – 14.77), respectively. The diagnostic odds ratio (DOR) represents a critical indicator that assists in a meta-analysis by focusing on diagnostic performance, and combines the advantages of both sensitivity and specificity, and describes the diagnostic value of a

TABLE 1 | Main characteristics of 16 studies included in the meta-analysis.

	First author	Year	Country	CircRNA	Regulation	Sample size		Cancer type	Specimen	Method	Diagnostic power			Source of the control group
						Case	Control				Sensitivity	Specificity	AUC	
1	Sun S	2018	China	hsa_circ_001242	downregulated	40	40	OSCC	tissue	qRT-PCR	0.725	0.775	0.784	adjacent normal tissues
2	Li B	2018	China	hsa_circ_0008309	downregulated	45	45	OSCC	tissue	qRT-PCR	0.512	0.913	0.7642	adjacent normal tissues
3	He T	2018	China	circPVT1	upregulated	50	50	OSCC	tissue	qRT-PCR	0.686	0.86	0.787	adjacent normal tissues
4	Zhao S	2018	China	hsa_circ_0001874 + hsa_circ_0001971	upregulated	93	85	OSCC	saliva	qRT-PCR	0.9268	0.7778	0.922	Healthy controls
5	Li X	2019	China	hsa_circ_0004491	downregulated	40	40	OSCC	tissue	qRT-PCR	0.73	0.68	0.751	adjacent normal tissues
6	Xia B	2019	China	circ-MMP9	upregulated	25	16	OSCC	plasma	qRT-PCR	0.889	0.81	0.91	Healthy controls
7	Su W	2019	China	hsa_circ_0005379	downregulated	37	37	OSCC	tissue	qRT-PCR	0.699	0.605	0.6805	adjacent normal tissues
8	Dou Z	2019	China	hsa_circ_0072387	downregulated	63	63	OSCC	tissue	qRT-PCR	0.714	0.698	0.746	adjacent normal tissues
9	Fan C	2019	China	circMAN1A2	upregulated	55	121	OSCC	serum	qRT-PCR	0.672	0.915	0.779	Healthy controls
10	Wang Z	2019	China	hsa_circ_009755	downregulated	27	27	OSCC	tissue	qRT-PCR	0.7037	0.7778	0.782	adjacent normal tissues
11	Yao Y	2020	China	circular RNA_0001742	upregulated	146	146	OSCC	tissue	qRT-PCR	0.775	0.808	0.87	adjacent normal tissues
12	Zhang H	2020	China	hsa_circ_0003829	downregulated	60	60	OSCC	tissue	qRT-PCR	0.7	0.8	0.81	adjacent normal tissues
13	Li L	2020	China	hsa_circ_0086414	downregulated	55	55	OSCC	tissue	qRT-PCR	0.655	0.873	0.749	adjacent normal tissues
14	Chen G	2020	China	circATRNL1	downregulated	48	48	OSCC	tissue	qRT-PCR	0.848	0.509	0.711	adjacent normal tissues
15	Zhang B	2020	China	hsa_circ_009755	downregulated	42	42	OSCC	tissue	qRT-PCR	0.69	0.885	0.83	adjacent normal tissues
16	Fan X	2021	China	circSPATA6	downregulated	46	25	OSCC	serum	qRT-PCR	0.79	0.69	0.7748	Healthy controls

circRNA (35). The summary receiver operator curve (SROC, **Figure 3F**) plot revealed an AUC of 0.83 (95% CI: 0.79 – 0.86). The bivariate boxplot in **Figure 3H** presents the heterogeneity details in the included studies. Fagan's nomogram was constructed to calculate the post-test probabilities of the circRNAs, in which the post-test possibility increased to 47% with a positive likelihood ratio (LR) of 4, with the post-test possibility decreasing to 8% with a negative LR of 0.33 (**Figure 4**). These findings indicated that circRNAs were a credible diagnostic biomarker with high accuracy and efficacy. **Figure 5** presents an LR scattergram plotted with the combined summary points.

Therefore, taken together, the results indicated that the circRNAs had good diagnostic accuracy for OSCC and could serve as effective biomarkers of OSCC.

Meta-Regression and Subgroup Analysis

Overall, the studies exhibited relatively high heterogeneity in sensitivity and specificity ($I^2 = 64.12$ and $I^2 = 75.08$, respectively). Thus, a meta-regression analysis was first conducted to investigate the heterogeneity source (**Appendix 4**). The meta-regression analysis demonstrated that three covariates (specimen type, expression status, and sample size) could explain 100% of the between-study variance.

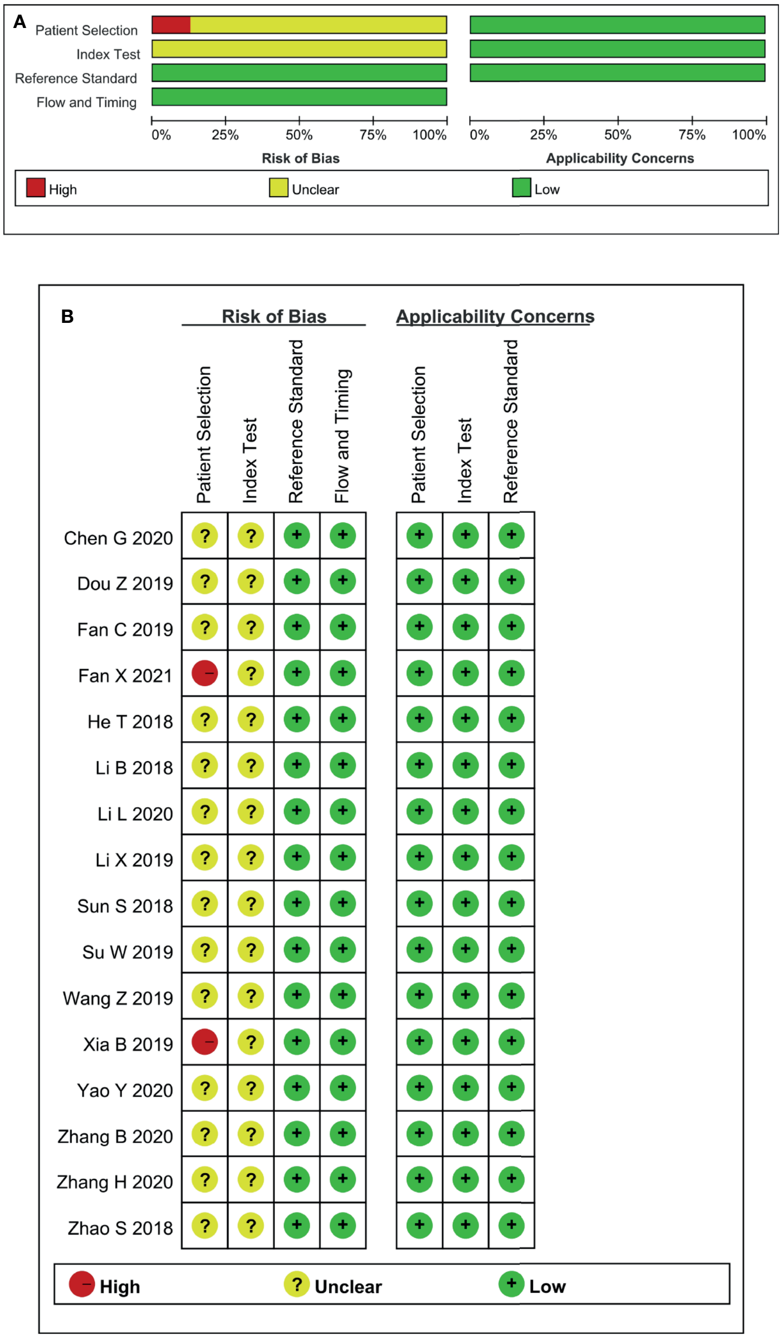

FIGURE 2 | Quality assessment of the included studies according to QUADAS-2 **(A)** Methodological quality graph; **(B)** Methodological quality summary.

Table 2 and **Figures 6–8** present further subgroup analyses to identify the source of the heterogeneity. Subgroups of studies utilizing serum (n = 2), plasma (n = 1), and saliva (n = 1) specimens exhibited better diagnostic performance with DOR (24.70 *vs.* 9.00) and the AUC (0.90 *vs.* 0.80) compared to the tissue (n = 12) subgroup. The pooled sensitivity and specificity were both greater than in the tissue subgroup. No significant heterogeneity was observed in the tissue subgroup (I^2 = 0.0, P = 0.450) or other specimen types (I^2 = 47.6%, P = 0.125). Therefore, the variance between these two subgroups of specimen types may account for the heterogeneity.

We analyzed the subgroups according to the expression status of dysregulated circRNAs. The studies on upregulated circRNAs (n = 5) had a significantly higher pooled DOR (20.35 *vs.* 7.49) and AUC (0.89 *vs.* 0.78) than those on downregulated circRNAs (n=11). In the forest plots, the results covered no heterogeneity in

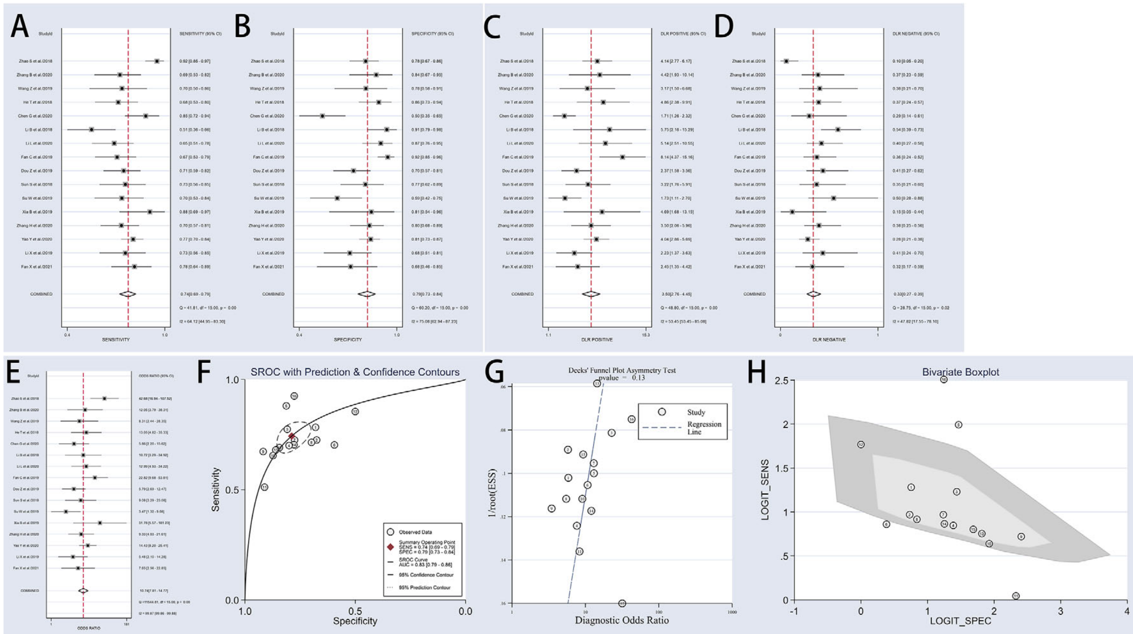

FIGURE 3 | Forest plots of sensitivity, specificity, PLR, NLR, DOR, AUC, and funnel plot for diagnosis of circRNAs in OSCC among 16 studies. **(A)** Sensitivity; **(B)** Specificity; **(C)** PLR; **(D)** NLR; **(E)** DOR; **(F)** AUC (SROC curve); **(G)** Deek's funnel plot; and **(H)** Bivariate boxplot. OSCC, oral squamous cell carcinoma; PLR, positive likelihood ratio;NLR, negative likelihood ratio; DOR, diagnostics odds ratio; SROC, Summary receiver operator characteristics curve; AUC, the area under SROC curve.

upregulated (I^2 = 18.4%, P = 0.298) and downregulated circRNAs (I^2 = 0.0, P = 0.797). Since no heterogeneity was observed in the subgroups, the difference between these two expression status subgroups may account for the heterogeneity.

An analysis of subgroups classified by the sample size of the included cohorts (≥ 100 and < 100) was also carried out. The ≥ 100 subgroup (n = 7) had a higher DOR (14.22 *vs.* 7.58) and AUC (0.86 *vs.* 0.79) than the < 100 subgroup (n = 9) (**Table 2**). In the former subgroup, evident heterogeneity was detected with a value of I^2 = 53.4 (P = 0.045). However, no heterogeneity was observed in the latter subgroup (I^2 = 0.0, P= 0.545). Hence, the subgroup analysis results indicated that the sample size of the enrolled cohorts might be the source of heterogeneity.

Publication Bias

Deek's funnel plot asymmetry tests were employed to assess the publication bias, as illustrated in **Figure 3G**, with the results indicating no obvious publication bias (P = 0.13). The funnel plot and Harbord test shown in **Figure 9** were used to track the potential publication bias in the meta-analysis. The P-value of both was > 0.05 (P = 0.13 and P = 0.175), suggesting no publication bias in the meta-analysis.

Sensitivity Analysis

A sensitivity analysis was carried out to explain the heterogeneity of each study. As shown in **Figure 10**, omitting any individual study had no substantial impact on the pooled statistics, indicating that the results were credible and reliable.

TSA Outcome

The overall required information size was calculated for the 1762 participants (**Appendix 5**). The z-curve crossed both the conventional and TSA monitoring boundaries. However, it failed to reach the RIS line, indicating statistical significance and sufficient evidence on the diagnostic performance of circRNAs as biomarkers for OSCC.

DISCUSSION

Previous cumulative investigations have demonstrated that dysregulated circRNAs played a critical role in the cell proliferation, metastasis, and occurrence of various cancers. The closed, covalent, and continuous circular structure of circRNAs makes them more steady than their linear counterparts (36). Moreover, dysregulated circRNAs have been discovered in plasma, tissues, and serum (37). The characteristics above render circRNAs favorable as molecular biomarkers of cancer.

Overall, 16 studies were included in this meta-analysis. The final results based on all the enrolled studies showed an AUC of 0.83 for circRNAs, with a sensitivity of 0.74 and specificity of 0.79 in distinguishing OSCC patients from healthy controls. The pooled sensitivity and specificity showed moderate diagnostic test accuracy, indicating that circRNAs had sufficient statistical ability to identify or exclude suspected cases to enhance the clinical diagnosis. A DOR of 10.74 (> 1.0) was obtained in the

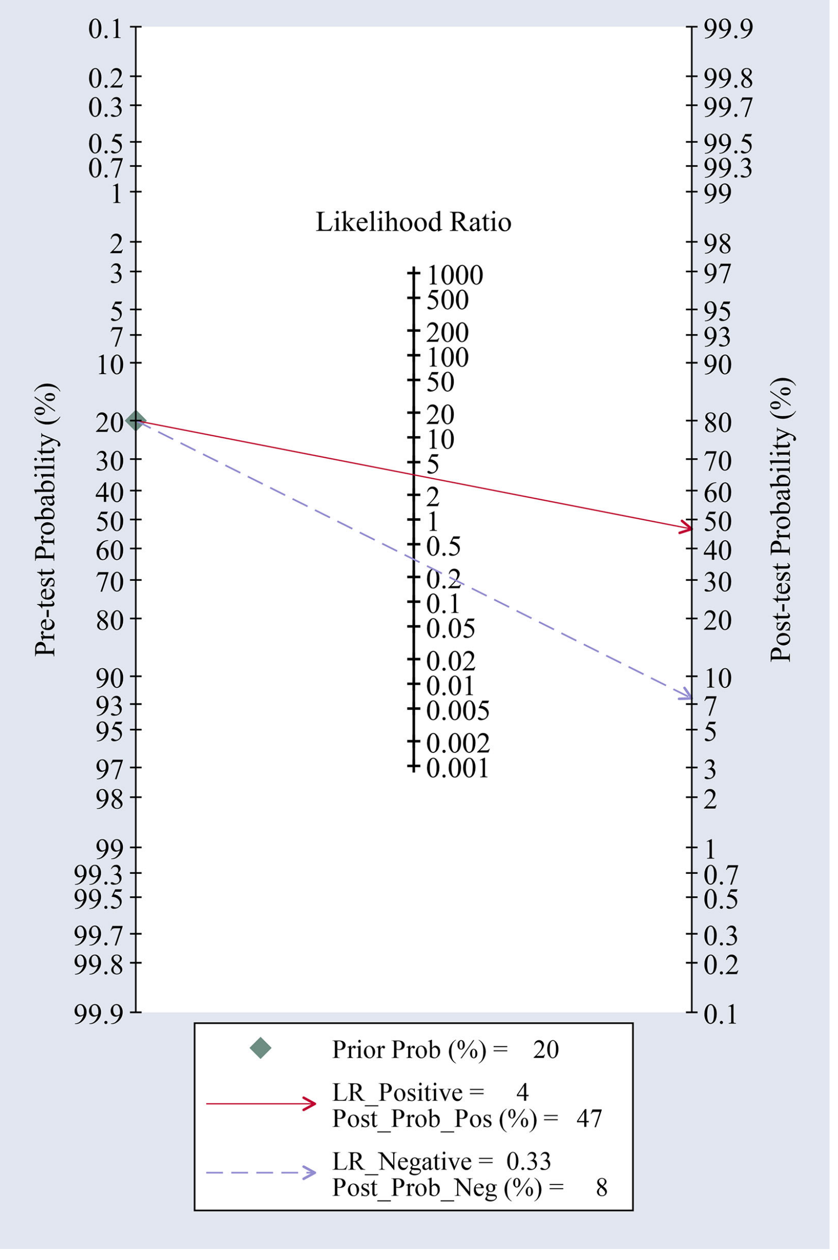

FIGURE 4 | Fagan's nomogram for likelihood ratios.

present analysis, indicating that the dysregulated circRNAs were effective predictive biomarkers for OSCC. Furthermore, the higher AUC value showed better performance in the balance of sensitivity and specificity. Notably, the high AUC value of 0.83 in the current analysis reflects the overall relatively high diagnostic accuracy of circRNAs in OSCC detection.

To the best of our knowledge, this study was the first systematic review and meta-analysis to estimate the diagnostic ability of circRNAs as biomarkers in OSCC patients and summarize their sensitivity and specificity. Other published systematic reviews have evaluated several biomarkers for OSCC diagnosis, such as microRNAs, mRNAs, and proteins. Rapado-Gonzalez et al. performed a systematic review of microRNAs in OSCC and summarized the clinical correlation, including proliferation and progression, with a relatively high AUC of 0.91 (38). Gaba et al. assessed the diagnostic value of a specific mRNA, DUSP1, which proved insufficient with an AUC of 0.66. In addition, Gaba et al. reviewed the clinical correlation of a protein named IL1-β protein and estimated its diagnostic value, which was considered good with an AUC of 0.82 (39).

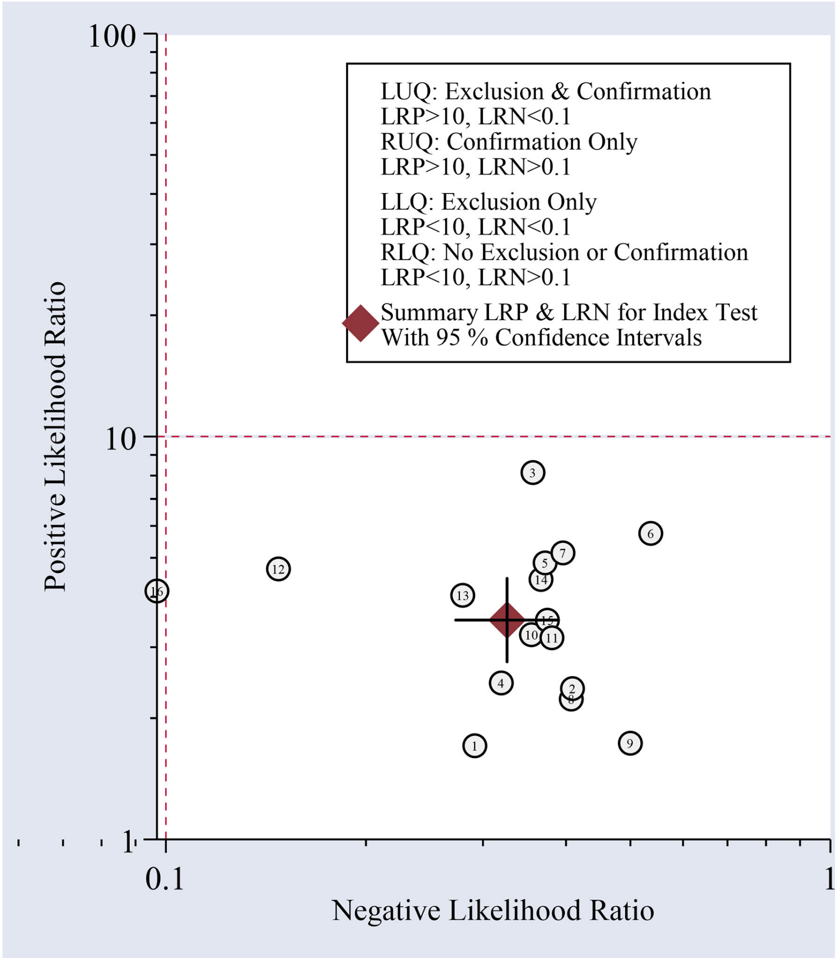

FIGURE 5 | Scatter plot of positive and negative likelihood ratios with combined summary points.

TABLE 2 | Results of subgroup analysis of cricRNAs reported by 16 studies in diagnostic meta-analysis.

Analysis	No. of studies	Sensitivity (95% CI)	Specificity (95% CI)	PLR (95% CI)	NLR (95% CI)	DOR (95% CI)	AUC(95%CI)	I²(%)	p-value
Overall	16	0.74(0.69-0.79)	0.79(0.73-0.84)	3.50(2.78-4.45)	0.33(0.27-0.39)	10.74(7.81-14.77)	0.83(0.79-0.86)	43.0	0.035
Sample type									
tissue	12	0.72(0.7-0.76)	0.78(0.71-0.84)	3.26(2.50-4.24)	0.36(0.32-0.42)	9.00(6.61-12.25)	0.80(0.76-0.83)	0.0	0.450
serum or plasma or saliva	4	0.83(0.71-0.91)	0.83(0.74-0.90)	4.93(3.32-7.33)	0.20(0.12-0.34)	24.70(14.37-42.44)	0.90(0.87-0.92)	47.6	0.125
Sample size									
≥100	7	0.75(0.66-0.82)	0.83(0.77-0.87)	4.36(3.33-5.70)	0.31(0.23-0.41)	14.22(9.41-24.50)	0.86(0.83-0.89)	53.4	0.045
<100	9	0.73(0.66-0.80)	0.73(0.64-0.81)	2.76(2.06-3.71)	0.36(0.30-0.45)	7.58(5.17-11.11)	0.79(0.76-0.83)	0.0	0.545
Expression									
downregulated	11	0.71(0.65-0.76)	0.75(0.67-0.82)	2.88(2.20-3.76)	0.38(0.33-0.45)	7.49(5.38-10.44)	0.78(0.74-0.82)	0.0	0.797
upregulated	5	0.80(0.68-0.88)	0.84(0.78-0.89)	4.94(3.75-6.50)	0.24(0.16-0.38)	20.35(13.10-31.62)	0.89(0.86-0.91)	18.4	0.298

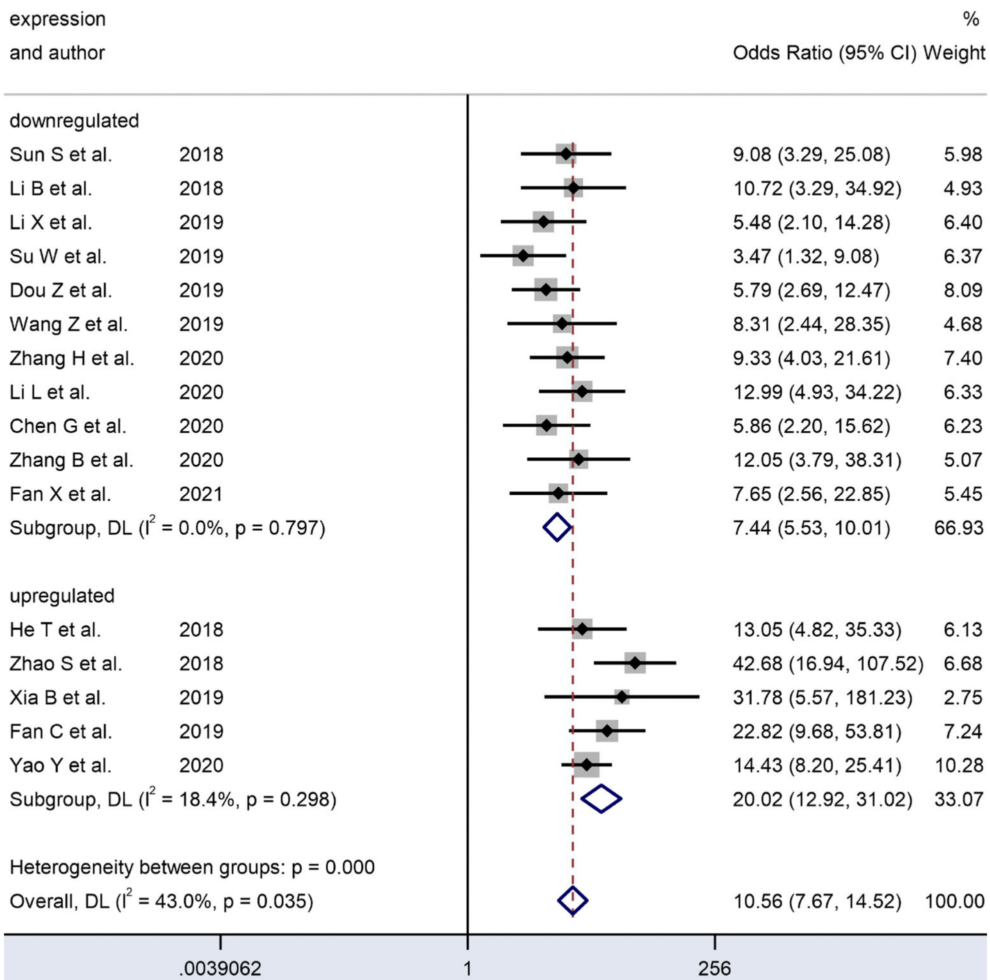

FIGURE 6 | Forest plots of subgroup analysis of the combined ORs with 95%CIs according to expression status of circRNAs in patients with OSCC.

However, despite the growing number of reviews and analyses based on diagnostic biomarkers for OSCC, no consensus has been reached on determining which biomarker has the best diagnostic performance for OSCC and what is the most accurate sample for testing.

Meta-regression and subgroup analyses of specimens, sample size, and the expression status of the dysregulated circRNAs were performed to explore the sources of the heterogeneity. The random-effects-based meta-regression analysis showed that these three covariates were the main sources of the heterogeneity. Studies that utilized serum, plasma, and saliva specimens performed significantly better in diagnosing OSCC patients compared to those using tissue specimens, with no heterogeneity detected. The subgroups with upregulated circRNAs and ≥ 100 samples were found to possess a much higher diagnostic accuracy than the downregulated circRNAs and those with < 100 samples and these two subgroups showed no heterogeneity. Apparent heterogeneity was found in the subgroup with ≥ 100 samples. Therefore, the heterogeneity might be related to the sample size, specimen type, and expression status.

We further considered the reasons for the differences in the diagnostic accuracy between the tissue and liquid biopsies. Concerning tissue biopsies, OSCC, as a solid tumor, exhibits tissue heterogeneity even for the same histological type. The proportion of tumor cells and mesenchymal cells vary in different patients and even in different parts of the same tumor. Therefore, the sample used for detection only accounts for part of the tumor. This cannot accurately reflect the whole tumor status, which is the potential reason for the lower accuracy in tissue samples than detection by body fluid specimens.

Currently, tissue-based diagnostic strategies require the testing of materials obtained through invasive procedures, such as biopsy or aspiration, which are usually associated with severe discomfort and medical costs (40). Compared to tissue biopsies, body fluids are a better choice for disease screening and diagnosis due to the advantages of accessibility, low invasion, low cost, and various sample types to monitor disease development (41).

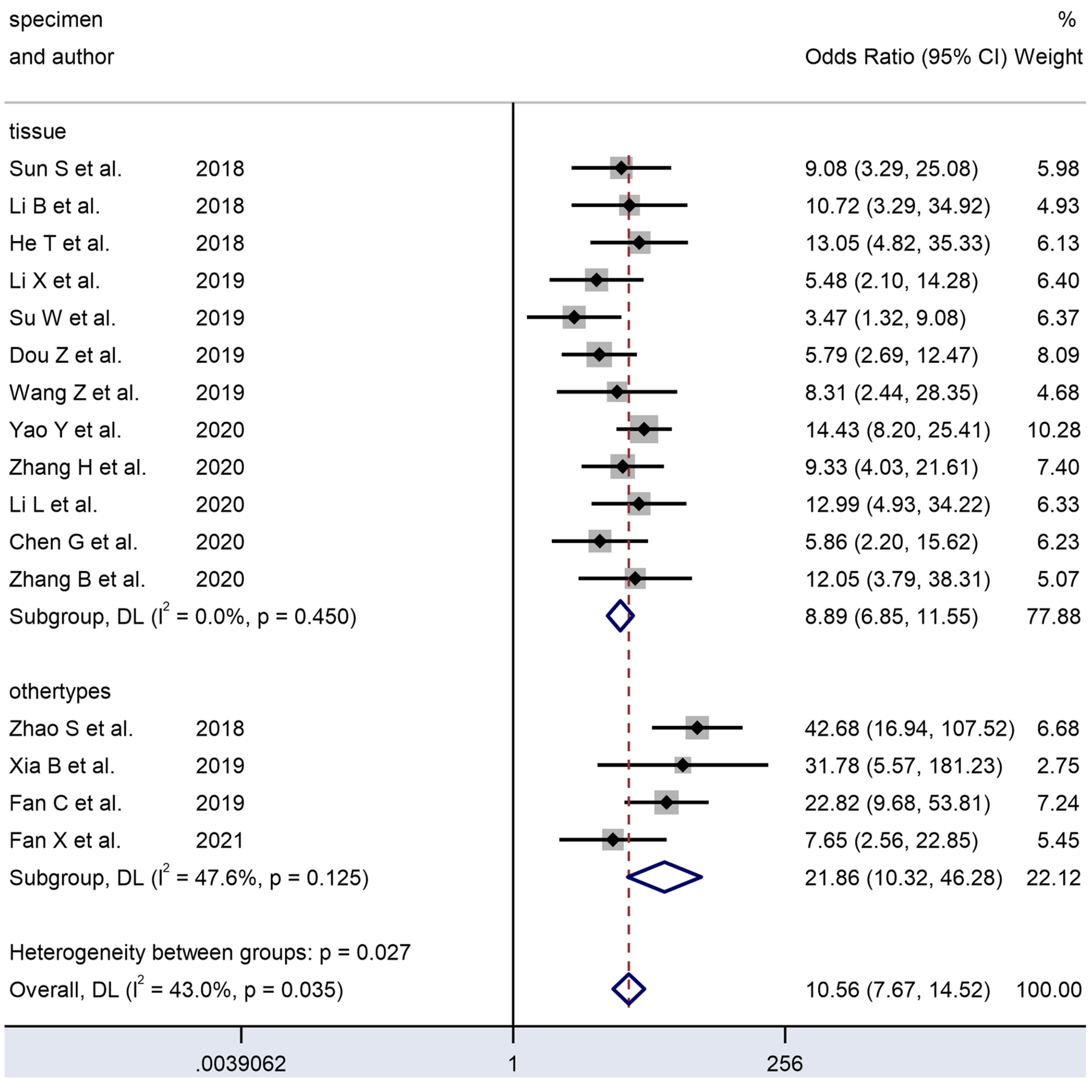

FIGURE 7 | Forest plots of subgroup analysis of the combined ORs with 95%CIs according to specimen type of circRNAs in patients with OSCC.

Several studies have reviewed the potential of mRNAs as diagnostic markers, illustrating the possible clinical application of OSCC-specific signals in body fluids (42, 43). These molecules can be prospective candidates for biomarkers due to their stable circulation in human body fluids and accessibility through non-invasive methods. Likewise, circRNA detection can be regarded as a novel method for body fluid-based biopsies, which would be helpful as significant diagnostic and monitoring tools in the clinic. At present, there is a shortage of research on the diagnostic value of circRNAs in body fluids for OSCC, which provides a new direction for researchers worldwide to utilize the saliva and serum of high-risk patients with lesions in the oral cavity suspected of oral squamous cell carcinoma.

Nevertheless, it is not yet possible to apply these molecular biomarkers in clinical diagnosis and monitoring. New techniques, such as digital PCR, make it possible to test cancer and phenotype-specific molecular changes to improve sensitivity and accuracy. After this technique is used more widely, the successful application of molecular markers in liquid biopsies of other tumors (e.g., lung carcinoma) will encourage further evaluation of this method in OSCC cases.

Several deficiencies in the present study merit consideration. (a) Based on our inclusion criteria, all samples and relevant statistics accidentally came from China. (b) Subgroup analysis of different circRNA should be further performed. (c) Conspicuous heterogeneity existed in the included studies. The sample size, specimen types, and expression status might be sources of the heterogeneity. (d) The sample size and number of the enrolled studies in this analysis were relatively small. Thus, more comprehensive high-quality studies that encompass larger scales, more regions, well-designed operations, and further exploration into the functional mechanisms are necessary.

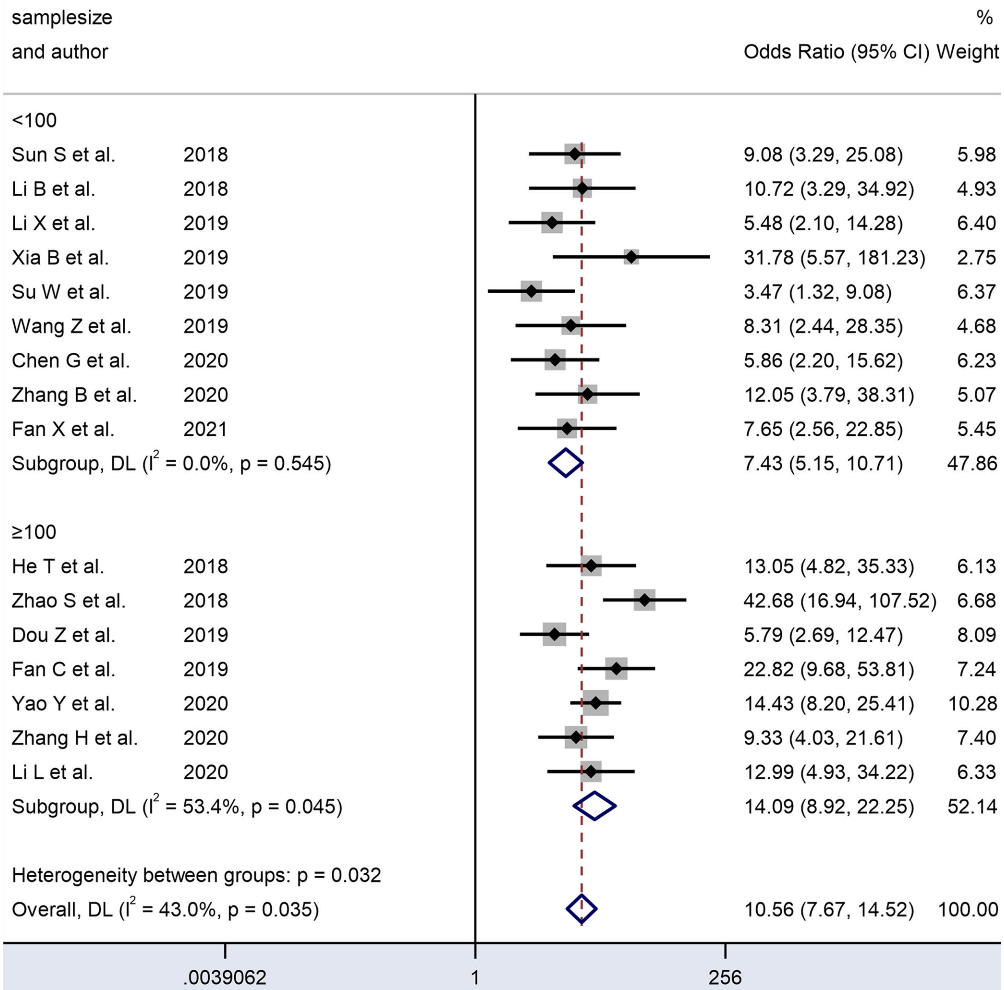

FIGURE 8 | Forest plots of subgroup analysis of the combined ORs with 95%CIs according to sample size of circRNAs in patients with OSCC.

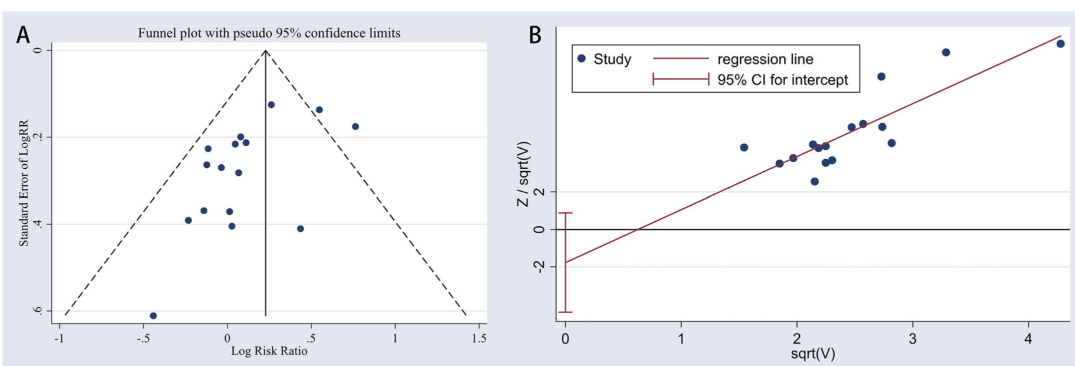

FIGURE 9 | Publication bias in the meta-analysis. **(A)**, funnel chart; **(B)**, Harbord test plot.

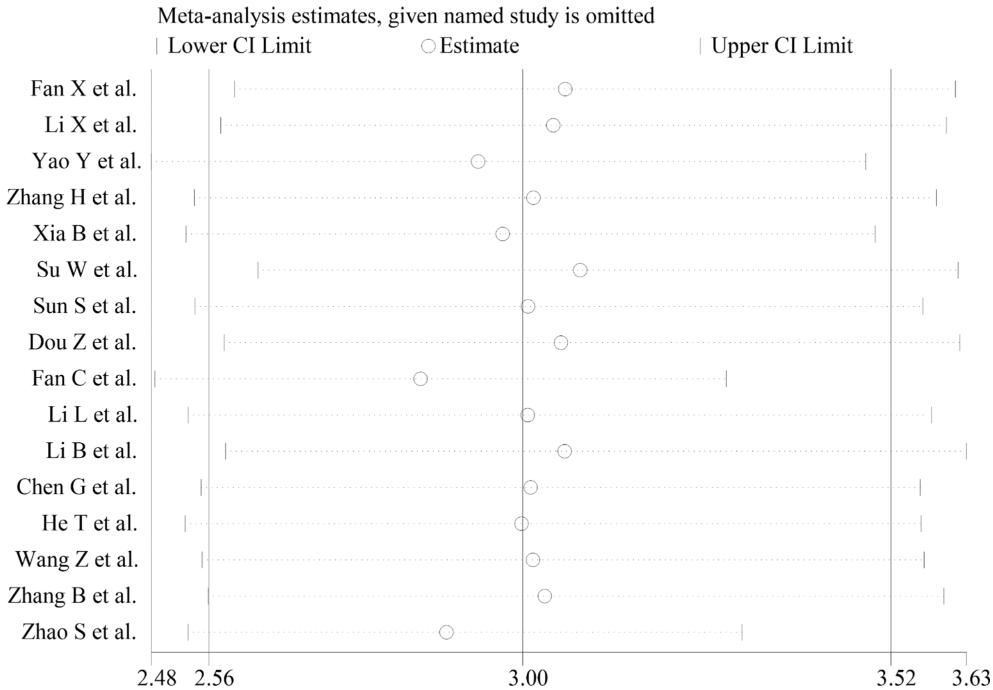

FIGURE 10 | Sensitivity analysis plot of overall included studies.

CONCLUSION

In summary, this meta-analysis revealed a strong association between the altered expression of circRNAs and the diagnosis of OSCC. Hence, circRNAs can potentially serve as promising biomarkers and therapeutic targets for OSCC. Nevertheless, the clinical application of cricRNAs for the detection of OSCC requires further research.

DATA AVAILABILITY STATEMENT

The original contributions presented in the study are included in the article/**Supplementary Material**. Further inquiries can be directed to the corresponding authors.

AUTHOR CONTRIBUTIONS

LZ contributed to conception, analysis, and drafted manuscript. MW contributed to conception and design, acquisition and interpretation of data, and critically revised manuscript. WR contributed to design, interpretation of data, and drafted manuscript. SL contributed to design, acquisition of data, and critically revised manuscript. KZ critically revised manuscript. JZ contributed to acquisition and analysis of data. LG contributed to analysis and interpretation of data, and drafted manuscript. All authors contributed to the article and approved the submitted version.

FUNDING

This work was supported by the Natural Science Foundation of Shandong Province (2019GSF108273, 2017WS215, and ZR2018BH021), the Qingdao Outstanding Health Professional Development Fund, and the Qilu Health Leading Talent Project.

SUPPLEMENTARY MATERIAL

The Supplementary Material for this article can be found online at: https://www.frontiersin.org/articles/10.3389/fonc.2021.693284/full#supplementary-material

REFERENCES

1. Argiris A, Karamouzis MV, Raben D, Ferris RL. Head and Neck Cancer. *Lancet (Lond Engl)* (2008) 371(9625):1695–709. doi: 10.1016/s0140-6736(08)60728-x
2. Bray F, Ferlay J, Soerjomataram I, Siegel RL, Torre LA, Jemal A. Global Cancer Statistics 2018: GLOBOCAN Estimates of Incidence and Mortality Worldwide for 36 Cancers in 185 Countries. *CA: Cancer J Clin* (2018) 68(6):394–424. doi: 10.3322/caac.21492
3. Chi AC, Day TA, Neville BW. Oral Cavity and Oropharyngeal Squamous Cell Carcinoma–an Update. *CA Cancer J Clin* (2015) 65(5):401–21. doi: 10.3322/caac.21293
4. Leemans CR, Braakhuis BJ, Brakenhoff RH. The Molecular Biology of Head and Neck Cancer. *Nat Rev Cancer* (2011) 11(1):9–22. doi: 10.1038/nrc2982

5. Chai AWY, Lim KP, Cheong SC. Translational Genomics and Recent Advances in Oral Squamous Cell Carcinoma. *Semin Cancer Biol* (2020) 61:71–83. doi: 10.1016/j.semcancer.2019.09.011
6. Leemans CR, Snijders PJF, Brakenhoff RH. The Molecular Landscape of Head and Neck Cancer. *Nat Rev Cancer* (2018) 18(5):269–82. doi: 10.1038/nrc.2018.11
7. Solomon B, Young RJ, Rischin D. Head and Neck Squamous Cell Carcinoma: Genomics and Emerging Biomarkers for Immunomodulatory Cancer Treatments. *Semin Cancer Biol* (2018) 52(Pt 2):228–40. doi: 10.1016/j.semcancer.2018.01.008
8. Yang EC, Tan MT, Schwarz RA, Richards-Kortum RR, Gillenwater AM, Vigneswaran N. Noninvasive Diagnostic Adjuncts for the Evaluation of Potentially Premalignant Oral Epithelial Lesions: Current Limitations and Future Directions. *Oral Surg Oral Med Oral Pathol Oral Radiol* (2018) 125 (6):670–81. doi: 10.1016/j.oooo.2018.02.020
9. Starke S, Jost I, Rossbach O, Schneider T, Schreiner S, Hung LH, et al. Exon Circularization Requires Canonical Splice Signals. *Cell Rep* (2015) 10(1):103–11. doi: 10.1016/j.celrep.2014.12.002
10. Guo JU, Agarwal V, Guo H, Bartel DP. Expanded Identification and Characterization of Mammalian Circular RNAs. *Genome Biol* (2014) 15 (7):409. doi: 10.1186/s13059-014-0409-z
11. Hentze MW, Preiss T. Circular RNAs: Splicing's Enigma Variations. *EMBO J* (2013) 32(7):923–5. doi: 10.1038/emboj.2013.53
12. van Heesch S, Witte F, Schneider-Lunitz V, Schulz JF, Adami E, Faber AB, et al. The Translational Landscape of the Human Heart. *Cell* (2019) 178 (1):242–60. doi: 10.1016/j.cell.2019.05.010
13. Shan K, Liu C, Liu BH, Chen X, Dong R, Liu X, et al. Circular Noncoding RNA HIPK3 Mediates Retinal Vascular Dysfunction in Diabetes Mellitus. *Circulation* (2017) 136(17):1629–42. doi: 10.1161/circulationaha.117.029004
14. Gomes CPC, Schroen B, Kuster GM, Robinson EL, Ford K, Squire IB, et al. Regulatory RNAs in Heart Failure. *Circulation* (2020) 141(4):313–28. doi: 10.1161/circulationaha.119.042474
15. Gasparini S, Del Vecchio G, Gioiosa S, Flati T, Castrignano T, Legnini I, et al. Differential Expression of Hippocampal Circular RNAs in the BTBR Mouse Model for Autism Spectrum Disorder. *Mol Neurobiol* (2020) 57(5):2301–13. doi: 10.1007/s12035-020-01878-6
16. Meng X, Li X, Zhang P, Wang J, Zhou Y, Chen M. Circular RNA: An Emerging Key Player in RNA World. *Brief Bioinform* (2017) 18(4):547–57. doi: 10.1093/bib/bbw045
17. McInnes MDF, Moher D, Thombs BD, McGrath TA, Bossuyt PM, Clifford T, et al. Preferred Reporting Items for a Systematic Review and Meta-analysis of Diagnostic Test Accuracy Studies: The Prisma-DTA Statement. *Jama* (2018) 319(4):388–96. doi: 10.1001/jama.2017.19163
18. Whiting PF, Rutjes AW, Westwood ME, Mallett S, Deeks JJ, Reitsma JB, et al. Quadas-2: a Revised Tool for the Quality Assessment of Diagnostic Accuracy Studies. *Ann Intern Med* (2011) 155(8):529–36. doi: 10.7326/0003-4819-155-8-201110180-00009
19. Fan X, Wang Y. Circular RNA Circspata6 Inhibits the Progression of Oral Squamous Cell Carcinoma Cells by Regulating TRAF6 Via Mir-182. *Cancer Manag Res* (2021) 13:1817–29. doi: 10.2147/cmar.S292074
20. Zhang H, Shen Y, Zhang B, Qian M, Zhang Y, Yang H. Hsa_Circ_0003829 Serves as a Potential Diagnostic Predictor for Oral Squamous Cell Carcinoma. *J Int Med Res* (2020) 48(9):300060520936880. doi: 10.1177/0300060520936880
21. Zhang B, Wang Z, Shen Y, Yang H. Silencing Circular RNA Hsa_Circ_009755 Promotes Growth and Metastasis of Oral Squamous Cell Carcinoma. *Genomics* (2020) 112(6):5275–81. doi: 10.1016/j.ygeno.2020.09.035
22. Yao Y, Bi L, Zhang C. Circular RNA_0001742 Has Potential to Predict Advanced Tumor Stage and Poor Survival Profiles in Tongue Squamous Cell Carcinoma Management. *J Clin Lab Anal* (2020) 34(8):e23330. doi: 10.1002/jcla.23330
23. Li L, Zhang ZT. Hsa_Circ_0086414 Might be a Diagnostic Biomarker of Oral Squamous Cell Carcinoma. *Med Sci Monit* (2020) 26:e919383. doi: 10.12659/msm.919383
24. Chen G, Li Y, He Y, Zeng B, Yi C, Wang C, et al. Upregulation of Circular Rna circATRNL1 to Sensitize Oral Squamous Cell Carcinoma to Irradiation. *Mol Ther Nucleic Acids* (2020) 19:961–73. doi: 10.1016/j.omtn.2019.12.031
25. Xia B, Hong T, He X, Hu X, Gao Y. A Circular RNA Derived From MMP9 Facilitates Oral Squamous Cell Carcinoma Metastasis Through Regulation of MMP9 mRNA Stability. *Cell Transplant* (2019) 28(12):1614–23. doi: 10.1177/0963689719875409
26. Wang Z, Tang J, Wang Y, Sun S, Chen Y, Shen Y, et al. Circular RNA Hsa_Circ_009755 Downregulation Correlates With Clinicopathology in Oral Squamous Cell Carcinoma. *Onco Targets Ther* (2019) 12:4025–31. doi: 10.2147/ott.S196618
27. Su W, Wang Y, Wang F, Sun S, Li M, Shen Y, et al. Hsa_Circ_0005379 Regulates Malignant Behavior of Oral Squamous Cell Carcinoma Through the EGFR Pathway. *BMC Cancer* (2019) 19(1):400. doi: 10.1186/s12885-019-5593-5
28. Li X, Zhang H, Wang Y, Sun S, Shen Y, Yang H. Silencing Circular RNA Hsa_Circ_0004491 Promotes Metastasis of Oral Squamous Cell Carcinoma. *Life Sci* (2019) 239:116883. doi: 10.1016/j.lfs.2019.116883
29. He T, Li X, Xie D, Tian L. Overexpressed circPVT1 in Oral Squamous Cell Carcinoma Promotes Proliferation by Serving as a miRNA Sponge. *Mol Med Rep* (2019) 20(4):3509–18. doi: 10.3892/mmr.2019.10615
30. Fan CM, Wang JP, Tang YY, Zhao J, He SY, Xiong F, et al. circMAN1A2 Could Serve as a Novel Serum Biomarker for Malignant Tumors. *Cancer Sci* (2019) 110(7):2180–8. doi: 10.1111/cas.14034
31. Dou Z, Li S, Ren W, Wang Q, Liu J, Kong X, et al. Decreased Expression of Hsa_Circ_0072387 as a Valuable Predictor for Oral Squamous Cell Carcinoma. *Oral Dis* (2019) 25(5):1302–8. doi: 10.1111/odi.13094
32. Zhao SY, Wang J, Ouyang SB, Huang ZK, Liao L. Salivary Circular Rnas Hsa_Circ_0001874 and Hsa_Circ_0001971 as Novel Biomarkers for the Diagnosis of Oral Squamous Cell Carcinoma. *Cell Physiol Biochem* (2018) 47(6):2511–21. doi: 10.1159/000491624
33. Sun S, Li B, Wang Y, Li X, Wang P, Wang F, et al. Clinical Significance of the Decreased Expression of Hsa_Circ_001242 in Oral Squamous Cell Carcinoma. *Dis Markers* (2018) 2018:6514795. doi: 10.1155/2018/6514795
34. Li B, Wang F, Li X, Sun S, Shen Y, Yang H. Hsa_Circ_0008309 May be a Potential Biomarker for Oral Squamous Cell Carcinoma. *Dis Markers* (2018) 2018:7496890. doi: 10.1155/2018/7496890
35. Glas AS, Lijmer JG, Prins MH, Bonsel GJ, Bossuyt PM. The Diagnostic Odds Ratio: A Single Indicator of Test Performance. *J Clin Epidemiol* (2003) 56 (11):1129–35. doi: 10.1016/s0895-4356(03)00177-x
36. Lei M, Zheng G, Ning Q, Zheng J, Dong D. Translation and Functional Roles of Circular RNAs in Human Cancer. *Mol Cancer* (2020) 19(1):30. doi: 10.1186/s12943-020-1135-7
37. Wang F, Nazarali AJ, Ji S. Circular RNAs as Potential Biomarkers for Cancer Diagnosis and Therapy. *Am J Cancer Res* (2016) 6(6):1167–76.
38. Rapado-González O, Martínez-Reglero C, Salgado-Barreira A, López-López R, Suárez-Cunqueiro MM, Muinelo-Romay L. miRNAs in Liquid Biopsy for Oral Squamous Cell Carcinoma Diagnosis: Systematic Review and Meta-Analysis. *Oral Oncol* (2019) 99:104465. doi: 10.1016/j.oraloncology.2019.104465
39. Gaba FI, Sheth CC, Veses V. Salivary Biomarkers and Their Efficacies as Diagnostic Tools for Oral Squamous Cell Carcinoma: Systematic Review and Meta-Analysis. *J Oral Pathol Med* (2021) 50(3):299–307. doi: 10.1111/jop.12791
40. Schafer CA, Schafer JJ, Yakob M, Lima P, Camargo P, Wong DT. Saliva Diagnostics: Utilizing Oral Fluids to Determine Health Status. *Monogr Oral Sci* (2014) 24:88–98. doi: 10.1159/000358791
41. Good DM, Thongboonkerd V, Novak J, Bascands JL, Schanstra JP, Coon JJ, et al. Body Fluid Proteomics for Biomarker Discovery: Lessons From the Past Hold the Key to Success in the Future. *J Proteome Res* (2007) 6(12):4549–55. doi: 10.1021/pr070529w
42. Li Y, St John MA, Zhou X, Kim Y, Sinha U, Jordan RC, et al. Salivary Transcriptome Diagnostics for Oral Cancer Detection. *Clin Cancer Res* (2004) 10(24):8442–50. doi: 10.1158/1078-0432.Ccr-04-1167
43. Denaro N, Merlano MC, Russi EG, Lo Nigro C. Non Coding RNAs in Head and Neck Squamous Cell Carcinoma (HNSCC): A Clinical Perspective. *Anticancer Res* (2014) 34(12):6887–96.

Conflict of Interest: The authors declare that the research was conducted in the absence of any commercial or financial relationships that could be construed as a potential conflict of interest.